Alaiz Experiment (ALEX17): Campaign and Data Report

NEWA Deliverable Report D2.21

Cantero, Elena ; Guillén, Fernando Borbón ; Rodrigo, Javier Sanz; De Azevedo Santos, Pedro Alvim; Mann, Jakob; Vasiljevic, Nikola; Courtney, Michael; Martínez-Villagrasa, Daniel ; Martí, Belén; Cuxart, Joan

Link to article, DOI:
10.5281/zenodo.3187482

Publication date:
2019

NEWA Deliverable Report D2.21

Alaiz Experiment (ALEX17): Campaign and Data Report

Elena Cantero, Fernando Borbón Guillén, Javier Sanz Rodrigo, Pedro Santos, Jakob Mann, Nikola Vasiljević, Michael Courtney, Daniel Martínez-Villagrasa, Belén Martí, Joan Cuxart

May 2019

Author: Elena Cantero, Fernando Borbón Guillén, Javier Sanz Rodrigo, Pedro Santos, Jakob Mann, Nikola Vasiljević, Michael Courtney, Daniel Martínez-Villagrasa, Belén Martí, Joan Cuxart
Title: Alaiz Experiment (ALEX17):
Campaign and Data Report

Monday 20th May, 2019

DOI: doi.org/zenodo

Abstract (max. 2000 char)

This report ALEX17, the acronym for ALaiz EXperiment 2017, is the last full-scale experiment within the NEWA (New European Wind Atlas) project, whose primary objective is to create a wind atlas of Europe that includes the state-of-the-art in modelling the wind resource, as well as the creation of a comprehensive database. ALEX17 aims to present a utility-scale measurements campaign to characterize the wind flow in complex terrain, through a combination of measurement technologies. Having finalized the measurements campaign and processed all the information, the wind flow in the area of study it can be characterized for different weather conditions. In addition, the experimental data will be able to validate the reliability of the numeric simulation models of wind flow in complex terrain, in order to reduce uncertainties when evaluating the wind resource.

Financial Support:
NEWA ERA-NET Plus

Topic:
FP7-ENERGY.2013.10.1.2

Grant number:
618122

Pages: 106
Tables: 37
Figures: 74
References: 17

Author Information

Name	Organization	E-mail
Elena Cantero	National Renewable Energy Centre (CENER)	ecantero@cener.com
Fernando Borbón Guillén	National Renewable Energy Centre (CENER)	fborbon@cener.com
Javier Sanz Rodrigo	National Renewable Energy Centre (CENER)	jsrodrigo@cener.com
Pedro Santos	Technical Universty of Denmark (DTU)	paas@dtu.dk
Jakob Mann	Technical Universty of Denmark (DTU)	jmsq@dtu.dk
Nikola Vasiljević	Technical Universty of Denmark (DTU)	niva@dtu.dk
Michael Courtney	Technical Universty of Denmark (DTU)	mike@dtu.dk
Daniel Martínez-Villagrasa	University of the Balearic Islands (UIB)	dani.martinez@uib.cat
Belén Martí	University of the Balearic Islands (UIB)	belen.marti@uib.cat
Joan Cuxart	University of the Balearic Islands (UIB)	joan.cuxart@uib.cat

Revision History

Version	Version Date	Summary
Version 1	30/04/2019	Original version
Version 2	15/05/2019	Text revision by all authors

Contents

Page

1 Introduction **8**
- 1.1 NEWA Context . . . 8
- 1.2 Scientific Objectives . . . 8

2 Campaign Setup **10**
- 2.1 Site Characterization . . . 10
  - 2.1.1 Topography . . . 10
  - 2.1.2 Land Cover . . . 11
- 2.2 The Experimental Layout . . . 12
  - 2.2.1 Measurement Campaign Timeline . . . 13
- 2.3 Long-Range Wind-Scanners . . . 13
  - 2.3.1 WindScanner Positions & Layout . . . 13
  - 2.3.2 Scanning Trajectories . . . 15
  - 2.3.3 Ridge Scans . . . 15
  - 2.3.4 Transect Scan . . . 16
  - 2.3.5 Virtual Masts . . . 17
  - 2.3.6 Pointing Accuracy & LOS Sanity Check . . . 19
- 2.4 Met Masts . . . 20
  - 2.4.1 Georeference (Leica) survey . . . 22
  - 2.4.2 MP5 . . . 23
  - 2.4.3 Sonic masts . . . 24
  - 2.4.4 Conventional masts . . . 25
- 2.5 Surface-layer stations, SLS . . . 26
- 2.6 WLS70 Profiler . . . 28
- 2.7 WindRASS and Surface Energy Budget station . . . 29
  - 2.7.1 Surface energy budget station . . . 29
  - 2.7.2 WindRASS . . . 30
- 2.8 MeteoNavarra Stations . . . 30

3 Data Management & Availability **32**
- 3.1 Terrain data . . . 32
- 3.2 WindScanner Data . . . 32
- 3.3 WLS70 Profiler . . . 34
- 3.4 MP5 Mast . . . 37
- 3.5 Sonic masts . . . 37
- 3.6 Conventional masts . . . 39
- 3.7 SLS network . . . 39
  - 3.7.1 SLS raw data files . . . 40
  - 3.7.2 SLS flux data files . . . 40
- 3.8 WindRASS and Surface Energy Budget station . . . 40
  - 3.8.1 SEB station data files . . . 41
  - 3.8.2 WindRASS data files . . . 42

4 Summary **43**

Bibliography **44**

A Tables **47**

B Sensors: Additional Information **79**
B.1 WindScanners . . . 79
B.2 WLS70 Profiler . . . 79
B.3 Sonic Masts . . . 79
B.4 MP5 Mast . . . 79
B.5 Conventional Masts . . . 79
B.6 Surface Layer Stations (SLS) . . . 80
B.7 Surface Energy Balance (SEB) Station . . . 80
B.8 RASS-Sodar Profiler . . . 80

C WindScanner & WLS70 Deployment **81**
C.1 WS1: Sirocco at Zulueta . . . 81
C.2 WS2: Koshava at Zabalegui . . . 82
C.3 WS3: Whittle at Elorz . . . 84
C.4 WS4: Brise at Monreal . . . 85
C.5 WS5: Sterenn at Otano . . . 87
C.6 WLS70 Deployment . . . 88

D Met Masts Deployment **90**
D.1 M1: Cup Mast at Elorz (North) . . . 90
D.2 M2: Sonic Mast at Otano . . . 91
D.3 M3: Sonic Mast at Tajonar #1 . . . 93
D.4 M5: Cup Mast at Elorz (South) . . . 94
D.5 M6: Sonic Mast at Tajonar #2 . . . 96
D.6 M7: Sonic Mast at Zabalegui . . . 97
D.7 MP5: Reference Mast at CENER's Test Site . . . 99

E Atmospheric & Land Cover Conditions **101**
E.1 Wind Regime . . . 101
E.2 Clouds and Fog . . . 103
E.3 Land Cover Change . . . 104

1 Introduction

1.1 NEWA Context

The New European Wind Atlas (NEWA) is a joint effort of research agencies of eight European countries, co-funded under the ERA NET Plus Program. The project is structured around two areas of work: development of dynamical downscaling methodologies and measurement campaigns to validate these methodologies, leading to the creation and publication of a European wind atlas in electronic form.

One of the main objectives of the NEWA project is to carry out large scale field experiments at a high spatial and temporal resolution, and provide a significant upgrade to the experimental databases currently available (Mann et al., 2017).

This document reports technical details on one of the NEWA experiments, where the focus was on testing of the model chain in complex terrain in an area with strong mesoscale variability.

The NEWA Alaiz experiment (ALEX17) was performed at Alaiz, located in Navarre region (Spain), a site consisting of a mountain range of 1000m above sea level (a.s.l.). To the North, along the prevailing wind direction (see Appendix A), measurement equipment are located at a valley 500m lower in altitude. The experimental layout aims to provide a high-quality database to explore wind flow phenomena and derive validation datasets of high-resolution mesoscale-to-microscale models with strong coupling between terrain and thermal stratification.

1.2 Scientific Objectives

The ALEX17 campaign complements other experiments from the NEWA project by instrumenting a site of large dimensions and elevation changes where strong coupling between mesoscale phenomena and microscale site effects are expected ((Sanz Rodrigo et al., 2013); (Badger et al., 2014)). The Alaiz mountain range hosts CENER's Test Site and several commercial wind farms operated by Acciona (figure 1). Hence, the experiment offers the opportunity to characterize the inflow conditions to obtain a better understanding of their impact on wind turbine and wind farm performance.

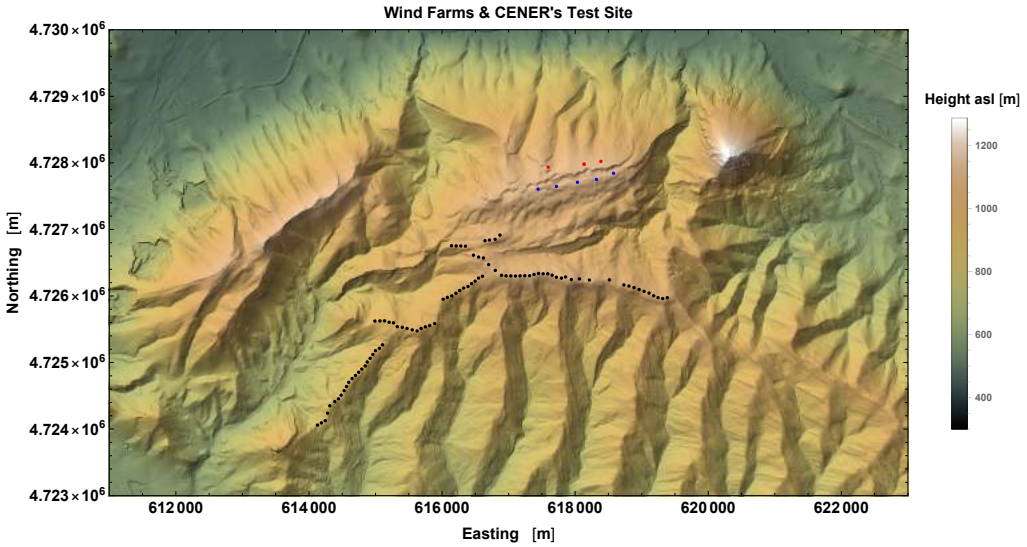

Figure 1. Layout of CENER's Test Turbines (blue dots) and 120m masts (red dots) along with commercial wind farms to the south (black dots).

The prevailing wind directions, shown in figure 67, naturally draws your attention to exploring

the interaction of the atmospheric boundary layer with Alaiz Mountain range, shown in figure 1, as well as the influence of the Tajonar ridge, located 6 km to the North, see section 2.1.1. This interaction will depend on the underlying large-scale forcing of the flow and the microscale flow generated between the valley and the ridge tops due to relative differences in surface temperatures along the diurnal cycle.

The experiment was designed with two objectives in mind:

First of all, ground-based instrumentation was deployed across the valley to characterize surface conditions and boundary-layer flux-profile quantities. It is important to make sure that the campaign spans at least one year to cover the seasonal variability of the wind climate, which can be extended to a multi-year assessment through the measurements at CENER's test site, that go back to 2010, and with the regional network of surface stations maintained by MeteoNavarra from the 90s.

A more detailed assessment aims to peer into micrometeorological flow patterns and flow-topography interaction. Hence, remote sensing instruments were added to to measure the flow field. Scanning lidar systems allow to access measurements over long distances without the logistics overhead that tall masts require. By scanning on vertical planes across the valley, it is possible to visualize the dynamics of large-scale flow patterns generated by the interaction between the ABL and the topography such us waves or flow-separation regions in the lee side of the ridges.

To achieve the planned wind field along a large area synchronized scanning lidar systems, known as WindScanners, were used in pairs and triplets allow the wind vector reconstruction on top of the ridges and across the valley. A position at the valley is defined as reference for wind conditions with a flux-profile mast and a WindRASS, a sodar system to measure the vertical profile of wind speed and potential temperature up to around 400 m. When all the systems are working together a very rich dataset will allow flow model developers to validate their codes and determine which wind conditions are the most impactful on turbine performance.

2 Campaign Setup

2.1 Site Characterization

The Alaiz test site is situated in the centre of the Navarre region. The site topography is characterized by the Cantabrian Mountains and the Pyrenees to the North and the Ebro valley to the south separating the Iberian System to the Southwest. These large topographic features combined by synoptic activity of opposite sign in the Cantabric and Mediterranean Seas create a characteristic channeled wind along the Ebro valley, called ”El Cierzo”. This wind regime is responsible for a significant share of the wind power produced in Spain.

The wind climate of the area has been the subject of numerous studies. For instance, Jiménez et al. (2013) show that the wind speed from a network of surface stations of the Navarre region has a correlation coefficient of 0.76 with the pressure difference between two stations located at each end of the Ebro Valley. This large-scale synoptic wind climate is modulated locally by the orography at Alaiz producing two distinct prevailing wind regimes from the north and from the south.

Figure 2. Picture of Alaiz Mountain from the North Ridge.

2.1.1 Topography

The focus area is about 20x20 km, as shown by the Digital Terrain Model (DTM) on figure 3). The selected site is suitable for the study of mesoscale-to-microscale models with strong coupling between terrain and thermal stratification, where several elements justify further investigation:

1. the interaction between the Alaiz mountain, called South Ridge, and an upstream hill, Tajonar and herein called North Ridge;
2. the wake effects from CENER’s test turbines and Acciona wind farm at the South Ridge;
3. the interactions between terrain and forest canopy.

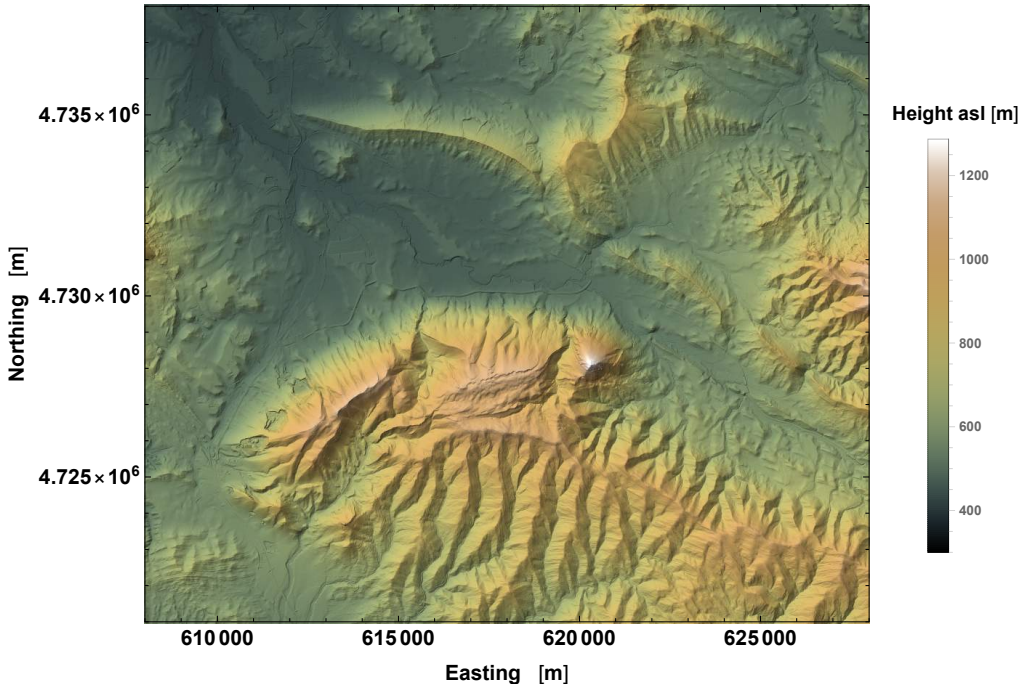

Figure 3. DTM of ALEX17 domain with 2m resolution. Source: TRACASA

.

2.1.2 Land Cover

Figure 4 depicts, with 2-m resolution, the heterogeneous land cover and obstacles present inside the studied domain. The color code represents height values of all these elements above ground level. Hence it is the Digital Terrain Model (DTM) subtracted from the Digital Surface Model (DSM).

Patches of high forested areas can be observed on the Alaiz mountain range, as well as on the north side of the North Ridge (Tajonar). The (DSM-DTM) values show canopy heights that can reach 20 m, therefore indicating a high associated roughness length in some areas. Figure 4 shows that terrain data is available to estimate a leaf area index (LAI) and, hence, derive roughness length (z_0) values for the studied domain.

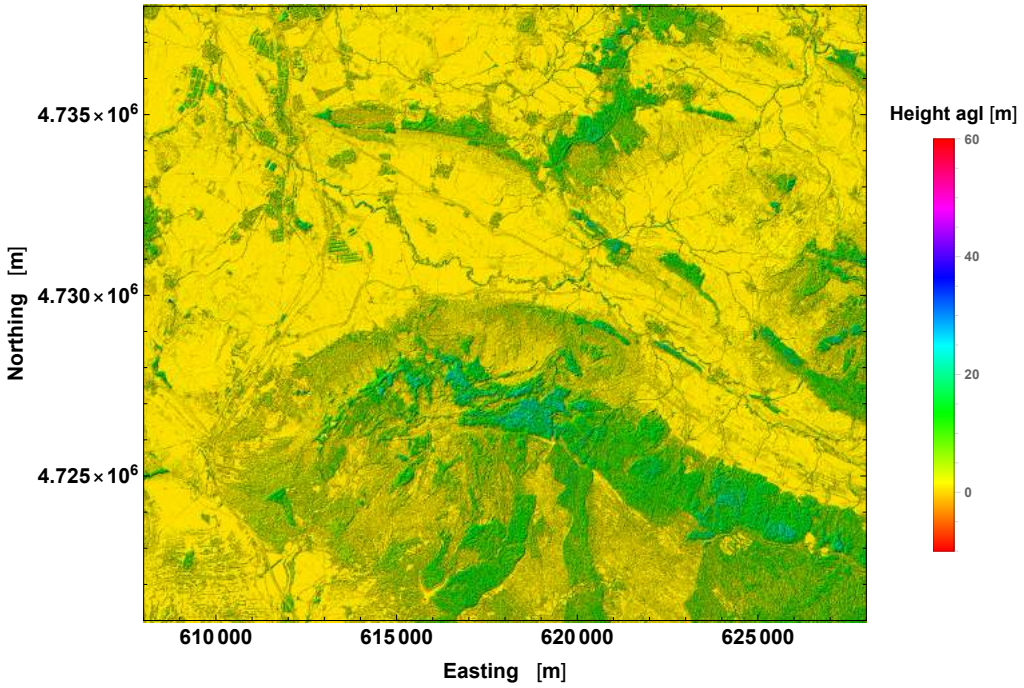

Figure 4. Land cover of ALEX17 domain with 2m resolution. Source: TRACASA

.

2.2 The Experimental Layout

The layout of ALEX17 is designed to obtain high-quality observations across an area previously meteorologically unexplored, shown in figure 3, hence complementing the wind measurements on top of the South Ridge, where turbines operate under a more favorable wind resource (figure 2).

To this end a series of sensors were deployed in the area, namely:

- 3 x Long-range WindScanner (LRWS) systems owned by the NEWA consortium and operated by DTU Wind Energy, see section 2.3;
- 2 x LRWS owned and operated by DTU Wind Energy, see section 2.3;
- 9 x Surface Layer Stations (SLS) owned and operated by UIB, see section 2.5;
- 1 x Surface Energy Budget Station (SEB) owned by the Catalan Met Service and operated by UIB, see section 2.7;
- 1 x 118m flux-profile meteorological mast (called MP5) owned and operated by CENER, see section 2.4.2;
- 1 x WindRASS sodar system owned by the Catalan Met Service and operated by UIB, see section 2.7;
- 1 x Windcube 70 (WLS70) lidar profiler owned and operated by DTU Wind Energy, see section 2.6;
- 22 x surface climatological stations owned and operated by Navarre Meteo Service with data curated by CENER, see section 2.8;
- 6 x meteorological masts, with lattice towers owned and installed by CENER, where:
  - 3 x 80m met masts equipped with GILL sonic anemometers owned and operated by DTU Wind Energy and with Rotronic temperature and humidity sensors owned and operated by CENER, see section 2.4.3;

- 1 x 60m met masts equiped with METEK sonic anemometers owned and operated by DTU Wind Energy and with Rotronic temperature and humidity sensors owned and operated by CENER, see section 2.4.3;
- 2 x 80m met masts equiped with cup anemometers owned and operated by CENER, see section 2.4.4;

It is worth mentioning the provision of met masts and conventional anemometric systems by Iberdrola as an in-kind contribution to the NEWA project.

2.2.1 Measurement Campaign Timeline

Considering all the sensors installed during the ALEX17 experiment, a Gantt chart shows the length of each dataset along with the overlapping period (figure 5) that defines the Intensive Observational Period (IOP), covering a period of 4 months from August-2018 to December-2018.

Apart from the 4-months IOP it is worth noticing that the WindScanner measurement campaign has a total of 9 months, which can be consider a long-term campaign for this kind of instrument. The met masts complete one year of measurements to account for the seasonal variability, along with the other vertical profilers and stations.

The periods shown in figure 5 don't consider data coverage and availability of each instrument and period, which are presented in the specific sections below.

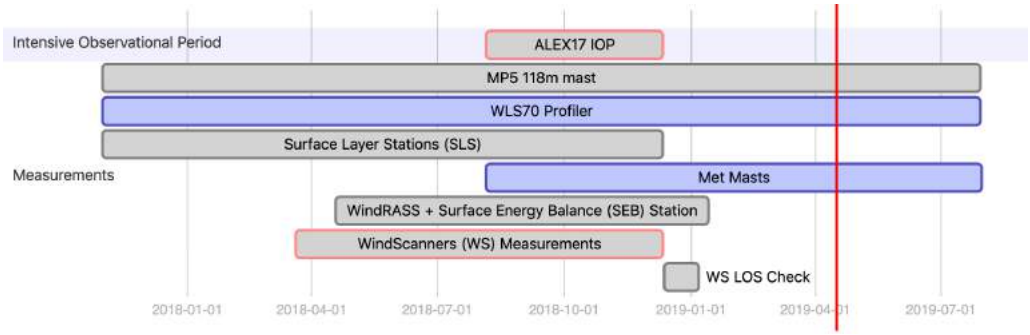

Figure 5. ALEX timeline with measurement periods and IOP. The red line points the end of NEWA.

2.3 Long-Range Wind-Scanners

In order to acquire a wind flow mapping of such a large area, a Long-Range WindScanner system (LRWS) composed by a set of 5 WindScanners (WS) were deployed (Vasiljević et al., 2016). The WS were be positioned inside the valley with the intention of, when combined, characterize the wind flow on top of both ridges (Tajonar Hill and Alaiz mountain), as well as capture flow patterns in the valley and, hence, the interaction between the two main topographic features of the experimental. Vasiljević et al. (2017) presents the best practices to conduct the WS campaign and the main aspects applied in this experiment are summarized below.

2.3.1 WindScanner Positions & Layout

ALEX17 uses a combination of 5 WS, which can be synchronized in space and time within 2 m and 10 ms, respectively (Vasiljevic, 2014). All the scanners are prototypes of the WLS200S commercial scanning lidar with several hardware modification and special DTU WindScanner Client Software (WCS) which allows complex and synchronized trajectories.

Figure 6 shows the position of each scanner together with the measured points with multi-lidar (ML) technique. Aspects worth noting:

- **Shaded areas**: WS pairs can be combined for dual Doppler measurements with at least 35° of beam intersecting angle, in order to maintain the wind reconstruction accuracy below 0.25 $m\,s^{-1}$ (Vasiljević et al., 2017):
  - **WS1 + WS3** for North Ridge (Tajonar Hill);
  - **WS2 + WS4** for South Ridge (Alaiz Mountain);

Based on the viable area, the measurement points of figure 6 were selected and divided in 3 patterns:

1. **Ridge Scans**: Dual-Doppler measurements that follow the top of each ridge at 125 m above ground level forming a 2 km line on each side, measured by the aforementioned combination of WS;
2. **Transect Scan**: ML measurements from WS2, WS3, WS4 and WS5 to form a 6 km line, also at 125 m above ground level, connecting both ridges and passing over WS3 and WS5.
3. **Virtual Masts (VM)**: ML measurements to form a wind profile at the specified positions
   - VM1: Dual-doppler measurement with WS5 and WS1;
   - VM2: ML measurement with WS2, WS4 and WS5.

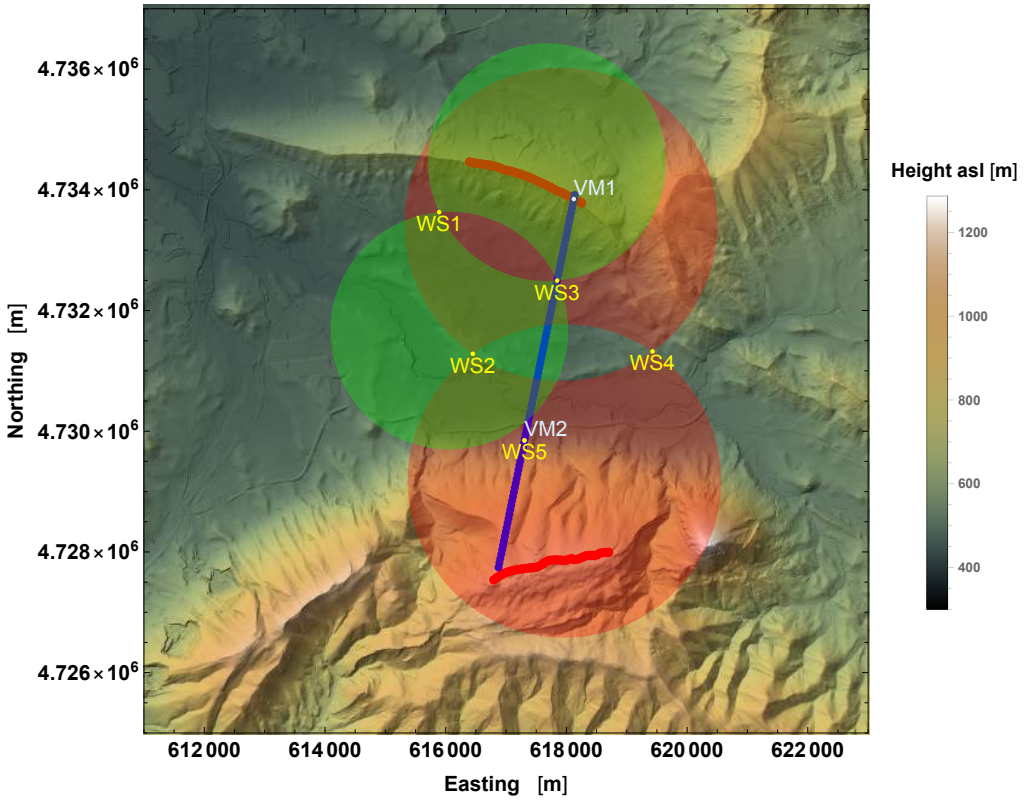

Figure 6. WS layout with shaded areas for at least 35° *intersection on ridge scans.*

This combination results in a 10-km long Z-shaped transect which is a unique feature of this experiment.

After deployment, the final positions of each scanners were acquired during the Leica campaign, described in section 2.4.1, with an accuracy of 1 cm. Table 1 in appendix A shows the XYZ coordinates of each system. Details of the deployment are in appendix C.

2.3.2 Scanning Trajectories

As presented in figure 6, the 3 types of scanning patterns were arranged in 10 min intervals, such that for 1 hour there are two (or more) scenarios scanned. Table 2 presents the order of the scanning trajectories for each WS.

2.3.3 Ridge Scans

The Ridge Scans are built of 40 points on each ridge which follows the maximum elevation of each region. The measurement height is 125 m a.g.l. The scanning trajectory is planned such that the total scan time is within 1 min, in order to have at least 10 samples per 10 min period.

The **lidar parameters** for each ridge scan are presented in Table 3. The scanning trajectories shown in figure 6 yields a sequence of azimuth (θ) and elevation (α) angles for each scanner, shown in figures 7 and 8. The color codes represent the LOS range, which means the lighter colors will have low CNR values and, therefore, low availability during the campaign.

North Ridge: Figure 7 shows the scanning angles for the pair WS1 and WS3.

- It's worth noticing the high elevation angles to perform this scan, which means that the reconstructed wind vector can't be directly related to the horizontal plane, since it depends on α as well as the flow inclination;
- In this ridge the LOS range is represented by hotter colors, which is good and means that high CNR values and availability are expected.

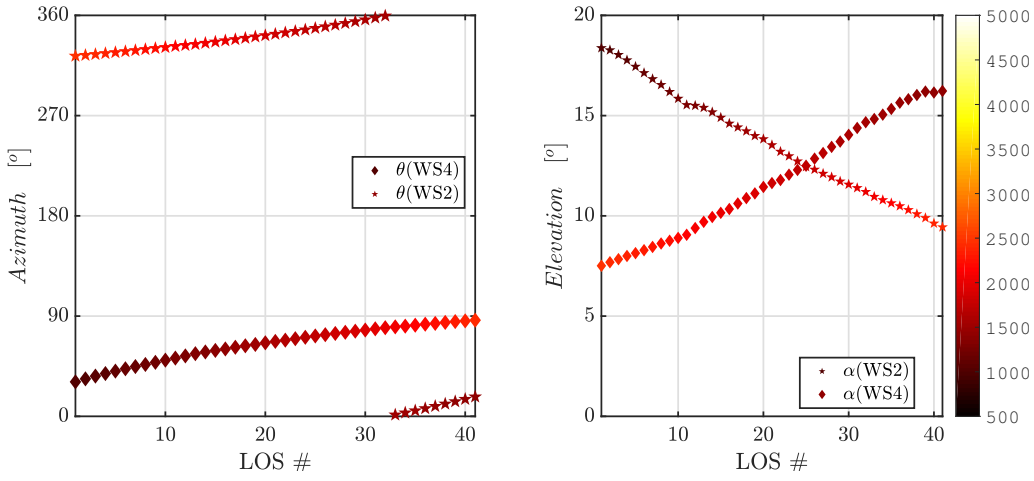

Figure 7. North Ridge: WS1 and WS3 scanning trajectory azimuth (θ) and elevation (α). The color code represents the LOS range (in meters)

South Ridge: Figure 8 shows the scanning angles for the pair WS2 and WS4.

- The elevation angles are lower, as noticed in figure 6, but still not possible to perform an accurate horizontal wind reconstruction;
- It's possible to see that a larger range is required for WSs to reach the measurements along this ridge, which might compromise data availability, hence the challenge of this measurement scenario;
- Specially for WS4 in the beginning of the South Ridge, the LOS range goes higher than 4500 m which will results in really low CNR and availability;
- According to the deployment report, see appendix C.4, WS4 will also loose the last two LOS points due to blockage by the fence next to the system.

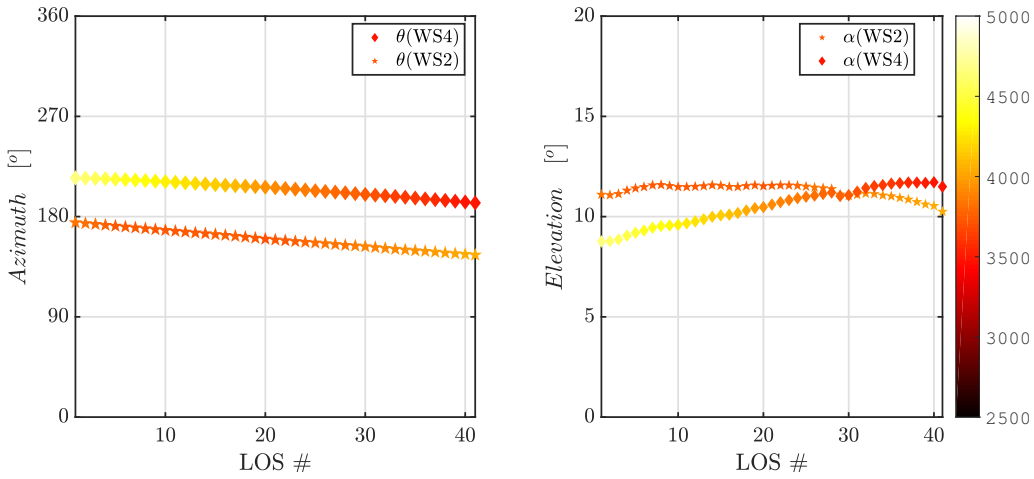

Figure 8. South Ridge: WS2 and WS4 scanning trajectory azimuth (θ) and elevation (α). The color code represents the LOS range (in meters)

2.3.4 Transect Scan

The transect scan is a combination of four WS from the layout. WS2 and WS4 are synchronized to acquire 85 points represented by the blue line in figure 6.

The transect is a straight line which connects WS3 and WS5 positions. All 85 measurements points follow the terrain profile and are located 125m a.g.l. Figure 9 shows the cross-section of the terrain containing the transect, hence also containing WS3 and WS5 positions.

It is possible to observe that the RHI scans from WS3 and WS5 will complement the dual-doppler measurements from the transect pair (WS2 and WS4). Notice that both RHIs cover the ”blind spot” where WS2 and WS4 are facing each other and the dual-doppler reconstruction wouldn’t be possible (Vasiljević et al., 2016).

With the transect scanning plan summarized in figure 9 there is a possibility of the 3D wind vector reconstruction along the entire 6 km transect line. Although WS2 and WS4 are synchronized to measure the transect line, the RHIs are only coordinated to measure in the same 10min slot.

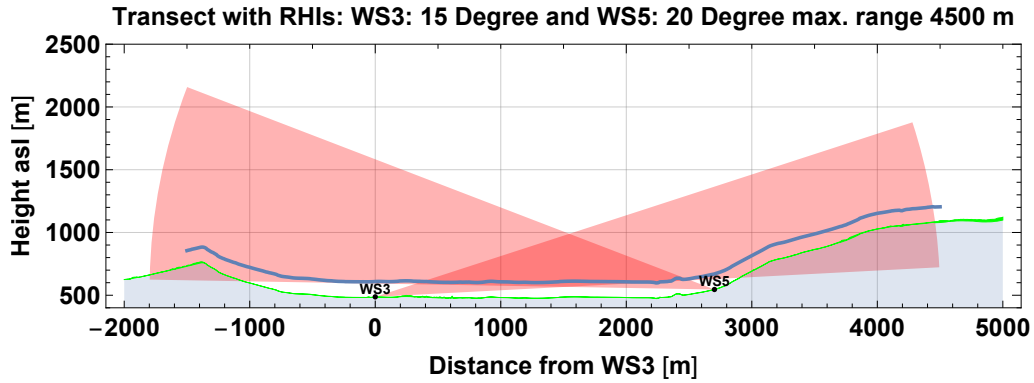

Figure 9. 125 m a.g.l. 6 km transect (WS2+WS4) complemented by RHIs

Transect scan: As in the ridge scans, figure 10 shows the scanning angles for WS2 and WS4 in order to perform the blue path planned on figure 9.

- It is clear that the first LOS starts in the South Ridge and follows the terrain to maintain a

measurement height of 125m a.g.l., with a wide range of elevation angles;

- The South ridge part of the transect has far LOS points for WS, represented by the lighter colors.
- As previously discussed, the scanners face each other with a low elevation angle in the middle of the valley, where more measurements (from the RHIs) or additional assumptions are needed to reconstruct the wind vector.

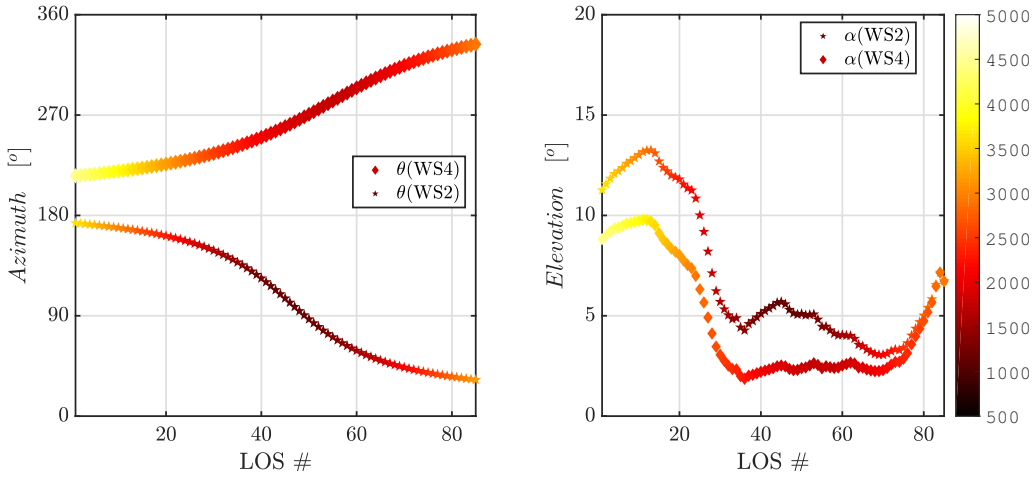

Figure 10. Transect Scan: WS2 and WS4 scanning trajectory azimuth (θ) and elevation (α). The color code represents the LOS range (in meters).

2.3.5 Virtual Masts

The Virtual Masts (VMs) are a scanning strategy where coordinated RHIs and/or LOS measurements are combined to reconstruct the wind vector at several distinct vertical heights. Figure 11 shows an overview of the VM trajectories, where VM1 is measured on the 2nd 10 min interval and VM2 on the 3rd interval (see table 2), such as:

- **VM1**: Dual-doppler measurements on the 2nd 10 min interval. WS5 RHI is combined with a dedicated RHI from WS1, see table 6 for the lidar parameters of each RHI;
- **VM2**: Triple-doppler measurements on the 3rd 10 min interval. Dedicated RHIs from WS2 and WS4 are coordinated between each other along with a LOS from WS5, which points upwards ($\alpha = 90°$). See table 6 for the lidar parameters of each RHI. Figure 12 shows the transect view of both dedicated VM2 RHI scans, which can also be used to analyze flow patterns.

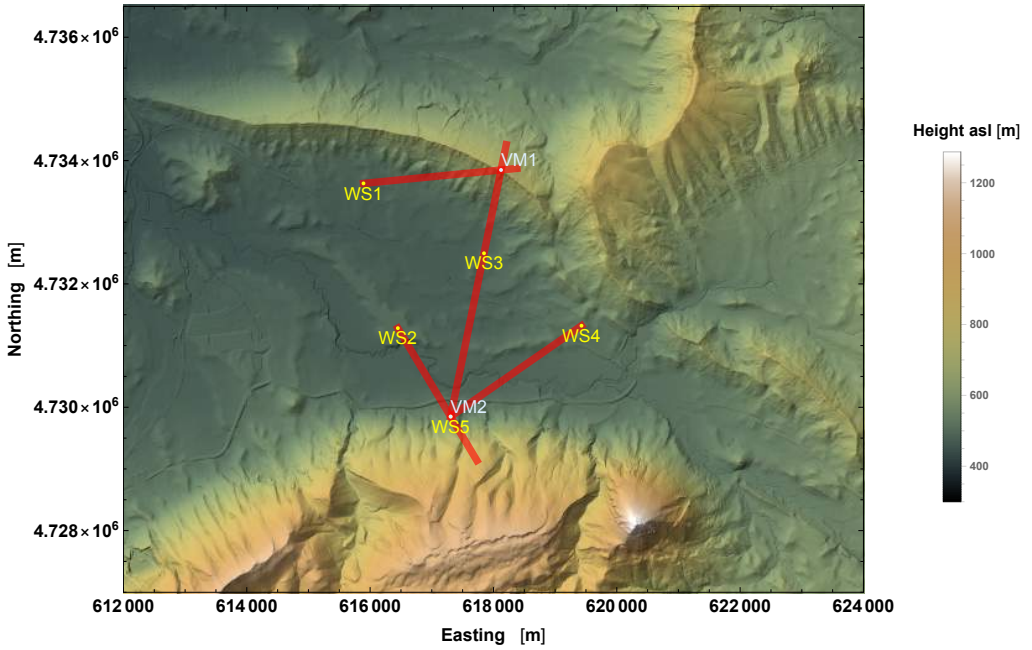

Figure 11. Virtual Masts scanning trajectory

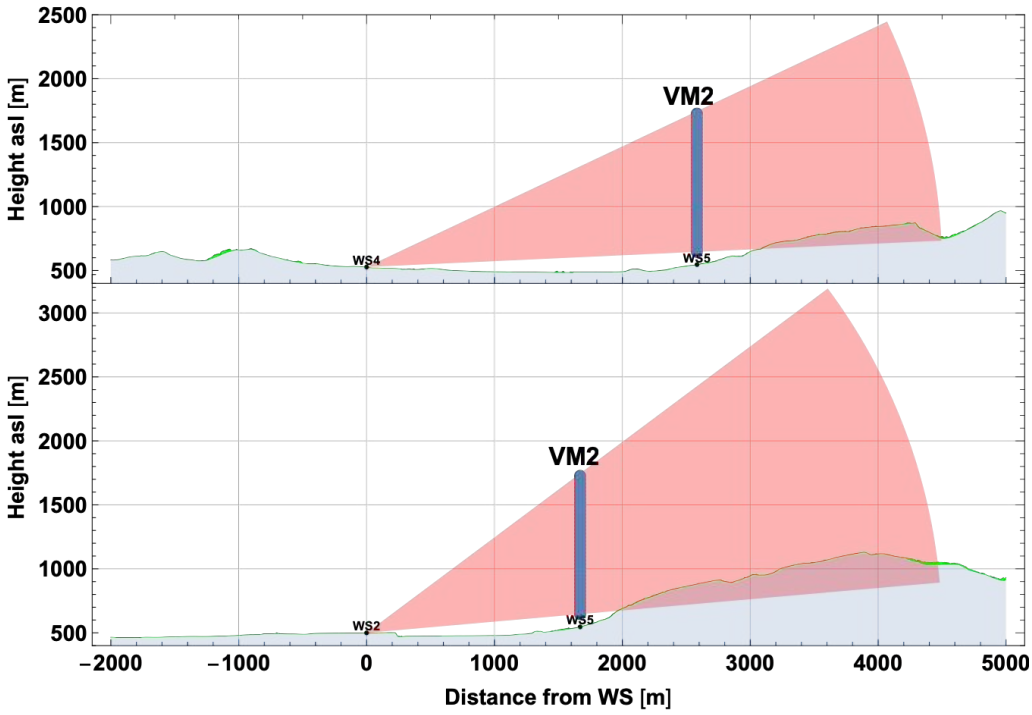

Figure 12. VM2 transect view

2.3.6 Pointing Accuracy & LOS Sanity Check

Once the WindScanner systems are deployed and georeferenced (see table 1) the final scanning trajectories can be uploaded to the systems in the planned order (table 2). However, before executing the trajectories all systems have to be leveled with the ground and oriented to the North. This is a crucial step for good quality measurements, since the range gates in the planned strategies can go up to 4.5 km.

Vasiljević et al. (2016) showed that with the WS system leveled and oriented, the pointing accuracy is within 0.05°(or 1 mrad) at 5 km. However, during the campaign, the system can loose the leveling and, hence, introducing uncertainty in the measurements. Figure 13 shows the static position error in heigth or horizontal distance, caused by a deviation in azimuth (θ) or elevation (α), as a function of the range gate.

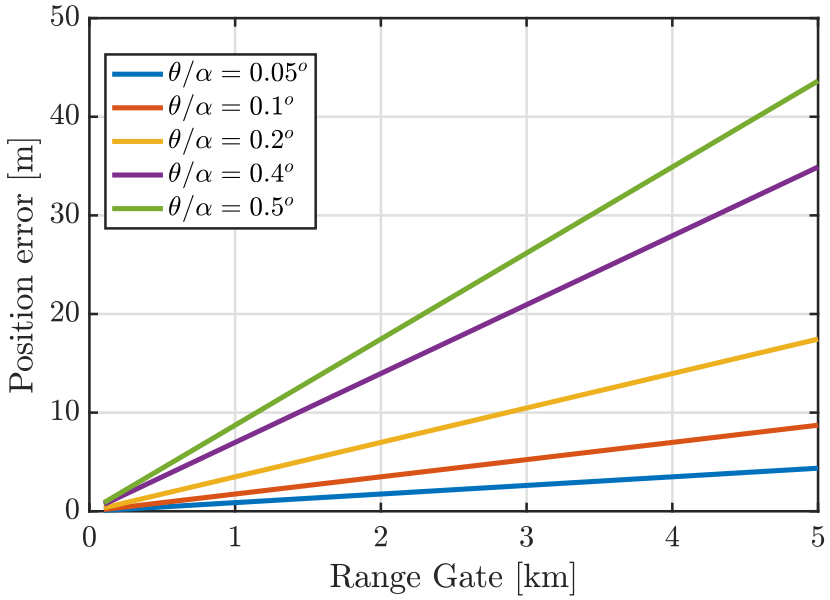

Figure 13. Position error as a function of range gate and azimuth,θ, or elevation, α

The actual pointing error of each system was determined with the CNR mapper procedure (Vasiljević et al., 2017), which consists of performing a series of subsequent PPI scans (TV scan) to map a reference point on which the laser will be almost totally reflected. Therefore, the reference points are hard targets, georeferenced within a centimeter accuracy (see section 2.4.1).

Figure 14 shows an example of the first CNR mapping done for WS3 before any previuos alignment, where the top of a church was used as a hard target. With a first scan it's possible to identify the target and, with this result, narrow the azimuth and elevation angles down to the selected target.

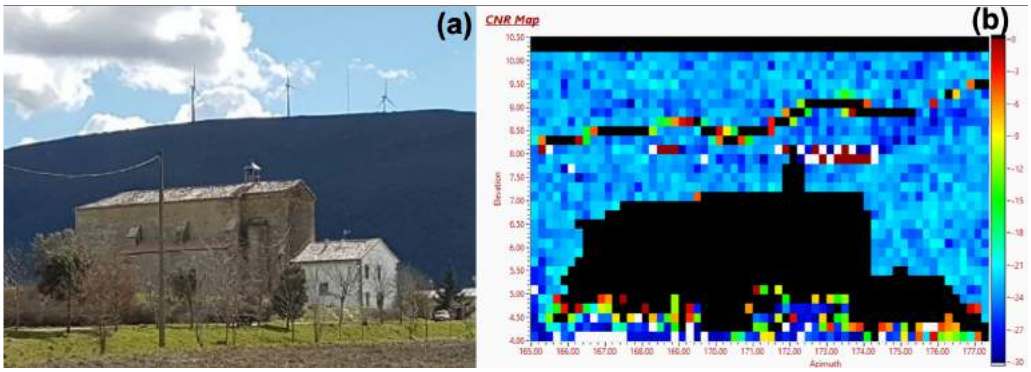

Figure 14. WS3 CNR Mapping before leveling: overview of Church (a) and TV scan result (b)

Figure 15c shows the selected target, which is the ball on top of the church's bell. This point was georeferenced by the Leica system and, with WS3 position, the calculated [Azimuth,Elevation,Range]=[173.968,5.857,209]. The result presented in figure 15d shows a pointing error of 3.34° in azimuth and 0.2° in elevation, hence WS3 was leveled and aligned accordingly.

In the beginning of the experiment, after alignment, all systems where within 1 mrad or 0.06° in azimuth and elevation, apart from the elevation of WS1 that was 0.22°. According to figure 13 this outlier will correspond to a pointing error of around 10 m at 3 km.

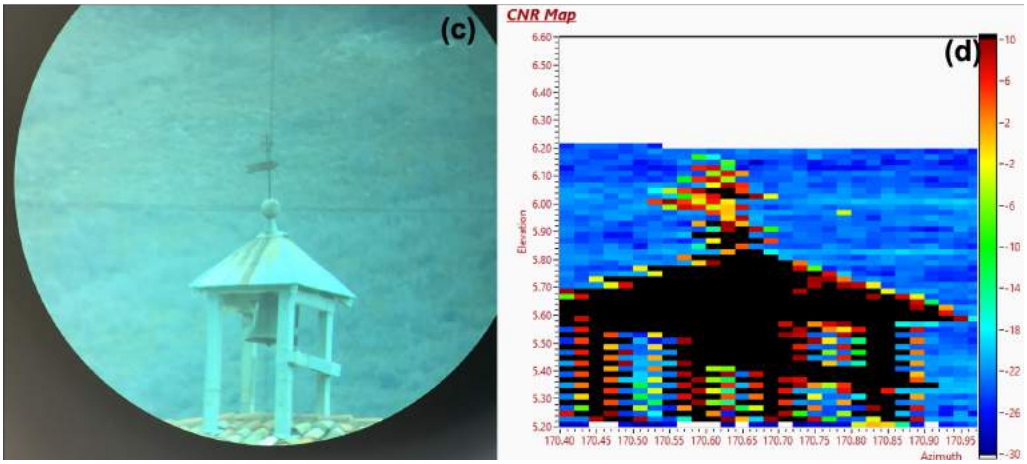

Figure 15. WS3 CNR Mapping before leveling: zoom at hard target (c) and mapping result (d)

Table 4 shows the pointing error (in degrees) for each system during the campaign. All WS systems were checked for pointing accuracy more than once during the campaign, in order to spot any misalignment and ensure a pointing error within a 0.2° maximum limit. It is possible to see that WS3 lost it's leveling between May and July, with this misalignment being corrected on 24/july/2018 by applying a new homing offset.

2.4 Met Masts

ALEX17 makes use of existing instrumentation and data management infrastructure of CENER's test site combined with six 80-meter-high masts installed in the valley for this purpose.

The test site has four 118m tall met masts situated in front of the turbine sites to the north: MP1, MP3, MP5 and MP6. See (figure 16).

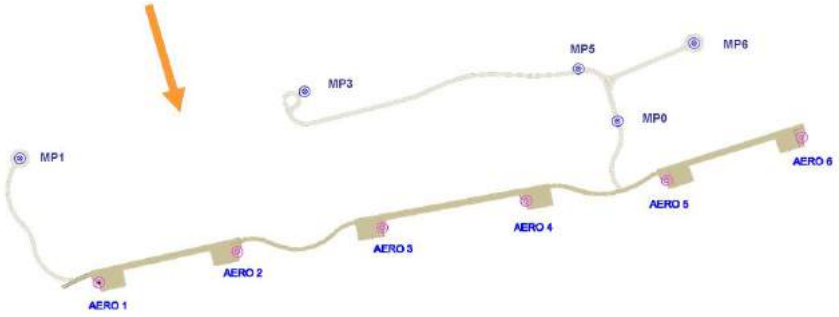

Figure 16. CENER-Alaiz Wind Turbine Test Site.

The standard instrumentation of the masts complies with the IEC standard for wind power performance tests.

For the measurement campaign, the MP5 mast was used as a reference.

The additional six masts, and the equipment installed in two of them, Mast 1 and Mast 5, have been donated by Iberdrola for this experiment.

Figure 17 shows the location of the six masts in the valley and the MP5 mast in the Alaiz test site.

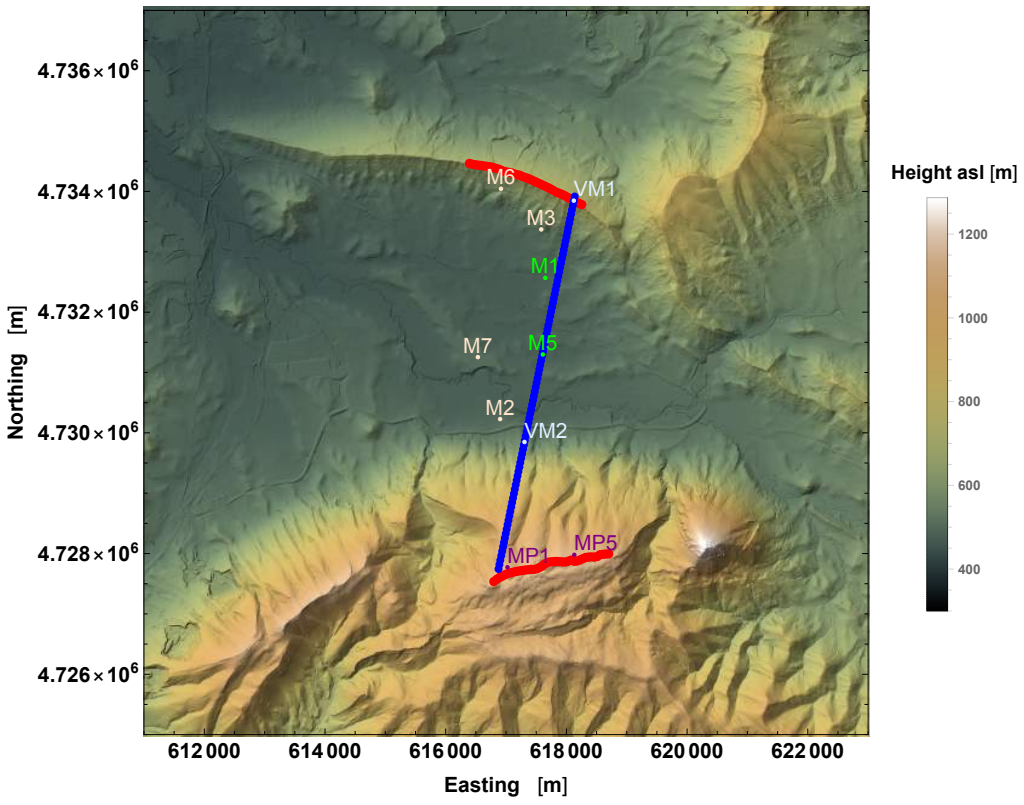

Figure 17. Met masts and Virtual Masts (VM) positions in relation to Z-transect

2.4.1 Georeference (Leica) survey

For all meteorological masts in ALEX17 a laser scan survey was conducted in order to determine with precision each sensor position in UTM Zone 30 coordinates, WGS84 system. A Leica TotalStation MS50 was used to conduct the survey, along with the Leica GSNN GS14 antenna to acquire the GPS signal. The procedure followed the best practices also conducted in previous experiments (Vasiljević et al., 2017):

1. More than 20 satellites were available to determine the multistation position. The local coordinate system was corrected in order to record all positions in UTM coordinates.
2. With a DGPS-RTK correction data the reported accuracy of all positions recorded with this system were **within 1 cm** in all directions (Easting, Northing and height);
3. All WS systems had their scanning head XYZ coordinates measured, see table 1, as well as all met mast's foundation, see tables 8 and 9;
4. Reference points were also taken at each sensor and the respective boom, see figures 18 and 19.
    - P3, P4 for the Gill sonics and P5,P6 for METEK sonics can provide the boom orientation and tilt;
    - P1, P2 show the instrument tilt with respect to the boom, expected to be within 1°;
    - The met mast base and top provide the tower tilt, also expected to be within 1°.
5. Both sonic sensors were installed such that the North indicator is aligned with the boom, pointing towards the tower.
    - GILL SONICS (M2, M3 AND M7) COORDINATES: The $+U$ axis is aligned with the N indicator. The $+V$ direction is 90 deg c-c-wise from the N indicator.
    - METEK SONICS (M6 AND MP5) COORDINATES: The +U axis is aligned with the N arrow. The +V direction is 90 deg c-wise (yes, clockwise) from the N indicator[1].

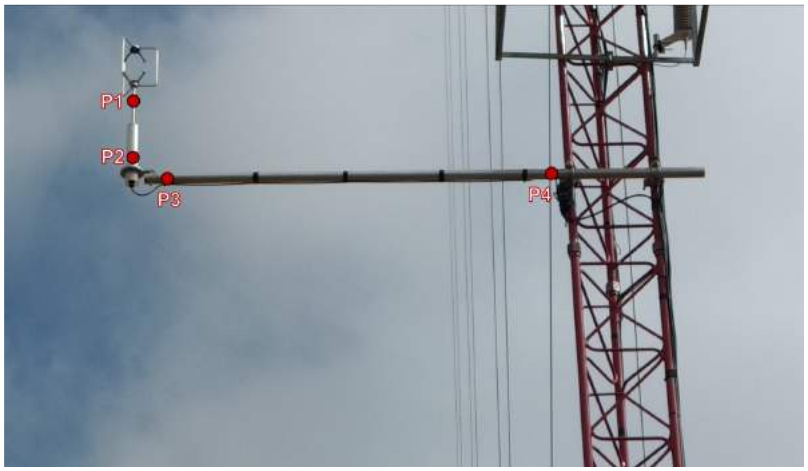

Figure 18. Measured georeferenced points for M2, M3 and M7 with Gill sonics (south view, boom towards the west)

[1] NCAR ISFS Documentation: https://www.eol.ucar.edu/content/isfs-documentation

Figure 19. Measured georeferenced points for M6 and MP5 with METEK sonics (north view, boom towards the west)

The boom orientation for the towers is shown in figure 20. A summary of the boom orientation and tilt angles is shown in table 7.

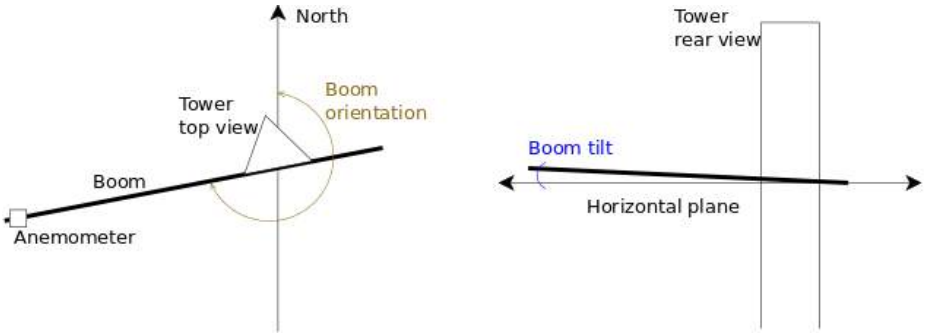

Figure 20. Boom orientation and tilt angles.

In order to have a clear reference point for ALEX17 WS measurements, at the end of the campaign all WS systems the CNR mapping was repeated towards M7 and all systems were re-leveled. Then a LOS scenario was fixed for one month, were all systems had wind and spectra (*.dsp files) stored while staring to the 80m 3D sonic of M7.

- **LOS Sanity Check**: All WS systems staring to a single reference point (M7@80m) for 1 month (Dec/18-Jan/19).

2.4.2 MP5

The mast MP5 (N 42.695º, W 1.558º) is 118 m height lattice permanent mast with nine measurement levels oriented to 360º and 180º, figure 21 shows a picture of MP5 mast. Wind speed and wind direction are measured at five levels (118, 102, 90, 78 and 40 m) with wind vanes and cup anemometers, and with sonic anemometers at 118, 78 and 40 meters. Temperature and relative humidity are measured at five levels (113, 97, 81, 38 and 2 m).

Figure 21. MP5 120m mast north of a wind turbine at the test site.

The data acquisition system consist on a real-time controller CompactRIO from National Instruments with 128 MB DRAM and 2 GB storage embedded in a chassis in connection with 8 modules of digital and analogue data acquisition. All connected to an Ethernet network.

The rate sample is 5 Hz for cup anemometers (Vector A100LK) and 20 Hz for sonic anemometers (METEK USA-1), wind vanes, pressure, humidity and temperature sensors.

All the cup anemometers have been calibrated at Ignacio da Riva Institute, centre belonging to MEASNET (Measuring Network of Wind Energy Institutes) and with ENAC accreditation according to UNE-EN ISO/IEC 17025. All calibration certificates are part of the metadata, i.e. provided along with the dataset.

The sonic anemometers have been calibrated in Deutsche Wind Guard Institute wind tunnel, IECRE and MEASNET approved test laboratory.

Wind vanes (Thies Compact) have not undergone specific calibration.

Pressure sensor (Vaisala PTB100A) and temperature and humidity sensors (Ammonit P6312) have been calibrated at "Alpe metrología industrial" with ENAC accreditation according to UNE-EN ISO/IEC 17025.

The spatial location of the MP5 tower and its sensors have been measured with the Leica GPS system. The tilt angles of the different components are summarized in table 7.

2.4.3 Sonic masts

The four masts (see table 8 for the coordinates of the masts) with sonic anemometers are lattice guyed masts.

Three of them Mast 2 (M2), Mast 3 (M3) and Mast 7 (M7) are 80 m masts with five Gill WindMaster PRO 3D sonic anemometers installed at 80, 60, 40, 20 and 10 meters oriented to 270º; and four Rotronic HM4 temperature and humidity sensors installed at 80, 40, 10 and 2 meters height oriented to 90º.

Mast 6 (M6) is a 60 m lattice mast with four METEK USA-1 3D sonic anemometers installed at 60, 40, 20 and 10 meters orientated to 270º; and four temperature and humidity sensors installed at 60, 40, 10 and 2 meters height oriented 90º.

Figure 22 shows the M3, one of the ”sonic mast” installed.

Figure 22. Picture of one of the sonic masts, M3.

The data acquisition system is centered at M2, with a DTU DAQWin data acquisition and transmission system. Each mast has a transmission antenna pointed to M2, which receives, stores and upload data from all masts to a database. For the temperature sensors the data acquisition system installed in each mast is a Campbell Scientific/CR1000.

The rate sample is 18 Hz for sonic anemometers and 1 Hz for temperature and humidity sensor (Rotronic, HygroMet4). All the temperature sensors have been calibrated at ”Alpe metrología industrial” with ENAC accreditation according to UNE-EN ISO/IEC 17025.

2.4.4 Conventional masts

The two masts (see in table 9 the coordinates of the masts) with conventional instrumentation are lattice guyed masts.

Both of them are 80 m masts with five cup anemometers installed at 80, 60, 40, 20 and 10 meters orientated to 270º; three wind vanes at 76, 60 and 20 meters oriented 90º, two vertical anemometers oriented 90º, two temperature and humidity sensors installed at 76 and 2 meters height oriented 180º and pressure sensor installed a 2 meters in and arm oriented 90º.

Figure 23 shows the picture of M1 with ”conventional” configuration.

The data acquisition system is a Campbell Scientific/CR1000 data logger. The rate sample is 1 Hz for all the sensors.

All the cup anemometers (Thies model 4.3350.00.000) have been calibrated at Ignacio da Riva Institute, centre belonging to MEASNET (Measuring Network of Wind Energy Institutes) and with ENAC accreditation according to UNE-EN ISO/IEC 17025.

Wind vanes (Thies Model 4.3121.33.000), vertical anemometers (Young model27106-T) and pressure sensor (Ammonit model AB 60) have not specific calibration.

Temperature and humidity sensors (Galtec model KPK 1/6) have been calibrated at ”Alpe metrología industrial” with ENAC accreditation according to UNE-EN ISO/IEC 17025.

Figure 23. Picture of one of the conventional masts, M1.

2.5 Surface-layer stations, SLS

The experimental layout deployed by the University of the Balearic Islands (UIB) includes nine surface-layer stations (SLS) distributed over the valley bottom and mountain slopes that were in operation for over a year (figure 24). These 2-m high stations provide both atmospheric and soil measurements to characterize their variability along the valley. Since they incorporate measurements of wind and two levels for air temperature and humidity, it is possible to estimate the turbulent fluxes through the flux-gradient approach (Moene and Dam, 2014) and the atmospheric stability within the surface layer.

Several SLS were located to cover the features of the valley bottom along its main axis (SLS01, SLS02, SLS08), with one observed point at the far eastern entrance (SLS03). Additional stations were distributed over the mountain slopes, with SLS09 and SLS07 on the northern side (Tajonar) and SLS05, SLS04 and SLS06 on the southern slope (Alaiz). These last three stations form a line from near the top of the Alaiz ridge (SLS05 is located few meters downslope from tower MP3), following the terrain slope down to the foothills. Some of the nine stations complement the information recorded at upper levels from the 80-m masts (i.e., SLS08 shares location with Mast05). The SLS01 site in Zabalegui holds additional instrumentation like a RASS-Sodar profiler and a complete surface energy budget (SEB) station (figure 26, see more details in section 2.7), an 80-m tower (Mast07) and one WindScanner. Such concentration of instrumentation at the central part of the valley makes this location a special site in the ALEX17 campaign. Geographical coordinates are described in table 10.

Most of the SLS stations have been designed and setup by members of the Meteorology Group at the Physics Department of the UIB (figure 25, left) and have been used in previous studies (Simó et al., 2019). Their structure consists on a tripod made of PVC cylinders, holding a two-dimensional sonic anemometer (Windsonic, Gill Instruments) at 2 m above ground. Three temperature and humidity sensors (HYT271, Innovative Sensor Tech.) are installed at 2.0, 1.0 and 0.2 m above ground level (agl), although the hygrothermometer in the middle was not maintained until the end of the ALEX17 campaign. These sensors are protected with a self-made radiation shield consisting in a double PVC cylinder covered with aluminium foil and holes at the bottom to favour the air circulation inside the shelter. This shield has been successfully tested previously against the standard multi-plate gill-type screen broadly used in the meteorology field.

The comparison of the HYT temperature and humidity measurements against a standard hygrothermometer (HC2S3, Rotronic AG) show a good performance for both outdoor and indoor

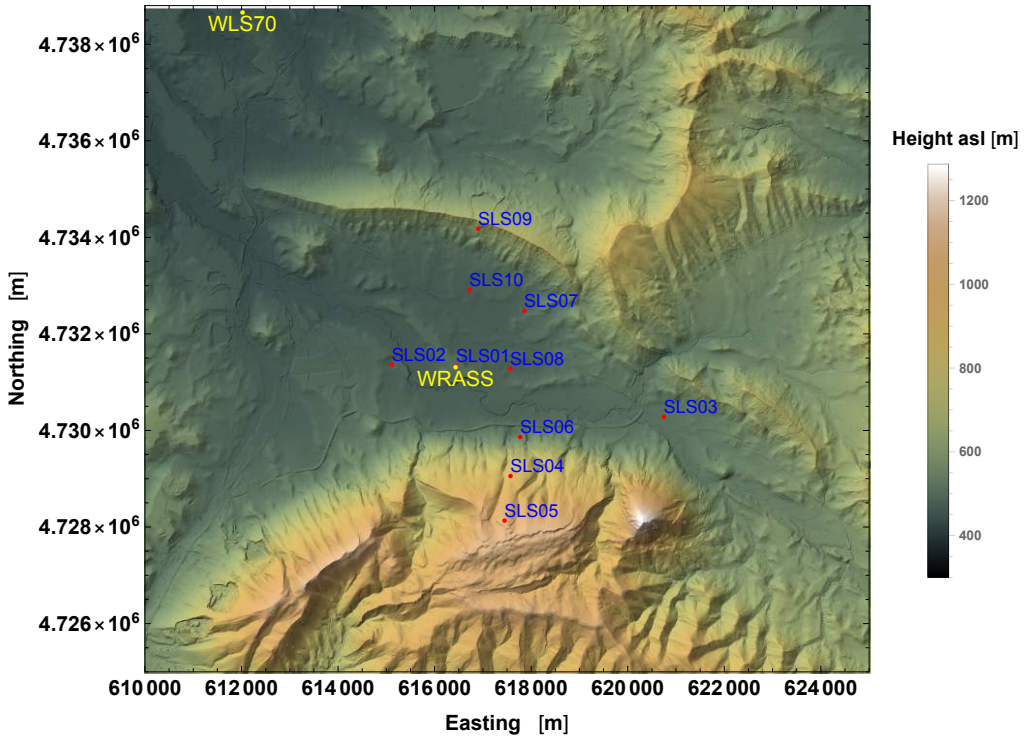

Figure 24. Terrain and surface-layer stations (SLS) of the ALEX17 campaign. Locations for the WindRASS and WLS70 are also indicated. The surface energy budget (SEB) station was installed at the same site as WindRASS and SLS01.

.

conditions. The outdoor test was performed during several months at the UIB campus, obtaining a RMSE and correlation coefficient of 0.3 °C and 0.997, respectively, for temperature records and 0.2 g kg^{-1} and 0.982 in the humidity case.

The buried instrumentation consists in a soil water content reflectometer (CS650/655, Campbell Sci.) located at 5 cm below the surface that monitors the volumetric water content over a volume at the upper part of the soil. This sensor includes a thermistor that provides the soil temperature at the specified depth. A heat flux plate (HFP01, Hukseflux) provides the soil heat flux at 8 cm deep. This measurement can be consistently extrapolated to the surface level after calculating the soil storage through the soil temperature and water recorded at the upper levels.

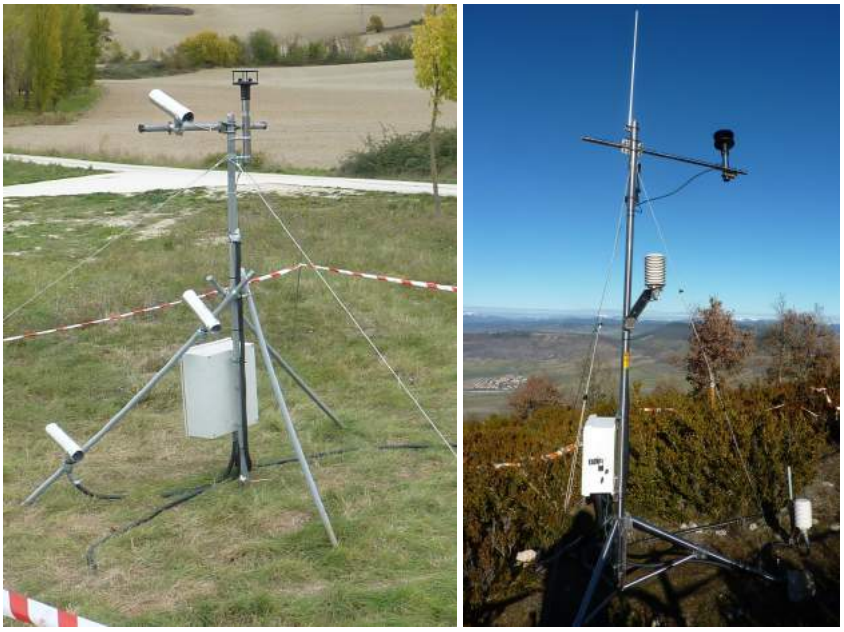

Figure 25. The design of all SLS stations is like SLS07 (left), except station SLS04 (right) which is assembled with commercial components only.

.

The data acquisition system has been developed locally using Arduino micro-controllers and self-programmed boards and the raw data were stored in a SD card. Each pole is powered by individual solar panels, making them fully autonomous. To optimize the energy use and data storage, sensors were interrogated once every 5 minutes. In the case of the windsonic, the interrogation was performed over 30 seconds at 1 Hz sampling rate; while for the HYT sensors, 20 measurements were acquired over one minute (i.e. one measure every 3 seconds). At the end, each station provides raw files with time series of 5 minutes that include samples of the soil data (temperature, humidity and heat flux), and one-minute averages of air temperature and humidity plus 30-second averages of wind speed and direction.

The remote location of SLS04, half-way between the Alaiz mountain ridge and its foothills, implied a different configuration with a more robust design (figure 25, right). Therefore, it was assembled on a 3-m high, stainless-steel tripod with commercial components only. The main differences compared to the rest of stations are the type of hygrothermometers (CS215, Campbell Sci.), their housing (Gill-type radiation shield) and the datalogging system (CR300, Campbell Sci.). The latter allowed for a sampling rate between 1 and 4 seconds, storing raw data files with time series of one-minute averages.

Table 11 describes all settings related to the mounting of the instrumentation, particularly the specific heights and depths for each sensor at the different SLS stations. The 2-D sonic anemometer was installed so that the wind was measured parallel to the ground. The surface was assumed to be horizontal except for those stations at the sloping sites (SLS04, 05, 06, 09). For these latter cases, the anemometers were oriented over a slope surface averaged by eye over a scale of tens of meters. The tilt angles are also included in table 11.

2.6 WLS70 Profiler

In order to have a reference wind profile at the North, a lidar profiler was installed in the edge of the domain, see figure 24. The profiler is called WLS70 after it's model Windcube70 from Vaisala LEOSPHERE. CENER had previous experience operating remote sensing equipment including lidar vertical profilers for wind energy research projects in complex terrain conditions at the Alaiz test site (Borbón, 2015).

The system was commissioned and started measuring on **31-October-2017**, launching the ALEX17 campaign. WLS70 continued measuring after the IOP finished to go cover the whole comapign until July-2019. Deployment details with pictures are presented in Appendix C.6.

The WLS70 is located within the city of Pamplona/Spain, inside the an University (UPNA) campus. The UTM Zone 30 coordinates are [Easting, Northing]= $[612021.99, 4738658.56]m$. This position, on the edge of the experiment domain (figure 24), was chosen after a sensitivity analysis were the uncertainty due to orography on the meso-scale models is low.

The main lidar parameters of the system are summarized in table 12.

2.7 WindRASS and Surface Energy Budget station

The Zabalegui site (where station SLS01 and M7 were installed, Fig. 26) hold a RASS-Sodar and a surface energy balance station from April 2018 to January 2019 (see their geographical coordinates in table 13). This equipment was rented to the Catalan Meteorological Service (MeteoCat) and has been operated in previous field campaigns (Cuxart et al., 2012, 2015).

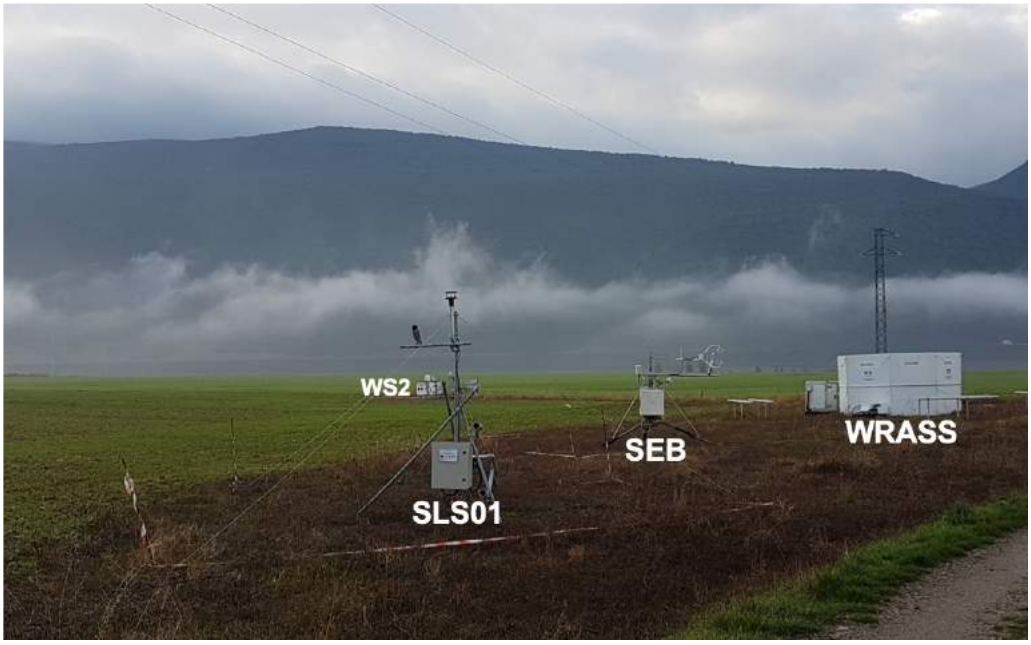

Figure 26. Overview of WRASS and SEB at the Zabalegui site with the Alaiz mountain range to the back. At the same site there are M7, WS2 and SLS01. Picture taken on July 2018.

.

2.7.1 Surface energy budget station

This station contains the needed instrumentation to estimate the 4 main terms of the surface energy balance, including a 4-component net radiometer (CNR1, Kipp&Zonen), and one eddy covariance system composed of an open-path gas analyser (LI7500, LI-COR Inc.), a sonic anemometer (CSAT3, Campbell Sci.) and a thermo-hygrometer (HMP45C, Vaisala). The ground heat flux is measured at four different locations with heat flux plates (HFP01SC, Hukseflux), which can be consistently extrapolated to the surface level after calculating the soil storage through two averaging soil temperature probes (TCAV, Campbell Sci.) and two soil water content reflectometers (CS616, Campbell Sci.). Sonic anemometer was installed considering that the underlying ground surface was horizontal, with the positive x-axis of the sonic coordinate system pointing into 100° (see figure 39). Details on the heights and depths for each sensor and corresponding sampling rates are described in table 14.

The data sampling has a frequency of 10 Hz and the final SEB fluxes are calculated for a time interval of 10 minutes. This station provides both files of raw and calculated flux data to the database.

2.7.2 WindRASS

A RASS-Sodar (WindRASS, Scintec) was installed to monitor the vertical profiles of wind and virtual temperature in the first few hundreds of meters at the centre of the valley. The WindRASS combines acoustic and electromagnetic radio waves to infer a profile of the sound speed and, from there, extract the wind and virtual temperature. This characteristic makes WindRASS different from conventional RASS, for which radio-acoustic sounding is used for temperature measurements only (Cuxart et al., 2012).

During ALEX17, the device has been configured to work at a vertical resolution of 10 m, with a range from 40 to 400 m, to produce vertical profiles every 15 min. The range of operation for temperature profiles is from $-50\,^{\circ}$C to $60\,^{\circ}$C with a nominal accuracy of $0.2\,^{\circ}$C, respectively, and for the wind speed 0-12 and $0.5\,\mathrm{m\,s^{-1}}$, with an estimated accuracy in wind direction of 15°. The operation of WindRASS is possible in the absence of atmospheric turbulence (therefore on clear calm nights) and it is apt for working in foggy or rainy conditions.

The obtained profiles usually lose statistical significance as the height increases because more echoes get lost from the upper part of the height range. This effect is specially important with wind speeds over 10 m $\mathrm{s^{-1}}$ and it is the main reason for not generating data at the upper part of the profiles.

The WindRASS provides daily files with the processed data as described above (*mnd* files). Original raw data are also included in binary files, giving the possibility to post-process them and generate new files with a different configuration (i.e. changing time averaging periods, vertical resolution or variable outputs). The post-process can be performed through the Scintec Sodar Operation software APRun (for more details, refer to the *Scintec Flat Array Sodar – Software Manual APRun*).

2.8 MeteoNavarra Stations

Navarre is located in the north of the Iberian Peninsula, where the orography of the region shows a variety of rich features broadly limited by two large mountain systems: the Iberic System in the South of Navarre and the Pyrenees in the North, which merge westward with the last foothills of the Cantabrian Mountains. Between them, the Ebro Valley crosses the region from northwest to southwest toward the Mediterranean. A closer look at the Navarre reveals a complex array of smaller mountain systems and valleys.

As a complementary dataset, 22 met stations from the meteorological network of Navarre (http://meteo.navarra.es/) are included as part of the experimental database. Figure 27 shows their geographical distribution.

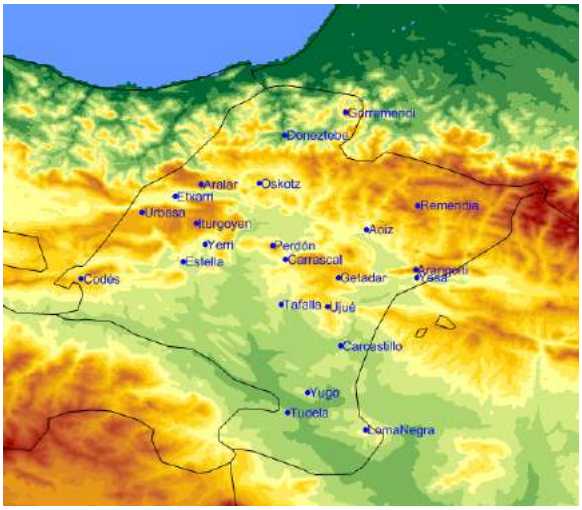

Figure 27. Synoptic stations on the elevation map over Navarre and surroundings.

The network of surface stations covers the ALEX17 period, from 1 of January 2002 to 31 December 2018, but most of them extend back to the 90s. Each station provides 10-min averaged wind speed and direction at 10 m a.g.l. Therefore, the stations provide long-term reference conditions for the regional wind climate. The UTM coordinates for all available stations and data availability are summarized in Appendix A, table 15.

3 Data Management & Availability

The ALEX17 dataset is compiled in one data collection DOI. The metadata card (link below) connects all individual datasets as well as papers, presentations and further results related to the experiment (including this report):

ALEX17 Dataset

doi.org/10.11583/DTU.c.4508597

3.1 Terrain data

For the terrain elevation and land cover, a Digital Elevation Model (DEM) for airbone lidar scans with 2m resolution of the entire domain is provided from the company TRACASA. All the domain maps presented on this report were plotted using this DEM.

The DEM contains a Digital Terrain Model (DTM), representing the last (ground) back scattered signal, as well as a Digital Surface Model (DSM) with the first (tree height/obstacles) signals form the laser scans. With this notation we define:

$$DEM = DTM + DSM \tag{1}$$

Within the DSM there is also other information regarding intermediate signals that can provide the LAI and PAD for the domain. The DSM post-processing gives useful products for modelling and wind energy purposes, such as maps for roughness lenght (z_o), vegetation leaf area index (LAI), vegetation density and displacement height.

The DEM will be available in the original 2 m resolution, as well as a smoothest 10 m resolution (for modelling purposes) in GeoTIFF, XYZ or grid files.

3.2 WindScanner Data

Figure 28 shows all important WindScanner Logbook entries during the campaign.

The Windscanner data is divided in files for each 10 min period, relating to a specific scanning trajectory according to table 2. The raw ASCII files retrieved from the scanners are stored in folders divided by 10 min periods, i.e. one for each scenario.

The folder naming scheme is according to each scenario, so that every 10 min a new folder is created following this naming `WS#/YYYYMMDDHHMMSS_XXXX`, where # is replaced by the scanner number and $XXXX$ by the scenario name and number as shows in table 16.

Other scenario names, such as PPIs, represent periods where the systems were being realigned with CNR mapping. Hence, in the dataset structure each 1 h period has to have 6 folders. In case a scanner fails during this period, a new folder is created and the scanning trajectory isn't complete.

For all the complete 10 min scenarios a CNR filter has applied and a NetCDF file created according to the e-WindLidar project proposed standards for FAIR lidar data (Vasiljevic et al., 2018).

The WindScanner availability is preliminary assessed considering only full 10 min scenario folders that were created by the systems. Therefore, what the results show is actually an operational fraction time, since the folder names only garantee that each scanner was working during the complete scanning trajectory.

Results for the operational fraction time are summarized in table 17. The period considered for the overall availability was the IOP from **09-May-2018 until 11-Dec-2018**. Before this period the systems were being calibrated and aligned with hard targets. After this period all the systems were performing a sanity check, staring continuously to the 80 m 3D sonic in M7.

All the Windscanners used in this experiment are Vaisala LEOSPHERE prototypes of the further WLS200S commercial model and were running almost nonstop for more than 4 years prior to

2018-04-16	Transect scan was first tested (v1).
2018-05-07	(15h UTC): WS3 being tested for pointing accuracy (PPI scenarios).
2018-05-08	(16h UTC): All scenarios launched and WS3 changed to v2. RHI angles were adapted, compare inifiles to see the changes.
2018-05-23	(08:40h UTC): New transect scan started. The old one was connected with the planned WS5 position ($\approx 100m$ to the east).
2018-07-17	(16h UTC): All systems stopped for remapping.
2018-08-02	(12h UTC): All systems were releveled, but only WS3 had a considerable offset.
2018-08-06	(7h UTC): Homing offset applied into PMAC, from now onwards it's not expected the systems to loose their home position.
2018-08-13	All systems are running in one Master PC with real-time sync.
2018-09-18	Sytems running in two Masters with real-time sync: [WS1,WS3,WS5] and [WS2,WS4].
2018-10-26	From 26-10-2018 to 09-11-2018: All systems were running in stand-alone mode (only client software, hence no real-time sync).
2018-11-08	A/C units are removed and humidity come back to normal levels.
2018-11-10	All systems back to Master + sync.

Figure 28. WindScanners Logbook

this campaign. Therefore, a lower laser power output and more failures than normal were already expected, as expressed in table 17.

Even with the aforementioned limitations, some challenges in multi-lidar measurements could be improved and ALEX17 presented higher availability than previous experiments (Mann et al., 2018).

It is possible to see that all the scanners that had synchronized trajectories (WS1+WS3 and WS2+WS4) presented lower data availability, $< 70\%$, proving the challenge of maintaining all the systems within 10 ms from each other. Hence, WS5 which was performing RHI and LOS scenarios had a better performance. WS2 had the lower availability due to a failure in the FPGA module.

When looking to the operational time series along the IOP a clearer picture can be drawn from each scanner. A description of the coincidence operational periods is shown in figure 29.

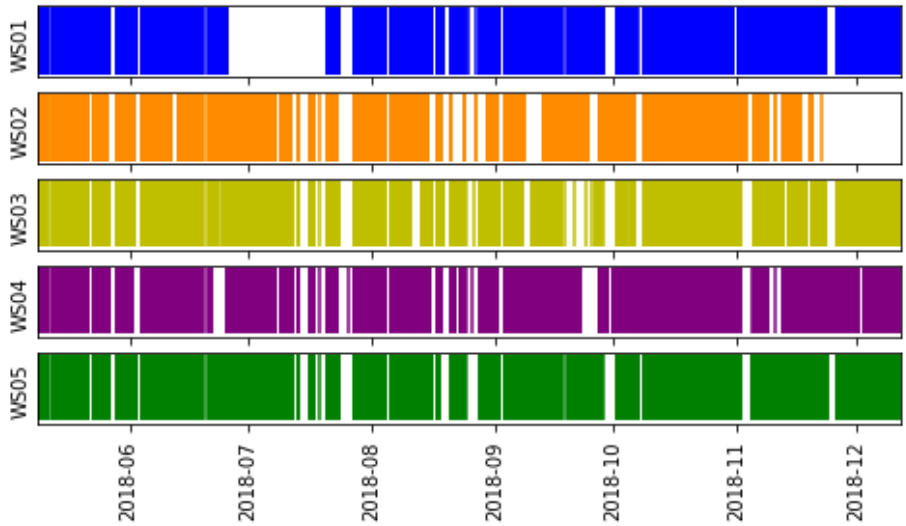

Figure 29. WS availability during IOP.

The IOP time series evidence the operational gaps of each scanner. It is worth noticing two main gaps:

- WS1 had a PC failure related to the RAM memory and had a data gap in July/2018, which was corrected;
- WS2 had a fatal failure on the FPGA module in late November/2018 and was down until the end of the campaign.

The overall monthly averages during the IOP period are showed on figure 30.

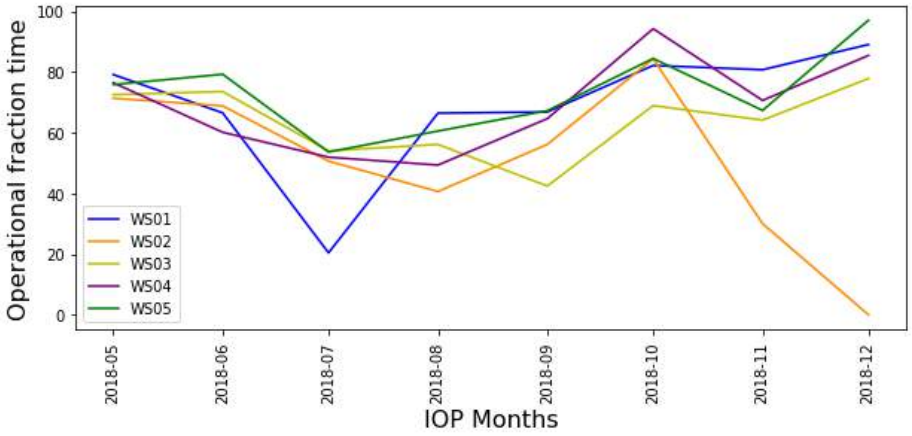

Figure 30. WS monthly operational fraction time during IOP.

3.3 WLS70 Profiler

Figure 31 shows important Logbook entries during the campaign.

2017-10-31	WLS70 measurements start: Data is in **UTC +1 time zone** (sync by NTP server 1.es.pool.ntp.org) and no day light saving time.
2017-12-01	From 31-10-2017 to 01-12-2017: system aligned with compass to 333°.
2018-04-11	From 01-12-2017 to 11-04-2018 (8h UTC): aligned with compass to 344°.
2018-05-18	WLS70 without connection due to a power cut at the University campus. On this date the connection and data transfer was reestablished but with data for at least 12 days..
2018-06-27	From 11-4-2018 to 23-07-2018: aligned to North ($\pm 2°$ uncertainty).
2018-07-21	**Final maintenance** (10h UTC): Optical table alignment, see figure 32, and $+4.87°$ offset found with Leica. Previous measurements are suspicious since the optical table was unleveled by $\approx 3°$ on both axis.

Figure 31. WLS70 Logbook

The WLS70 lidar profiler has all data stored in `mysql` schemes as follows:

1. `windcube_wls70_0001_10min`: 10min average data;
2. `windcube_wls70_0001_fast`: Raw LOS measurements from DBS scan, taken every 6 s and shifted by 90° in azimuth between them;
3. `windcube_wls70_0001_rundef`: log of each 10min average value;
4. `windcube_wls70_0001_setup`: All lidar parameters;

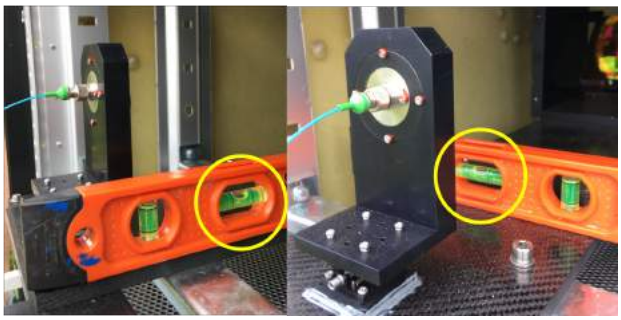

Figure 32. WLS70 leveled optical table in 21-07-2018

The focus point for this campaign was set at around 500 m, in order to have maximum recovery rate in and above the ASL. Although the WLS70 system can measure up to 2 km, the ABL height and the fast decrease in CNR with height make it possible to capture a smaller portion of the measurement range. The quality and recovery rate results presented below refers to the period between **November/2017 to March/2019**, but the WLS70 system will continue to measure at least until July/2019 in the same position.

Figure 33(left) shows the profile with mean CNR levels with one σ error bars. It's possible to see that above 1 km the signal quality decreases below the accepted threshold of -30dB. The results is a lower data recovery rate with height, as expected.

Figure 33(right) shows the average recovery rate profile for all aforementioned period as well as a the profile with filtered for data with CNR ≥ -30dB. As expected the highest recovery is close to the focus point and around 50% **of full profiles** (meaning all heights available at once) up to 1000 m are captured.

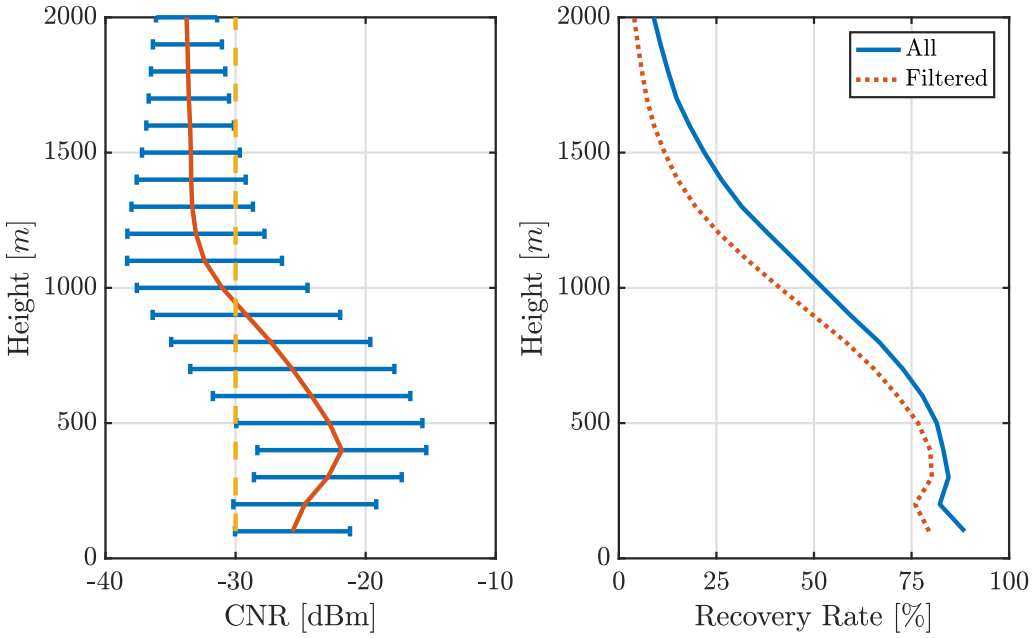

Figure 33. WLS70 average recovery rate profile (left) and CNR profile (right

Concerning monthly averages, figure 34 shows the color coded monthly recovery rate of filtered data for each height. In May/2018, as stated in the logbook (figure 31), the system was down for almost half of the month. The values of monthly recovery rate are expressed in tables and for all and filtered data respectively.

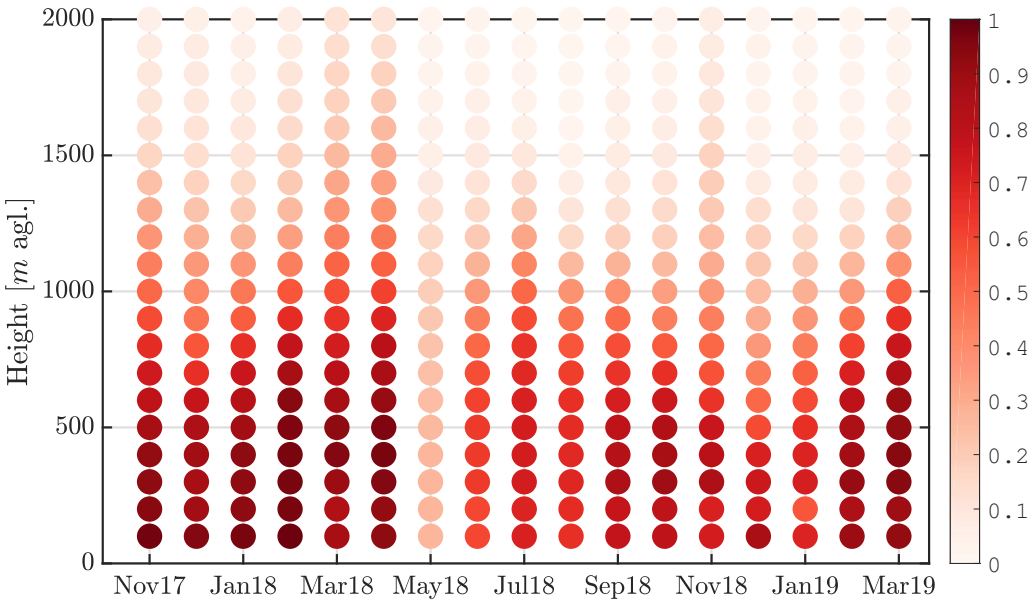

Figure 34. WLS70 monthly recovery rate (color coded)filtered by CNR$\geq -30dB$

3.4 MP5 Mast

The data base provides as .csv file with 10 minutes filtered data from MP5 in the period between July 2018 and March 2019.

The explanation of each column is in table 20.

Tables 21 and 22 shows the monthly recovery rate for each sensor from July 2018 to February 2019.

In July 2018 due to a electrical storm several sensors of the MP5 met mast were damaged so the recovery rate is lower than the others months.

3.5 Sonic masts

Figure 35 shows important Logbook entries during the campaign.

2018-08-06	Sonic measurements start: Data is in **UTC +1 time zone**.
2018-08-07	All sonics are online!.
2018-08-07	Boom direction offset: From 20180807_1000 (UTC+1) onwards the offset is applied to the variable WD_hor only.
2018-08-09	PV panels are now properly installed. 10m and 20m sonic measurements are good from now onwards.
2018-09-04	Time synchronization has not been running and the computer time was 53s ahead. A NTP server (1.es.pool.ntp.org) has been applied. From 20180904_1510 (UTC+1) onwards, time will be synchronized with the timeserver (still UTC+1, no daylight saving will be applied).

Figure 35. Sonic Masts Logbook

For the sonic met masts, the data from the sonic anemometers are stored in the following `mysql` schemes:

1. `channel_names`: Variable names;
2. `caldata_yyyy_mm_18Hz`: fast (20Hz) raw data divided by month;
3. `calmeans`: 10-min unfiltered average data;
4. `calmaxs`: 10-min average maximums;
5. `calmins`: 10-min average minimums;
6. `calstdvs`: 10-min average standard deviations;
7. `data_treatments`: log of post-processment (if any);
8. `channel_specifications`: version control and time zone of each logger configuration;
9. `channel_specs`: metadata of each variable;
10. `run_def`: log of each 10-min mean value.

Since all the masts are connected to a single logger at M2, we can define an **overall recovery rate of 83.25%** concerning the period from Aug/18 to Mar/19, which counts for data collection from all the masts. The monthly results for all sonic anemometers are shown in figure 36, where practically all sonics where working concurrently. Table 23 details the recovery of each sonic.

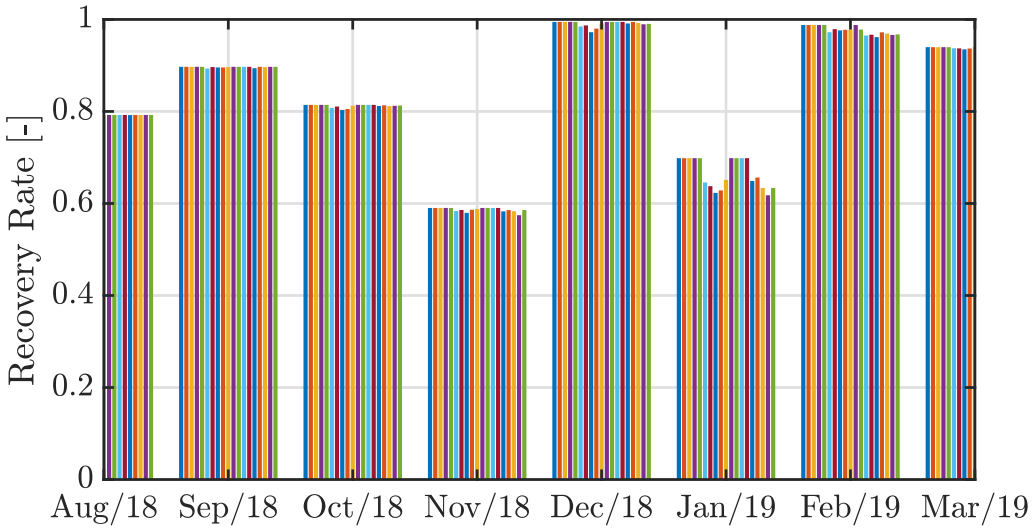

Figure 36. Recovery rate of all 19 3D sonic anemometers from DTU masts

It is clear that all sonic results were fully dependent on the quality of data transmission and operational time of M2, since it's was housing the Master Computer & logger (see section 2.4.3, making this mast a bottleneck of data collection. The data transmission between the masts was not a problem, since all masts reported a similar recovery rate.

However, with an unstable 3G network on site and with data package limitations the masts had times where no monitoring was possible. Without 3G connection the data could be stored in the M2 computer, but when M2 failed due to a power or computer issues ALL data was lost. It is worth to highlight this case happening on the months of November/18 and January/19.

The Temperature and humidity data was recorded in a separated logger, see section 2.4.3, and its recovery rate is showed in tables 24, 25, 26 and 27.

Some days after the installation there were problems with the power supply and data logger configuration, these were resolved in September 2018.

Some of the temperature and humidity sensors had malfunction problems and had to be replaced. This has meant not having data in some height levels until its replacement.

This data is provided as .csv file with 10 minutes filtered data in the period between July 2018 and March 2019.

The explanation of each column is in table 28.

3.6 Conventional masts

The data base provides as .csv file with 10 minutes filtered data from M1 and M5 in the period between July 2018 and March 2019.

All the data in **UTC time zone** without server synchronization. At it is explained in 2.4.4 the sampling rate is 1 Hz and data is stored in 10 min averaged table.

The explanation of each column is in table 29.

Tables 30 and 31 shows the monthly recovery rate in both masts for each sensor from July 2018 to February 2019.

Like in sonic masts Some days after the installation there were problems with the power supply and data logger configuration, these were resolved in September 2018. In M1 the wind vane at 60 presents a problem since some days after installation so its data has been filtered.

3.7 SLS network

The database provides two types of data files related to each surface-layer station (SLS): a raw data file and a flux file. Data are organized on a weekly basis: for each station, there is a folder indicating the year and the corresponding sub-folders therein named after the week of the year. All the files are initially provided in ASCII format. However, new versions of the same data files will be included to the database in NetCDF format and after the application of an accurate quality control procedure.

The SLS network was deployed in several phases along Autumn 2017 and Spring 2018, providing different measurement periods for each station. The first installation correspond to SLS04 in July 2017, and the latter stations (SLS01, SLS02) were deployed in April 2018, at the same time as the Wind-RASS, the SEB station and WindScanners. All the stations were taken down in December 2018, providing a measurement period of 8 months with a full operative SLS network. Table 32 shows the particular starting and ending dates of operation for each station. Most of them provided time series with several gaps that appeared mainly due to technical problems in the logger system or to battery damages. Figure 37 gives a detail of the data availability at each SLS between October 2017 and December 2018 to quickly check those periods where all the stations were working concurrently.

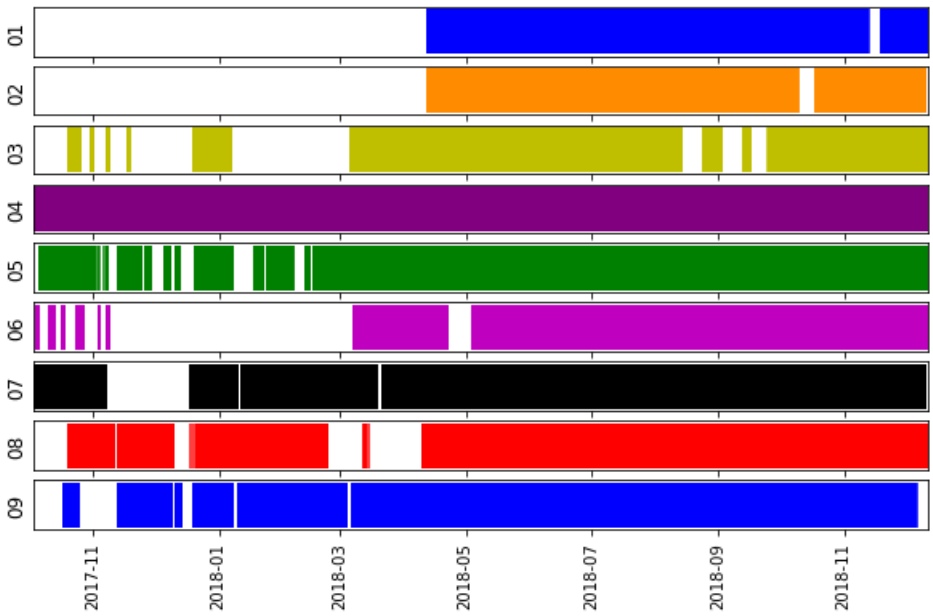

Figure 37. Data availability for each surface-layer station (SLS) between 3 October 2017 and 11 December 2018. SLS04 was set up on 30 July 2017.

3.7.1 SLS raw data files

The raw data files contain the parameters directly measured by the SLS stations with a sampling period of 5 minutes. Soil variables (volumetric water content, temperature and heat flux) are monitored with one sample every five minutes, while atmospheric parameters are provided after averaging several consecutive samples: temperature and humidity are built with 20 samples along one minute (0.33 Hz sampling rate), and wind is represented by the average of 30 samples along 30 seconds (1 Hz sampling rate). Table 33 provides a detailed list of the output variables included in the raw data files.

SLS04 represents an exception since its logger system was different from the rest. In this case, the raw data files provide time series of one-minute averages from a sampling rate of 1 second (T107 and HFP01) or 4 seconds (Windsonic, CS655 and CS215), depending on the sensor (table 34).

3.7.2 SLS flux data files

The flux data files will provide the estimated turbulent fluxes using the flux-gradient approach (Moene and Dam, 2014) every 30 minutes. The methodology is currently assessed at the Zabalegui site by comparing the estimated results from SLS01 against the fluxes obtained through the eddy-covariance technique with the SEB measurements. Data format and details on the assessment of turbulent fluxes will be provided in the future versions of this report.

3.8 WindRASS and Surface Energy Budget station

The WindRASS (WR) and SEB station were installed at the Zabalegui site from 19 April 2018 to 14 January 2019, with few gaps in the time series (fig. 38). Software issues on the WR system at the beginning of this period delayed the starting date for operational measurements. Additional missing data was mainly due to a failure in the SEB regulator affecting this station from 25 May to 8 June. A problem with the power supply at the Zabalegui site caused a three-day gap in mid-June that affected both sensors.

As for the SLS stations, this instrumentation contributes to the database with two types of data

files: a file containing the raw data and a second one with post-processed data. All the files are initially provided in ASCII format although NetCDF will be included in the subsequent database updates.

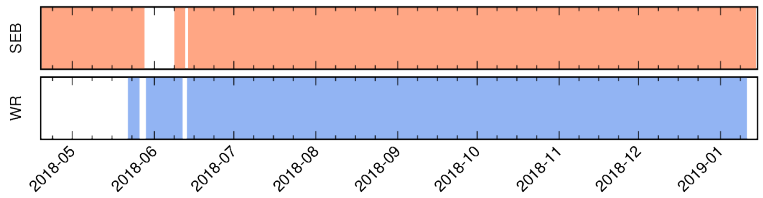

Figure 38. Data availability for SEB station and WindRASS (WR) between 19 April 2018 and 14 January 2019.

The following sections describe in detail the data files characteristics for both sensors.

3.8.1 SEB station data files

SEB station files are organized on a weekly basis, with the same architecture as for the SLS network: a first directory for the year that contains the corresponding sub-folders named after the week of year. Inside each week directory, there is a raw data file (*ts_data*) with measurements at a high sampling rate (10 Hz) from the sensors that compound the Eddy-Covariance system: the sonic anemometer (CSAT3), the gas analyser (LI-7500) and the thermo-hygrometer (HMP45C). The rest of sensors also operate at 10 Hz, but only 10-minute averages are included in a second data file, the so-called *flux* file, together with the 10-min statistics from the Eddy-Covariance system. Tables 35 and 36 include a detailed description of both file types. In all these measurements, wind data (i.e., wind vector and the rest of related variables such as variances, covariances or turbulent fluxes) are described in the sonic anemometer coordinate system. The CSAT3 sonic anemometer was oriented with the positive x-axis forming an azimuth angle of 100° respect to the geographical North (fig. 39).

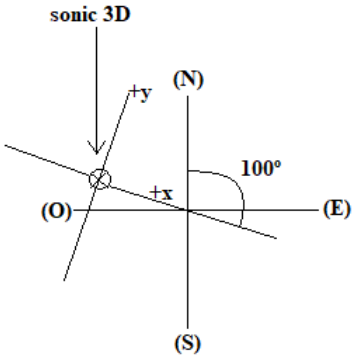

Figure 39. Orientation of the sonic anemometer CSAT3 from the SEB station respect to the Geographical coordinate system.

The flux file contains the turbulent fluxes computed online by the datalogger from the measured data. It saves all the cross products that are required to rotate the online fluxes into natural wind coordinates in post processing as described in Kaimal and Finnigan (1994). Online turbulent fluxes concerning the air components H_2O and CO_2 are corrected for density fluctuations, the so-called WPL-correction (Webb et al., 1980).

The sign convention for the fluxes, except net radiation, is positive away from the surface and negative towards the surface. The datalogger has introduced lags into the CSAT3, LI-7500, and

datalogger panel temperature data so that all measurements are aligned in time.

3.8.2 WindRASS data files

WindRASS measurements are stored in daily files under three main folders depending on the data format. Raw data are contained within binary files (*.raw*). These files hold primary information that can be re-processed to generate data with the configuration defined by the user. This post-processing can be performed through the Scintec Sodar Operation software APRun (for more details, refer to the *Scintec Flat Array Sodar - Software Manual APRun*).

The database also provides already processed data with the following configuration: vertical profiles of wind speed and direction, mean and standard deviation of the vertical wind component, and the air and virtual temperature. These vertical profiles are given every 15 minutes within a range from 40 to 400 m above ground level at a vertical resolution of 10 m. These data can be found in ASCII format (*.mnd*) or NetCDF (*.nc*).

4 Summary

The present reports describes the ALEX17 experiment and dataset, which focuses on mean flow and flux measurements over a large area, of around 20 km by 20 km, to characterize complex flow in complex terrain. With the combination of WindScanner systems, met masts and turbulence flux measurements preliminary results have shown some examples of complex flow in complex terrain, such as gravity waves or wind turbine wakes interacting with sloping terrain (Santos, 2019).

The dataset includes the following data:

- Digital Elevation Model (DEM);
- Equipment positions (UTM Z30, WGS84);
- Scanning trajectories (UTM Z30, WGS84);
- Metadata, when not embedded in the data files;
- Measurement data described in chapter 3

Further details can be found in the Appendix below, regarding sensors technical sheets (B), deployment of lidar systems on site (C) as well as met mast deployment (2.4). Details on atmospheric conditions and land cover change are also analyzed with pictures (E).

Bibliography

Badger, J., Frank, H., Hahmann, A. N., and Giebel, G.: Wind-climate estimation based on mesoscale and microscale modeling: Statistical-dynamical downscaling for wind energy applications, Journal of Applied Meteorology and Climatology, 53, 1901–1919, https://doi.org/10.1175/JAMC-D-13-0147.1, 2014.

Borbón, F.: Lidar uncertainty in complex terrain: Development of a bias correction methodology, Ph.D. Thesis, Technical University of Madrid, Madrid, Spain, URL http://oa.upm.es/33794/, 2015.

Cuxart, J., Cunillera, J., Jiménez, M. A., Martínez, D., Molinos, F., and Palau, J. L.: Study of Mesobeta Basin Flows by Remote Sensing, Bound.-Layer Meteorol., 143, 143–158, 2012.

Cuxart, J., Conangla, L., and Jiménez, M. A.: Evaluation of the surface energy budget equation with experimental data and the ECMWF model in the Ebro Valley, Journal of Geophysical Research: Atmospheres, 120, 1008–1022, 2015.

Jiménez, P. A., Dudhia, J., González-Rouco, J. F., Montávez, J. P., García-Bustamante, E., Navarro, J., Vilà-Guerau de Arellano, J., and Muñoz-Roldán, A.: An evaluation of WRF's ability to reproduce the surface wind over complex terrain based on typical circulation patterns, Journal of Geophysical Research: Atmospheres, 118, 7651–7669, https://doi.org/10.1002/jgrd.50585, URL https://agupubs.onlinelibrary.wiley.com/doi/abs/10.1002/jgrd.50585, 2013.

Kaimal, J. C. and Finnigan, J. J.: Atmospheric boundary layer flows: their structure and measurement, Oxford University Press, New York, 1994.

Mann, J., Angelou, N., Arnqvist, J., Callies, D., Cantero, E., Arroyo, R. C., Courtney, M., Cuxart, J., Dellwik, E., Gottschall, J., Ivanell, S., Kühn, P., Lea, G., Matos, J. C., Palma, J. M. L. M., Pauscher, L., Peña, A., Rodrigo, J. S., Söderberg, S., Vasiljevic, N., and Rodrigues, C. V.: Complex terrain experiments in the New European Wind Atlas, Philosophical Transactions of the Royal Society A: Mathematical, Physical and Engineering Sciences, 375, 20160 101, https://doi.org/10.1098/rsta.2016.0101, URL http://rsta.royalsocietypublishing.org/lookup/doi/10.1098/rsta.2016.0101, 2017.

Mann, J., Menke, R., Vasiljević, N., Berg, J., and Troldborg, N.: Challenges in using scanning lidars to estimate wind resources in complex terrain, Journal of Physics: Conference Series, 1037, 072 017, https://doi.org/10.1088/1742-6596/1037/7/072017, URL https://doi.org/10.1088/1742-6596/1037/7/072017, 2018.

Moene, A. F. and Dam, J. C. v.: Transport in the Atmosphere-Vegetation-Soil Continuum, Cambridge University Press, https://doi.org/10.1017/CBO9781139043137, 2014.

Santos, P.: The Alaiz Experiment (ALEX17): vizualing the flow in complex terrain with multi scanning lidars, https://doi.org/10.5281/zenodo.2620505, URL https://doi.org/10.5281/zenodo.2620505, 2019.

Sanz Rodrigo, J., Borbón Guillén, F., Gómez Arranz, P., Courtney, M. S., Wagner, R., and Dupont, E.: Multi-site testing and evaluation of remote sensing instruments for wind energy applications, Renewable Energy, 53, 200–210, https://doi.org/10.1016/j.renene.2012.11.020, URL http://dx.doi.org/10.1016/j.renene.2012.11.020, 2013.

Simó, G., Cuxart, J., Jiménez, M. A., Martínez-Villagrasa, D., Picos, R., López-Grifol, A., and Martí, B.: Observed atmospheric and surface variability on heterogeneous terrain at the hectometre scale and related advective transports, Journal of Geophysical Research: Atmospheres, submitted, 2019.

Vasiljevic, N.: A time-space synchronization of coherent Doppler scanning lidars for 3D measurements of wind fields, Ph.D. thesis, Denmark, 2014.

Vasiljević, N., L. M. Palma, J. M., Angelou, N., Carlos Matos, J., Menke, R., Lea, G., Mann, J., Courtney, M., Frölen Ribeiro, L., and M. G. C. Gomes, V. M.: Perdigão 2015: methodology for atmospheric multi-Doppler lidar experiments, Atmospheric Measurement Techniques, 10, 3463–3483, https://doi.org/10.5194/amt-10-3463-2017, URL https://www.atmos-meas-tech.net/10/3463/2017/, 2017.

Vasiljevic, N., Klaas, T., Pauscher, L., Lopes, J. C., Gomes, D. F., Abreuand, R., and Bardal, L. M.: e-WindLidar: making wind lidar data FAIR, https://doi.org/10.5281/zenodo.2478051, URL https://doi.org/10.5281/zenodo.2478051, 2018.

Vasiljević, N., Lea, G., Courtney, M., Cariou, J.-P., Mann, J., and Mikkelsen, T.: Long-Range WindScanner System, Remote Sensing, 8, https://doi.org/10.3390/rs8110896, URL http://www.mdpi.com/2072-4292/8/11/896, 2016.

Webb, E. K., Pearman, G. I., and Leuning, R.: Correction of flux measurements for density effects due to heat and water vapour transfer, Quarterly Journal of the Royal Meteorological Society, 106, 85–100, 1980.

Acknowledgements

The NEWA project is supported by a European Commission's ERA-Net Plus project, number 618122, joining national projects from 9 funding agencies from 8 member states:

- Public Service of Wallonia, Department of Energy and Sustainable Building (Belgium);
- Department of Economy, Science and Innovation Flemish Government (Belgium);
- Danish Energy Authority (Denmark);
- Federal Ministry for the Economic Affairs and Energy, on the basis of the decision by the German Bundestag (Germany);
- Latvijas Zinatnu Akademija (Latvia);
- Fundação para a Ciência e a Tecnologia (Portugal);
- Ministerio de Economía, Industria y Competitividad (Spain);
- The Swedish Energy Agency (Sweden);
- The Scientific and Technological Research Council of Turkey (Turkey).

A Tables

WindScanner	Easting [m]	Northing [m]	Altitude [m]
WS1	615892.37	4733629.98	486.44
WS2	616449.58	4731282.79	499.46
WS3	617846.80	4732496.43	487.21
WS4	619427.57	4731322.15	527.31
WS5	617305.59	4729848.75	545.92

Table 1. WindScanner coordinates: UTM Zone 30, WGS84

	10min Intervals		
Windscanner	1st	2nd	3rd
WS1	N Ridge (125m)	Virtual Mast (N Ridge)	N Ridge (125m)
WS2	S Ridge (125m)	Transect (N-S Ridge)	Virtual Mast (u, v)
WS3	N Ridge (125m)	RHI (South Ridge)	N Ridge (125m)
WS4	S Ridge (125m)	Transect (N-S Ridge)	Virtual Mast (u, v)
WS5	RHI (North Ridge)	RHI (North Ridge)	Virtual Mast (w)

Table 2. WS scanning scenarios

Parameters	North Ridge (WS1/WS3)	South Ridge (WS2/WS4)
Pulse Length	400ns	400ns
Accumulation Time	1000ms	1000ms
FFT Size	128 points	128 points
Full Width Half Maximum	75m	75m
(Min,Max) Range	$(100, 5000)$m	$(100, 5000)$m
Range Gates / LOS	112	112
Dynamic Range Gates	No	No
# of LOS	40	40
Ridge Length	2000m	2000m
Total scan time	43000ms	43000ms
Speed up/down time	500ms	500ms
Measurement time	40000ms	40000ms
Return time	2000ms	2000ms

Table 3. Ridge Scans: Lidar parameters

	07/May/2018		17/July/2018		24/October/2018	
	Azimuth [^{o}]	Elevation [^{o}]	Azimuth [^{o}]	Elevation [^{o}]	Azimuth [^{o}]	Elevation [^{o}]
WS1	-0.02	-0.22	0.46	0.05	-0.24	0.31
WS2	-0.04	-0.02	-0.01	-0.17	-0.94	-0.53
WS3	-0.06	0.02	1.67	-1.79	0.08	0.20
WS4	0.01	-0.05	0.16	0.32	0.11	-0.13
WS5	-0.06	-0.01	0.44	-0.02	-0.55	-0.11

Table 4. WS pointing error for each leveling period

Parameters	WS3 RHI	WS5 RHI (VM1)
Range Gates	[100 : 20 : 5000]m	[100 : 20 : 5000]m
# of LOS	30	30
Azimuth Angle	191.55°	11.55°
Elevation Angles	3°-18°	1.58°-21.56°
Scan Speed	0.5°/s	0.66°/s

Table 5. Transect Scan: Lidar parameters

Parameters	WS1 RHI (VM1)	WS2 RHI (VM2)	WS4 RHI (VM2)
Measurement Heights a.g.l.	[100 : 50 : 1400]m	[100 : 50 : 1200]m	[100 : 50 : 1200]m
# of LOS	30	30	30
Azimuth Angle	84.43°	149.17°	235.22°
Elevation Angles	4.39°-36.73°	5.02°-36.73°	2.63°-25.25°
Scan Speed	1.078°/s	1.057°/s	0.754°/s

Table 6. Virtual Masts (VM): Lidar parameters

Mast	Sensor	Boom height [m]	Orientation [º]	Tilt [º]
M2	Gill sonic	9.883	264.002	-0.408
M2	Gill sonic	20.151	260.674	-0.246
M2	Gill sonic	41.823	253.302	-1.089
M2	Gill sonic	61.161	254.514	-1.27
M2	Gill sonic	82.2	251.629	-1.255
M3	Gill sonic	9.609	302.065	1.167
M3	Gill sonic	20.209	298.249	0.615
M3	Gill sonic	40.952	292.062	-2.995
M3	Gill sonic	61.606	292.707	-1.945
M3	Gill sonic	82.215	293.16	-0.573
M7	Gill sonic	7.706	267.39	-0.143
M7	Gill sonic	17.882	266.636	-1.58
M7	Gill sonic	38.946	265.997	-0.564
M7	Gill sonic	58.778	263.56	-1.107
M7	Gill sonic	79.251	259.572	-1.782
M6	Metek sonic	9.603	264.924	0.469
M6	Metek sonic	20.12	261.603	-2.79
M6	Metek sonic	41.227	255.266	-1.51
M6	Metek sonic	60.595	251.351	-2.529
M1	Cup anemometer	10	unmeasured	unmeasured
M1	Cup anemometer	20.099	263.772	-0.566
M1	Cup anemometer	39.618	255.722	0.475
M1	Cup anemometer	59.53	266.213	-0.37
M1	Cup anemometer	79.577	266.815	-0.15
M5	Cup anemometer	9.707	267.277	0.22
M5	Cup anemometer	19.675	268.006	0.008
M5	Cup anemometer	39.708	268.865	-0.902
M5	Cup anemometer	59.622	268.314	0.159
M5	Cup anemometer	79.691	270.513	-0.527
MP5	Metek sonic	39.573	259.807	-0.921
MP5	Metek sonic	75.032	260.714	-1.109
MP5	Metek sonic	115.631	261.154	-0.986
MP5	Metek sonic	117.516	260.907	-0.292

Table 7. Boom orientation and tilt angles.

Mast	Easting [m]	Northing [m]
M2	616903	4730230
M3	617584	4733372
M6	616917	4734045
M7	616502	4731256

Table 8. Masts with sonic anemometer coordinates: UTM Zone 30, WGS84

Mast	Easting [m]	Northing [m]
M1	617650	4732567
M5	617609	4731301

Table 9. Conventional Masts coordinates: UTM Zone 30, WGS84

Station	Easting [m]	Northing [m]	Altitude [m]
SLS01	616444	4731332	497
SLS02	615114	4731366	475
SLS03	620750	4730282	509
SLS04	617572	4729055	874
SLS05	617448	4728132	1089
SLS06	617774	4729865	541
SLS07	617858	4732478	484
SLS08	617566	4731281	474
SLS09	616901	4734179	635

Table 10. SLS stations coordinates: UTM Zone 30, WGS84

Station	Wind		T + RH			VWC + ST	HF
	h [cm]	tilt [°]	h1 [cm]	h2 [cm]	h3 [cm]	d [cm]	d [cm]
SLS01	230	0	36	100	200	-5	-8
SLS02	229	0	36	100	200	-5	-8
SLS03	217	0	36	100	193	-5*	-10*
SLS04	290	12	30	–	205	-5[(1)]	-8
SLS05	225	7	36	100	209	-5	-8
SLS06	233	18	36	100	206	-5	-8
SLS07	232	0	36	109	220	-5	-8
SLS08	219	0	36	100	201	-5*	-8*
SLS09	222	25	36	100	209	-5*	-8*

Table 11. Details on the sensor position at each SLS station, indicating the heights (h) and depths (d) for the monitored variables: Wind, Air temperature (T) and humidity (RH), Soil volumetric water content (VWC) and soil temperature (ST) and soil heat flux (HF). Wind sensor was tilted approximately following the slope angle at those stations over mountain slopes. T and RH were measured at three levels, although sensor 2 was not maintained until the end of the campaign (see the text for more details). Numbers with an asterisk (*) indicates that VWC and HF sensors were initially located at -8 and -5 cm deep, respectively, and were changed to the indicated depths during 18-19/12/2017. [(1)] Soil temperature was additionally measured at -3 cm with an additional thermistor.

WLS70 Lidar parameters	Value
Sampling Frequency [MHz]	250
AOM Frequency [MHz]	49.971
Nb Pulses / Ligne of Sight	40000
FFT Window Width	150
Scan Cone Angle [^{o}]	14.677
Wavelenght [μm]	1.543
Altitudes [m]	[100:100:2000]

Table 12. WLS70 profiler lidar parameters

Station	Easting [m]	Northing [m]	Altitude (m)
SEB	616442	4731321	498
WR	616435	4731311	498

Table 13. Coordinates for the surface energy budget station (SEB) and WindRASS (WR): UTM Zone 30, in WGS84

Sensor	Sampling rate [Hz]	h/d [cm]
CNR1	10	122
LI7500	10	170
CSAT3	10	170
HMP45C	10	150
TCAV	10	-2,-6
CS616	10	-2.5
HFP01SC	10	-8

Table 14. Characteristics of the sensors at the SEB stations, indicating the sampling rates and the heights (h) or depths (d, negative values) for each instrument: 4-component net radiometer (CNR1), open-path gas analyser (LI7500), sonic anemometer (CSAT3), thermo-hygrometer (HMP45C), soil temperature probes (TCAV), soil water content reflectometers (CS616) and heat flux plates (HFP01SC). Each TCAV is formed by four thermistors that are inserted in pairs into the soil at two different depths. Sonic anemometer was installed parallel to an underlying flat surface by eye, with the positive x-axis of the sonic coordinate system pointing into 100° (see fig. 39).

Station	Easting [m]	Northing [m]	Time length
Aoiz	633391	4738896	Jul91-Dic18
Aralar	584587	4756228	Jan91-Dic18
Arangoiti	648048	4723086	Mar91-Dic18
Bardenas LomaNegra	634596	4658940	Apr91-Dic18
Bardenas Yugo	617057	4673622	Mar91-Dic18
Carcastillo	626546	4692335	Jun91-Dic18
Carrascal	609782	4726483	Apr91-Dic18
Doneztebe	608664	4776228	Jun99-Dic18
El Perdón	605764	4731975	Apr91-Dic18
Erremendia	648311	4748978	Sep01-Dic18
Estella	579641	4725294	Jan92-Dic18
Etxarri	576893	4751250	Jan92-Dic18
Getadar	625315	4719527	Jul00-Dic18
Gorramendi	626312	4785420	Mar91-Dic18
Oskotz	601469	4756679	May01-Dic18
Tafalla	608751	4708585	Nov91-Dic18
Trinidad Iturgoyen	583309	4740553	Mar91-Dic18
Tudela Montes de Cierzo	611406	4665422	Ago97-Dic18
Urbasa	567405	4744821	Oct01-Dic18
Villanueva Yerri	586031	-4732034	Jan98-Dic18
Yesa	648440	4720094	May91-Dic18

Table 15. UTM Zone30 coordinates, WGS84, of met stations along with dataset time coverage

	Folder names at 10min Intervals		
Windscanner	1st	2nd	3rd
WS1	_HMD1	_RHI1	_HMD1
WS2	_HMD1	_HMD2	_RHI1
WS3	_HMD1	_RHI1	_HMD1
WS4	_HMD1	_HMD2	_RHI1
WS5	_RHI1	_RHI1	_LOS1

Table 16. Folder names for each scanning trajectoy

WindScanner	Total [%]	May	June	July	Aug.	Sept.	Oct.	Nov.	Dec.
WS1	66.6	79.1	66.5	20.4	66.4	66.8	82.1	80.7	89.0
WS2	54.0	71.3	68.8	50.6	40.6	56.1	84.3	30.0	0.0
WS3	62.1	72.5	73.5	54.0	56.1	42.4	68.9	64.1	77.8
WS4	67.3	76.4	60.1	51.9	49.3	64.6	94.2	70.6	85.4
WS5	70.8	75.8	79.2	53.6	60.5	67.2	84.4	67.3	97.0

Table 17. Overall WindScanner operational time fraction during IOP

z [m]	Nov/17	Dec/17	Jan/18	Feb/18	Mar/18	Apr/18	May/18	Jun/18	Jul/18	Ago/18	Sep/18	Oct/18	Nov/18	Dec/18	Jan/19	Feb/19	Mar/19
2000	8.5	10.2	6	10.9	15.9	22.5	2.8	4.3	15.4	7.3	6.1	4.3	21.3	4.1	4.1	5	3.6
1900	12.9	12.1	8.2	13.6	19.1	25.8	3.3	5.1	16.8	8.3	7.6	5.2	23.1	4.4	5.2	6.4	4.9
1800	16.3	14.5	10.2	16.6	22	28.8	3.9	6.6	20.4	9	9.3	6.3	24.8	5	6.6	8.4	6.5
1700	19.4	16.4	12.8	19.8	24.1	32.5	5.2	8.8	24.1	10.6	12.5	7.8	27.1	5.1	8.3	9.4	8.7
1600	23.8	18.8	16.6	24.3	28.6	37.3	7.3	11	29.6	13.3	15.2	10.2	31.7	6.1	10.4	11.9	12.8
1500	28.6	22.5	19.6	27.6	34.9	42.7	10.5	13.7	34.4	16.4	17.6	14.5	36	8.4	13	14.5	18.5
1400	35.3	27	24.5	30.8	41.7	48.7	13.1	16.6	39.1	20.8	20.8	19.5	38.7	12.2	16.1	17.1	25.2
1300	41.6	31.8	29.8	36.5	48.5	53.3	15.9	21.6	45.9	27	27	24.9	40.3	18.5	19	20.6	33.4
1200	47.1	38.2	38.1	44.7	58	59.8	18.6	27.9	53.9	35.3	35.1	31.4	43.5	23.9	23.1	27.8	45.1
1100	52.7	44.6	46.8	54.2	66.4	67.7	20.7	34.9	59.2	44.5	43.9	38.8	48.5	26.8	29	36.6	56.8
1000	58.5	49.9	54.5	65.3	73.5	76.6	22.3	42.8	63.5	51.9	52.5	46.7	52.4	30.8	36.2	46.9	66.1
900	65	57	63.9	74.4	78.6	83.4	23.2	49.6	67.2	57.2	59.8	56.4	59	36.3	44.3	58.5	75.6
800	72.1	64.3	76.5	84.4	84.9	89.3	24.4	55.9	70.1	62.1	67	68.3	65.1	44.8	52.3	69.7	84.8
700	77.4	74.6	83.1	91.6	90.4	93.5	25.2	60.3	72.7	65.1	74	76.7	72.3	52.2	61	79.2	90.8
600	84.9	83.8	87.6	95.8	94	95.8	25.4	62.7	74.4	67.9	80.1	85.6	80.9	58.6	67.9	86.4	94.8
500	91.9	89.2	92.9	97.2	96.6	98.1	25.7	63.8	75.4	68.8	83.3	89.6	85.7	67.9	75.9	90	95.8
400	94.9	91.1	95.7	98.4	97.2	98.7	26.4	63.6	75.1	69.2	85.5	90.9	87.5	74.9	78.5	92.7	96.4
300	96	91.2	96.1	98.1	95.4	98.2	26.5	63.2	75.1	69.3	88.6	93.5	91.2	79.4	84.4	95.6	97.3
200	99	92.8	96.6	98.6	93.9	97.1	26.5	62.6	73.8	68.2	85.7	88.1	84.1	79.3	69.9	91.4	93.2
100	99.9	99.1	99.9	99.2	99	99.4	26.5	65.9	86	71.4	92	94.7	93.2	95.5	92.5	96.8	97.6

Table 18. WLS70 monthly recovery rate (in %) profile without filtering

z [m]	Nov-17	Dec-17	Jan-18	Feb-18	Mar-18	Apr-18	May-18	Jun-18	Jul-18	Aug-18	Sep-18	Oct-18	Nov-18	Dec-18	Jan-19	Feb-19	Mar-19
2000	4.9	6	3.4	6.5	11.5	10.4	1.9	2.2	0.9	0.3	1.5	2.6	6.5	2.8	1.7	1.6	2.1
1900	7.5	7.1	4.1	7.8	13.7	13.3	2.4	2.6	1.2	0.2	1.8	3.2	7.9	3.3	2.2	2.1	2.6
1800	9.5	8.4	5.5	10.1	16.1	17.1	2.7	3.2	2	0.3	2.6	3.7	9.3	2.9	2.8	2	2.8
1700	10.3	9.3	7.2	12	17.9	20.6	3.5	4.4	3.6	0.6	4.2	4.6	10.8	3	3.4	2.5	4.2
1600	12.5	11.1	9.7	14.8	20.7	25.4	4.2	6.1	6	2	5.4	6.3	13.6	3.5	4.4	3.2	5
1500	17	13.4	11.9	18	25.3	30	5.8	8.1	9.6	4	7.4	8.8	17.4	5	6.1	4.3	8.1
1400	23.2	17.5	15.7	20.8	31	33.2	8.7	11.1	14.7	6.6	9.4	11.1	19.4	7.4	7.6	7.6	11.7
1300	29.9	22.9	20.5	25.1	36.3	39	12.3	15.3	22	10.1	13	14.7	20.8	13.2	10.9	10.7	18
1200	36.4	28.7	27.7	33.2	43.1	45.5	15.4	20.9	31.2	15.5	18.9	19	24.4	18.7	15.7	17.9	26.9
1100	43.9	35.1	36.3	43.6	51	52.1	17.6	27.6	41.8	25.6	27.2	25.2	29.9	21.1	21.2	26.6	38.8
1000	50.9	40.7	45.3	55.5	57.5	60.4	19.7	35.7	50.6	37.8	38.8	33.6	35.9	24.1	28.2	35.6	52.6
900	58.2	46.9	53.5	66.8	64.9	69.8	21.5	43.6	58.2	47.7	50	43.5	44	29.3	36.4	47.2	65.2
800	66.6	55.3	65.1	77.6	72.9	80.8	22.6	51	64.5	55.8	57.3	54.8	50.5	35.9	44.4	60.2	75.2
700	73.4	65	75.7	86.3	80.6	85.9	24	57.3	68	61.1	64.9	65.6	56.4	44.2	52.8	70.5	83.4
600	78.9	76.1	81.7	93	86.7	90.2	24.9	60.8	70.5	65.4	71.8	74.5	64.8	50.8	58.8	79.3	89.8
500	86.2	84.2	87.7	95.3	92.3	95.4	25.2	63	72.4	66.7	78.7	83.6	75.2	58.8	65.5	84.6	91.9
400	92	87.5	92.9	96.3	94.1	96.8	26.2	62.8	72.9	68	81.5	87	80.8	70.3	69.2	87.9	93.1
300	92.4	86.6	92.9	96.2	89.1	94.1	26.4	62.2	72.2	68	84.1	88.5	84.1	74.5	71.4	90.5	93.6
200	93.8	87.5	92	96	83.7	91.9	26.5	59.8	69.7	66.3	76	78.6	70.9	72.6	55.6	84.5	88.6
100	97.5	94.9	96.6	98.6	86.9	92.2	26.5	59.4	70.5	65.9	77.7	78.6	72.6	85.7	69.6	89.6	91.4

Table 19. WLS70 monthly recovery rate (in %) profile with CNR≥ -30dBm filter

Table 20: MP5 column description, including number of column, variable, unit and short description.

Begin table			
Col	Variable	Unit	Description
1	”Date/Time”	–	Beginning of the 10-min block in format DD-MM-YYYY hh:mm
2	”Vr118_md”	m/s	10 minutes mean wind speed at the main 118 meters cup anemometer
3	”Vr118_mx”	m/s	10 minutes maximum wind speed at the main 118 meters cup anemometer
4	”Vr118_mn”	m/s	10 minutes minimum wind speed at the main 118 meters cup anemometer
5	”Vr118_sd”	m/s	10 minutes standard deviation of the wind speed at the main 118 meters cup anemometer
6	”Vc118_md”	m/s	10 minutes secondary wind speed at the main 118 meters cup anemometer
7	”Vc118_mx”	m/s	10 minutes maximum wind speed at the secondary 118 meters cup anemometer
8	”Vc118_mn”	m/s	10 minutes minimum wind speed at the secondary 118 meters cup anemometer
9	”Vc118_sd”	m/s	10 minutes standard deviation of the wind speed at the secondary 118 meters cup anemometer
10	”D118_md”	º	10 minutes mean wind direction at the 118 meters wind vane
11	”D118_mx”	º	10 minutes maximum wind direction at the 118 meters wind vane
12	”D118_mn”	º	10 minutes minimum wind direction at the 118 meters wind vane
13	”D118_sd”	º	10 minutes standard deviation of the wind direction at the 118 meters wind vane
14	”Vr78_md”	m/s	10 minutes mean wind speed at the main 78 meters cup anemometer
15	”Vr78_mx”	m/s	10 minutes maximum wind speed at the main 78 meters cup anemometer
16	”Vr78_mn”	m/s	10 minutes minimum wind speed at the main 78 meters cup anemometer
17	”Vr118_sd”	m/s	10 minutes standard deviation of the wind speed at the main 78 meters cup anemometer
18	”Vc78_md”	m/s	10 minutes secondary wind speed at the main 78 meters cup anemometer
19	”Vc78_mx”	m/s	10 minutes maximum wind speed at the secondary 78 meters cup anemometer
20	”Vc78_mn”	m/s	10 minutes minimum wind speed at the secondary 78 meters cup anemometer
21	”Vc78_sd”	m/s	10 minutes standard deviation of the wind speed at the secondary 78 meters cup anemometer
22	”D78_md”	º	10 minutes mean wind direction at the 78 meters wind vane
23	”D78_mx”	º	10 minutes maximum wind direction at the 78 meters wind vane
24	”D78_mn”	º	10 minutes minimum wind direction at the 78 meters wind vane
25	”D78_sd”	º	10 minutes standard deviation of the wind direction at the 78 meters wind vane
26	”Vr40_md”	m/s	10 minutes mean wind speed at the 40 meters cup anemometer
27	”Vr40_mx”	m/s	10 minutes maximum wind speed at the 40 meters cup anemometer
28	”Vr40_mn”	m/s	10 minutes minimum wind speed at the 40 meters cup anemometer
29	”Vr40_sd”	m/s	10 minutes standard deviation of the wind speed at the 40 meters cup anemometer
30	”H113_md”	%	10 minutes mean relative humidity from 113 meters temperature and humidity sensor
31	”H113_mx”	%	10 minutes maximum relative humidity from 113 meters temperature and humidity sensor
32	”H113_mn”	%	10 minutes minimum relative humidity from 113 meters temperature and humidity sensor
33	”H113_sd”	%	10 minutes standard deviation of the relative humidity from 113 meters temperature and humidity sensor
34	”T113_md”	°C	10 minutes mean temperature from 113 meters temperature and humidity sensor
35	”T113_mx”	°C	10 minutes maximum temperature from 113 meters temperature and

Continuation of Table 20			
Col	Variable	Unit	Description
			humidity sensor
36	”T113_mn”	°C	10 minutes minimum temperature from 113 meters temperature and humidity sensor
33	”T113_sd”	°C	10 minutes standard deviation of the temperature from 113 meters temperature and humidity sensor
34	”H97_md”	%	10 minutes mean relative humidity from 97 meters temperature and humidity sensor
35	”H97_mx”	%	10 minutes maximum relative humidity from 97 meters temperature and humidity sensor
36	”H97_mn”	%	10 minutes minimum relative humidity from 97 meters temperature and humidity sensor
37	”H97_sd”	%	10 minutes standard deviation of the relative humidity from 97 meters temperature and humidity sensor
38	”T97_md”	°C	10 minutes mean temperature from 97 meters temperature and humidity sensor
39	”T97_mx”	°C	10 minutes maximum temperature from 97 meters temperature and humidity sensor
40	”T97_mn”	°C	10 minutes minimum temperature from 97 meters temperature and humidity sensor
41	”T97_sd”	°C	10 minutes standard deviation of the temperature from 97 meters temperature and humidity sensor
42	”H81_md”	%	10 minutes mean relative humidity from 81 meters temperature and humidity sensor
43	”H81_mx”	%	10 minutes maximum relative humidity from 81 meters temperature and humidity sensor
44	”H81_mn”	%	10 minutes minimum relative humidity from 81 meters temperature and humidity sensor
45	”H81_sd”	%	10 minutes standard deviation of the relative humidity from 81 meters temperature and humidity sensor
46	”T81_md”	°C	10 minutes mean temperature from 81 meters temperature and humidity sensor
47	”T81_mx”	°C	10 minutes maximum temperature from 81 meters temperature and humidity sensor
48	”T81_mn”	°C	10 minutes minimum temperature from 81 meters temperature and humidity sensor
49	”T81_sd”	°C	10 minutes standard deviation of the temperature from 81 meters temperature and humidity sensor
50	”P_md”	mbar	10 minutes mean pressure
51	”P_mx”	mbar	10 minutes maximum pressure
52	”P_mn”	mbar	10 minutes minimum pressure
53	”P_sd”	mbar	10 minutes standard deviation of the pressure
54	”H38_md”	%	10 minutes mean relative humidity from 38 meters temperature and humidity sensor
55	”H38_mx”	%	10 minutes maximum relative humidity from 38 meters temperature and humidity sensor
56	”H38_mn”	%	10 minutes minimum relative humidity from 38 meters temperature and humidity sensor
57	”H38_sd”	%	10 minutes standard deviation of the relative humidity from 38 meters temperature and humidity sensor
58	”T38_md”	°C	10 minutes mean temperature from 38 meters temperature and

Continuation of Table 20			
Col	Variable	Unit	Description
			humidity sensor
59	”T38_mx”	°C	10 minutes maximum temperature from 38 meters temperature and humidity sensor
60	”T38_mn”	°C	10 minutes minimum temperature from 38 meters temperature and humidity sensor
61	”T38_sd”	°C	10 minutes standard deviation of the temperature from 38 meters temperature and humidity sensor
62	”H2_md”	%	10 minutes mean relative humidity from 2 meters temperature and humidity sensor
63	”H2_mx”	%	10 minutes maximum relative humidity from 2 meters temperature and humidity sensor
64	”H2_mn”	%	10 minutes minimum relative humidity from 2 meters temperature and humidity sensor
65	”H2_sd”	%	10 minutes standard deviation of the relative humidity from 2 meters temperature and humidity sensor
66	”T2_md”	°C	10 minutes mean temperature from 2 meters temperature and humidity sensor
67	”T2_mx”	°C	10 minutes maximum temperature from 2 meters temperature and humidity sensor
68	”T2_mn”	°C	10 minutes minimum temperature from 38 meters temperature and humidity sensor
69	”T2_sd”	°C	10 minutes standard deviation of the temperature from 38 meters temperature and humidity sensor
70	”Vs118_md”	m/s	10 minutes wind speed at the 118 meters sonic anemometer
71	”Vs118_mx”	m/s	10 minutes maximum wind speed at 118 meters sonic anemometer
72	”Vs118_mn”	m/s	10 minutes minimum wind speed at 118 meters sonic anemometer
73	”Vs118_sd”	m/s	10 minutes standard deviation of the wind speed at 118 meters sonic anemometer
74	”Ds118_md”	º	10 minutes mean wind direction from the 118 meters sonic anemometer
75	”D118_mx”	º	10 minutes maximum wind direction from the 118 meters sonic anemometer
76	”D118_mn”	º	10 minutes minimum wind direction from the 118 meters sonic anemometer
77	”D118_sd”	º	10 minutes standard deviation of the wind direction from the 118 meters sonic anemometer
78	”Z118_md”	m/s	10 minutes mean wind speed vertical component from 118 meters sonic anemometer
79	”Z118_mx”	m/s	10 minutes maximum wind speed vertical component from 118 meters sonic anemometer
80	”Z118_mn”	m/s	10 minutes minimum wind speed vertical component from 118 meters sonic anemometer
81	”Z118_sd”	m/s	10 minutes standard deviation of the wind speed vertical component from 118 meters sonic anemometer
82	”Ts118_md”	°C	10 minutes mean temperature from 118 meters sonic anemometer
83	”Ts118_mx”	°C	10 minutes maximum temperature from 118 meters sonic anemometer
84	”Ts118_mn”	°C	10 minutes minimum temperature from 118 meters sonic anemometer
85	”Ts118_sd”	°C	10 minutes standard deviation of the temperature from 118 meters sonic anemometer
86	”Vs78_md”	m/s	10 minutes wind speed at the 78 meters sonic anemometer
87	”Vs78_mx”	m/s	10 minutes maximum wind speed at 78 meters sonic anemometer
88	”Vs78_mn”	m/s	10 minutes minimum wind speed at 78 meters sonic anemometer
89	”Vs118_sd”	m/s	10 minutes standard deviation of the wind speed at 78 meters

Continuation of Table 20			
Col	Variable	Unit	Description
			sonic anemometer
90	”Ds78_md”	º	10 minutes mean wind direction from the 78 meters sonic anemometer
91	”D78_mx”	º	10 minutes maximum wind direction from the 78 meters sonic anemometer
92	”D78_mn”	º	10 minutes minimum wind direction from the 78 meters sonic anemometer
93	”D78_sd”	º	10 minutes standard deviation of the wind direction from the 78 meters sonic anemometer
94	”Z78_md”	m/s	10 minutes mean wind speed vertical component from 78 meters sonic anemometer
95	”Z78_mx”	m/s	10 minutes maximum wind speed vertical component from 78 meters sonic anemometer
96	”Z78_mn”	m/s	10 minutes minimum wind speed vertical component from 78 meters sonic anemometer
97	”Z78_sd”	m/s	10 minutes standard deviation of the wind speed vertical component from 78 meters sonic anemometer
98	”Ts78_md”	°C	10 minutes mean temperature from 78 meters sonic anemometer
99	”Ts78_mx”	°C	10 minutes maximum temperature from 78 meters sonic anemometer
100	”Ts78_mn”	°C	10 minutes minimum temperature from 78 meters sonic anemometer
101	”Ts78_sd”	°C	10 minutes standard deviation of the temperature from 78 meters sonic anemometer
102	”Vs40_md”	m/s	10 minutes wind speed at the 40 meters sonic anemometer
103	”Vs40_mx”	m/s	10 minutes maximum wind speed at 40 meters sonic anemometer
104	”Vs40_mn”	m/s	10 minutes minimum wind speed at 40 meters sonic anemometer
105	”Vs40_sd”	m/s	10 minutes standard deviation of the wind speed at 40 meters sonic anemometer
106	”Ds40_md”	º	10 minutes mean wind direction from the 40 meters sonic anemometer
107	”D40_mx”	º	10 minutes maximum wind direction from the 40 meters sonic anemometer
108	”D40_mn”	º	10 minutes minimum wind direction from the 40 meters sonic anemometer
109	”D40_sd”	º	10 minutes standard deviation of the wind direction from the 40 meters sonic anemometer
110	”Z40_md”	m/s	10 minutes mean wind speed vertical component from 40 meters sonic anemometer
111	”Z40_mx”	m/s	10 minutes maximum wind speed vertical component from 40 meters sonic anemometer
112	”Z40_mn”	m/s	10 minutes minimum wind speed vertical component from 40 meters sonic anemometer
113	”Z40_sd”	m/s	10 minutes standard deviation of the wind speed vertical component from 40 meters sonic anemometer
114	”Ts40_md”	°C	10 minutes mean temperature from 40 meters sonic anemometer
115	”Ts40_mx”	°C	10 minutes maximum temperature from 40 meters sonic anemometer
116	”Ts40_mn”	°C	10 minutes minimum temperature from 40 meters sonic anemometer
117	”Ts40_sd”	°C	10 minutes standard deviation of the temperature from 40 meters sonic anemometer
End of Table 20			

Year-Month	Vr118	Vc118	D118	Sonic118	Vr78	Vc78	D78	Sonic78	Vr40	Sonic40
18 Jul	0.0%	2.4%	0.0%	88.1%	2.4%	88.1%	0.0%	0.0%	88.1%	0.0%
18 Aug	75.6%	78.2%	75.6%	80.6%	78.4%	80.6%	34.3%	45.5%	80.6%	45.5%
18 Sep	96.5%	96.5%	96.5%	96.5%	96.5%	96.5%	96.5%	96.5%	96.5%	96.5%
18 Oct	95.6%	95.6%	95.6%	99.6%	95.6%	95.6%	95.6%	99.6%	95.6%	99.1%
18 Nov	95.4%	95.4%	95.4%	95.4%	23.2%	95.4%	23.2%	95.4%	95.4%	95.4%
18 Dec	100.0%	100.0%	100.0%	100.0%	43.9%	100.0%	100.0%	100.0%	100.0%	100.0%
19 Jan	88.2%	88.2%	88.2%	87.1%	83.8%	83.8%	83.8%	88.2%	83.8%	88.2%
19 Feb	98.3%	98.3%	98.3%	90.1%	98.3%	98.3%	98.3%	98.3%	98.3%	98.3%
All data	80.9%	81.5%	80.9%	92.2%	64.9%	92.2%	59.0%	77.5%	92.2%	77.5%

Table 21. Cup anemometers, wind vanes and sonic anemometers recovery rate in MP5

Year-Month	T113	T97	T81	T38	T2	H113	H97	H81	H38	H2
18 Jul	90.0%	90.0%	90.0%	90.0%	90.0%	90.0%	90.0%	90.0%	90.0%	90.0%
18 Aug	80.6%	80.6%	80.6%	80.6%	80.6%	80.6%	80.6%	80.6%	80.6%	80.6%
18 Sep	96.5%	96.5%	96.5%	96.5%	96.5%	96.5%	96.5%	96.5%	96.5%	96.5%
18 Oct	99.6%	99.6%	99.6%	99.6%	99.6%	99.6%	99.6%	99.6%	99.6%	99.6%
18 Nov	95.4%	95.4%	95.4%	95.4%	95.4%	95.4%	95.4%	95.4%	95.4%	95.4%
18 Dec	100.0%	100.0%	76.8%	100.0%	100.0%	100.0%	100.0%	100.0%	100.0%	100.0%
19 Jan	92.2%	92.2%	0.0%	92.2%	92.2%	92.2%	92.2%	92.2%	92.2%	92.2%
19 Feb	98.3%	43.7.3%	7.2%	98.3%	98.3%	98.3%	98.3%	98.3%	98.3%	98.3%
All data	94.0%	87.7%	68.8%	94.0%	94.0%	94.0%	94.0%	94.0%	94.0%	94.0%

Table 22. Temperature and Humidity recovery rate in MP5

Sonic \Month	Aug-18	Sep-18	Oct-18	Nov-18	Dec-18	Jan-19	Feb-19	Mar-19
M2@80m	79.2	89.7	81.4	59.0	99.5	69.8	98.8	94.0
M2@60m	79.2	89.7	81.4	59.0	99.5	69.8	98.8	94.0
M2@40m	79.2	89.7	81.4	59.0	99.5	69.8	98.8	94.0
M2@20m	79.2	89.7	81.4	59.0	99.5	69.8	98.8	94.0
M2@10m	79.2	89.7	81.4	59.0	99.5	69.8	98.8	94.0
M3@80m	79.2	89.3	80.8	58.4	98.5	64.6	97.2	93.7
M3@60m	79.2	89.7	81.1	58.6	98.7	63.8	97.9	93.7
M3@40m	79.2	89.6	80.3	58.0	97.2	62.3	97.6	93.5
M3@20m	79.2	89.6	80.5	58.6	98.0	62.8	97.7	93.7
M3@10m	79.2	89.7	81.3	58.8	99.1	65.1	97.8	94.0
M6@60m	79.2	89.7	81.4	59.0	99.5	69.8	98.8	94.0
M6@40m	79.2	89.7	81.4	59.0	99.5	69.8	97.8	94.0
M6@20m	79.2	89.7	81.4	59.0	99.5	69.8	96.5	94.0
M6@10m	79.2	89.7	81.4	59.0	99.5	69.8	96.7	94.0
M7@80m	79.2	89.4	81.2	58.3	99.1	64.9	96.2	93.7
M7@60m	79.2	89.7	81.3	58.6	99.5	65.6	97.2	93.8
M7@40m	79.2	89.6	81.2	58.3	99.3	63.4	96.9	93.7
M7@20m	79.2	89.7	81.2	57.5	98.9	61.8	96.6	93.8
M7@10m	79.2	89.7	81.3	58.6	99.0	63.4	96.8	93.8

Table 23. Sonic Mast's monthly recovery rate (in %)

Year-Month	T80	T40	T10	T2	HR80	HR40	HR10	HR2
18 Jul	46.1%	46.0%	27.1%	22.0%	46.1%	46.0%	27.1%	22.0%
18 Aug	39.9%	39.9%	0.0%	39.9%	39.9%	39.9%	0.0%	39.9%
18 Sep	58.6%	58.6%	0.0%	58.6%	58.6%	58.6%	0.0%	58.6%
18 Oct	100.0%	100.0%	0.0%	100.0%	100.0%	100.0%	0.0%	100.0%
18 Nov	87.0%	87.0%	0.0%	87.0%	87.0%	87.0%	0.0%	87.0%
18 Dec	72.9%	74.1%	0.0%	74.1%	72.9%	74.1%	0.0%	74.1%
19 Jan	70.2%	72.8%	0.0%	72.8%	70.2%	72.8%	0.0%	72.8%
19 Feb	29.2%	87.3%	29.4%	87.3%	79.8%	87.3%	29.4%	87.3%
19 Mar	100.0%	100.0%	100.0%	100.0%	100.0%	100.0%	100.0%	100.0%
All data	67.5%	73.8%	17.4%	71.1%	72.6%	73.8%	17.4%	71.1%

Table 24. Temperature and Humidity recovery rate in mast M2

Year-Month	T80	T40	T10	T2	HR80	HR40	HR10	HR2
18 Jul	43.2%	43.2%	43.2%	43.2%	43.2%	43.2%	43.2%	43.2%
18 Aug	39.7%	39.7%	39.7%	39.7%	39.7%	39.7%	39.7%	39.7%
18 Sep	0.0%	58.8%	58.8%	58.8%	0.0%	58.8%	58.8%	58.8%
18 Oct	0.0%	99.1%	99.1%	99.1%	0.0%	99.1%	99.1%	99.1%
18 Nov	0.0%	77.5%	77.5%	77.5%	0.0%	77.5%	77.5%	77.5%
18 Dec	0.0%	74.8%	74.8%	74.8%	0.0%	74.8%	74.8%	74.8%
19 Jan	23.6%	70.7%	70.7%	70.7%	22.9%	70.7%	70.7%	70.7%
19 Feb	90.5%	90.5%	90.5%	90.5%	90.5%	90.5%	90.5%	90.5%
19 Mar	98.6%	98.6%	98.6%	98.6%	98.6%	98.6%	98.6%	98.6%
All data	32.4%	72.4%	72.4%	72.4%	32.4%	72.4%	72.4%	72.4%

Table 25. Temperature and Humidity recovery rate in mast M3

Year-Month	T60	T40	T10	T2	HR60	HR40	HR10	HR2
18 Jul	46.1%	9.7%	46.1%	46.1%	46.1%	9.7%	46.1%	46.1%
18 Aug	100.0%	0.0%	100.0%	100.0%	100.0%	0.0%	100.0%	100.0%
18 Sep	100.0%	0.0%	100.0%	100.0%	100.0%	0.0%	100.0%	100.0%
18 Oct	97.6%	0.0%	97.6%	97.6%	97.6%	0.0%	97.6%	97.6%
18 Nov	90.1%	0.0%	90.1%	90.1%	90.1%	0.0%	90.1%	90.1%
18 Dec	93.2%	0.0%	93.2%	93.2%	93.2%	0.0%	93.2%	93.2%
19 Jan	79.6%	32.3%	79.6%	79.6%	79.6%	32.3%	79.6%	79.6%
19 Feb	96.3%	96.3%	96.3%	96.3%	96.3%	96.3%	96.3%	96.3%
19 Mar	100.0%	100.0%	100.0%	100.0%	100.0%	100.0%	100.0%	100.0%
All data	89.1%	25.9%	89.1%	89.1%	89.1%	25.9%	89.1%	89.1%

Table 26. Temperature and Humidity recovery rate in mast M6

Year-Month	T80	T40	T10	T2	HR80	HR40	HR10	HR2
18 Jul	22.8%	7.82%	31.12%	31.12%	22.8%	7.82%	31.03%	31.03%
18 Aug	0.0%	0.0%	0.0%	0.0%	0.0%	0.0%	0.0%	0.0%
18 Sep	58.5%	0.0%	58.5%	58.5%	58.5%	0.0%	58.5%	58.5%
18 Oct	97.4%	0.0%	97.4%	97.4%	97.4%	0.0%	97.4%	97.4%
18 Nov	96.4%	0.0%	96.4%	96.4%	96.4%	0.0%	96.4%	96.4%
18 Dec	87.5%	0.0%	87.5%	87.5%	87.5%	0.0%	87.5%	87.5%
19 Jan	88.1%	0.0%	88.1%	88.1%	88.1%	0.0%	88.1%	88.1%
19 Feb	98.3%	29.2%	98.3%	98.3%	98.3%	29.2%	98.3%	98.3%
19 Mar	100.0%	100.0%	100.0%	100.0%	100.0%	100.0%	100.0%	100.0%
All data	71.8%	15.2%	72.7%	72.7%	71.8%	15.2%	72.7%	72.7%

Table 27. Temperature and Humidity recovery rate in mast M7

Table 28: Sonic masts column description, including number of column, variable, unit and short description.

Begin table			
Col	Variable	Unit	Description
1	”Date/Time”	–	Beginning of the 10-min block in format DD-MM-YYYY hh:mm
2	”T80_Avg”	°C	10 minutes mean temperature from 80 meters temperature and humidity sensor
3	”T80_Max”	°C	10 minutes maximum temperature from 80 meters temperature and humidity sensor
4	”T80_Min”	°C	10 minutes minimum temperature from 80 meters temperature and humidity sensor
5	”T80_Std”	°C	10 minutes standard deviation of the temperature from 80 meters temperature and humidity sensor
6	”T40_Avg”	°C	10 minutes mean temperature from 40 meters temperature and humidity sensor
7	”T40_Max”	°C	10 minutes maximum temperature from 40 meters temperature and humidity sensor
8	”T40_Min”	°C	10 minutes minimum temperature from 40 meters temperature and humidity sensor
9	”T40_Std”	°C	10 minutes standard deviation of the temperature from 40 meters temperature and humidity sensor
10	”T10_Avg”	°C	10 minutes mean temperature from 10 meters temperature and humidity sensor
11	”T10_Max”	°C	10 minutes maximum temperature from 10 meters temperature and humidity sensor
12	”T10_Min”	°C	10 minutes minimum temperature from 10 meters temperature and humidity sensor
13	”T10_Std”	°C	10 minutes standard deviation of the temperature from 10 meters temperature and humidity sensor
14	”T2_Avg”	°C	10 minutes mean temperature from 2 meters temperature and humidity sensor
15	”T2_Max”	°C	10 minutes maximum temperature from 2 meters temperature and humidity sensor
16	”T2_Min”	°C	10 minutes minimum temperature from 2 meters temperature and humidity sensor
17	”T2_Std”	°C	10 minutes standard deviation of the temperature from 2 meters temperature and humidity sensor
18	”H80_Avg”	%	10 minutes mean relative humidity from 80 meters temperature and humidity sensor
19	”H80_Max”	%	10 minutes maximum relative humidity from 80 meters temperature and humidity sensor
20	”H80_Min”	%	10 minutes minimum relative humidity from 80 meters temperature and humidity sensor
21	”H80_Std”	%	10 minutes standard deviation of the relative humidity from 80 meters temperature and humidity sensor
22	”H40_Avg”	%	10 minutes mean relative humidity from 40 meters temperature and humidity sensor
23	”H40_Max”	%	10 minutes maximum relative humidity from 40 meters temperature and humidity sensor
24	”H40_Min”	%	10 minutes minimum relative humidity from 40 meters temperature and humidity sensor
25	”H40_Std”	%	10 minutes standard deviation of the relative humidity from 40 meters

Continuation of Table 28			
Col	Variable	Unit	Description
			temperature and humidity sensor
26	”H10_Avg”	%	10 minutes mean relative humidity from 10 meters temperature and humidity sensor
27	”H10_Max”	%	10 minutes maximum relative humidity from 10 meters temperature and humidity sensor
28	”H10_Min”	%	10 minutes minimum relative humidity from 10 meters temperature and humidity sensor
29	”H10_Std”	%	10 minutes standard deviation of the relative humidity from 10 meters temperature and humidity sensor
30	”H2_Avg”	%	10 minutes mean relative humidity from 2 meters temperature and humidity sensor
31	”H2_Max”	%	10 minutes maximum relative humidity from 2 meters temperature and humidity sensor
32	”H2_Min”	%	10 minutes minimum relative humidity from 2 meters temperature and humidity sensor
33	”H2_Std”	%	10 minutes standard deviation of the relative humidity from 2 meters temperature and humidity sensor
34	”TLogger_Avg”	°C	10 minutes mean temperature from the data logger
35	”TLogger_Max”	°C	10 minutes maximum temperature from the data logger
36	”Bateria_Avg”	V	10 minutes mean voltage from the batteries
37	”Bateria_Min”	V	10 minutes minimum voltage from the batteries
End of Table 28			

Table 29: Conventional masts column description, including number of column, variable, unit and short description.

Begin table			
Col	Variable	Unit	Description
1	”Date/Time”	–	Beginning of the 10-min block in format DD-MM-YYYY hh:mm
2	”T76_Avg”	°C	10 minutes mean temperature from 76 meters temperature and humidity sensor
3	”T76_Max”	°C	10 minutes maximum temperature from 76 meters temperature and humidity sensor
4	”T76_Min”	°C	10 minutes minimum temperature from 76 meters temperature and humidity sensor
5	”T76_Std”	°C	10 minutes standard deviation of the temperature from 76 meters temperature and humidity sensor
6	”T2_Avg”	°C	10 minutes mean temperature from 2 meters temperature and humidity sensor
7	”T2_Max”	°C	10 minutes maximum temperature from 2 meters temperature and humidity sensor
8	”T2_Min”	°C	10 minutes minimum temperature from 2 meters temperature and humidity sensor
9	”T2_Std”	°C	10 minutes standard deviation of the temperature from 2 meters temperature and humidity sensor
10	”H76_Avg”	%	10 minutes mean relative humidity from 76 meters temperature and humidity sensor
11	”H76_Max”	%	10 minutes maximum relative humidity from 76 meters temperature and humidity sensor
12	”H76_Min”	%	10 minutes minimum relative humidity from 76 meters temperature and humidity sensor
13	”H76_Std”	%	10 minutes standard deviation of the relative humidity from 76 meters temperature and humidity sensor
14	”H2_Avg”	%	10 minutes mean relative humidity from 2 meters temperature and humidity sensor
15	”H2_Max”	%	10 minutes maximum relative humidity from 2 meters temperature and humidity sensor
16	”H2_Min”	%	10 minutes minimum relative humidity from 2 meters temperature and humidity sensor
17	”H2_Std”	%	10 minutes standard deviation of the relative humidity from 2 meters temperature and humidity sensor
18	”P_Avg”	mbar	10 minutes mean pressure
19	”P_Max”	mbar	10 minutes maximum pressure
20	”P_Min”	mbar	10 minutes minimum pressure
21	”P_Std”	mbar	10 minutes standard deviation of the pressure
22	”V80_Avg”	m/s	10 minutes wind speed at the 80 meters cup anemometer
23	”D76_Avg”	º	10 minutes mean wind direction at the 76 meters wind vane
24	”D76_Std”	º	10 minutes standard deviation of the wind direction at the 76 meters wind vane
25	”V80_Max”	m/s	10 minutes maximum wind speed at the 80 meters cup anemometer
26	”V80_Std”	m/s	10 minutes standard deviation of the wind speed at the 80 meters cup anemometer
27	”D76_Max”	º	10 minutes maximum wind direction at the 76 meters wind vane
28	”V60_Avg”	m/s	10 minutes wind speed at the 60 meters cup anemometer
29	”D60_Avg”	º	10 minutes mean wind direction at the 60 meters wind vane

Continuation of Table 29			
Col	Variable	Unit	Description
30	”D60_Std”	º	10 minutes standard deviation of the wind direction at the 60 meters wind vane
30	”V60_Max”	m/s	10 minutes maximum wind speed at the 60 meters cup anemometer
31	”V60_Std”	m/s	10 minutes standard deviation of the wind speed at the 60 meters cup anemometer
32	”D60_Max”	º	10 minutes maximum wind direction at the 60 meters wind vane
33	”V20_Avg”	m/s	10 minutes wind speed at the 20 meters cup anemometer
34	”D20_Avg”	º	10 minutes mean wind direction at the 20 meters wind vane
35	”D20_Std”	º	10 minutes standard deviation of the wind direction at the 20 meters wind vane
36	”V20_Max”	m/s	10 minutes maximum wind speed at the 20 meters cup anemometer
37	”V20_Std”	m/s	10 minutes standard deviation of the wind speed at the 20 meters cup anemometer
38	”D20_Max”	º	10 minutes maximum wind direction at the 20 meters wind vane
39	”V40_Avg”	m/s	10 minutes mean wind speed at the 40 meters cup anemometer
40	”V40_Max”	m/s	10 minutes maximum wind speed at the 40 meters cup anemometer
41	”V40_Min”	m/s	10 minutes minimum wind speed at the 40 meters cup anemometer
42	”V40_Std”	m/s	10 minutes standard deviation of the wind speed at the 40 meters cup anemometer
43	”V10_Avg”	m/s	10 minutes mean wind speed at the 10 meters cup anemometer
44	”V10_Max”	m/s	10 minutes maximum wind speed at the 10 meters cup anemometer
45	”V10_Min”	m/s	10 minutes minimum wind speed at the 10 meters cup anemometer
46	”V10_Std”	m/s	10 minutes standard deviation of the wind speed at the 10 meters cup anemometer
47	”Vv80_Avg”	m/s	10 minutes mean vertical wind speed at the 80 meters vertical anemometer
48	”Vv80_Max”	m/s	10 minutes maximum vertical wind speed at the 80 meters vertical anemometer
49	”Vv80_Min”	m/s	10 minutes minimum vertical wind speed at the 80 meters cup anemometer
50	”Vv80_Std”	m/s	10 minutes standard deviation of the vertical wind speed at the 80 meters vertical anemometer
51	”Vv40_Avg”	m/s	10 minutes mean vertical wind speed at the 40 meters vertical anemometer
52	”Vv40_Max”	m/s	10 minutes maximum vertical wind speed at the 40 meters vertical anemometer
53	”Vv40_Min”	m/s	10 minutes minimum vertical wind speed at the 40 meters cup anemometer
54	”Vv40_Std”	m/s	10 minutes standard deviation of the vertical wind speed at the 40 meters vertical anemometer
55	”TLogger_Avg”	°C	10 minutes mean temperature from the data logger
56	”TLogger_Max”	°C	10 minutes maximum temperature from the data logger
57	”Bateria_Avg”	V	10 minutes mean voltage from the batteries
58	”Bateria_Min”	V	10 minutes minimum voltage from the batteries
End of Table 29			

Year-Month	V80	V60	V40	V20	V10	D76	D60	D20	VV80	VV40	T76	H76	T2	H2	P
18 Jul	40.7%	40.7%	40.7%	40.7%	40.7%	40.7%	0.0%	40.7%	40.7%	40.7%	40.7%	40.7%	40.7%	40.7%	40.7%
18 Aug	39.7%	39.7%	39.7%	39.7%	39.7%	39.7%	0.0%	39.7%	39.7%	39.7%	39.7%	39.7%	39.7%	39.7%	39.7%
18 Sep	58.8%	58.8%	58.8%	58.8%	58.8%	58.8%	0.0%	58.8%	58.8%	58.8%	58.8%	58.8%	58.8%	58.8%	58.8%
18 Oct	100.0%	100.0%	100.0%	100.0%	100.0%	100.0%	0.0%	100.0%	100.0%	100.0%	100.0%	100.0%	100.0%	100.0%	100.0%
18 Nov	100.0%	100.0%	100.0%	100.0%	100.0%	100.0%	0.0%	100.0%	100.0%	100.0%	100.0%	100.0%	100.0%	100.0%	100.0%
18 Dec	96.2%	96.2%	96.2%	96.2%	96.2%	96.2%	0.0%	96.2%	96.2%	96.2%	96.2%	96.2%	96.2%	96.2%	96.2%
19 Jan	88.7%	88.7%	88.7%	88.7%	88.7%	88.7%	0.0%	88.7%	88.7%	88.7%	88.7%	21.2%	88.7%	88.7%	88.7%
19 Feb	40.7%	40.7%	40.7%	40.7%	40.7%	40.7%	0.0%	40.7%	40.7%	40.7%	40.7%	40.7%	40.7%	40.7%	40.7%
19 Mar	100.0%	100.0%	100.0%	100.0%	100.0%	100.0%	0.0%	100.0%	100.0%	100.0%	100.0%	100.0%	100.0%	100.0%	100.0%
All data	80.2%	80.2%	80.2%	80.2%	80.2%	80.2%	0.0%	80.2%	80.2%	80.2%	80.2%	72.6%	80.2%	80.2%	80.2%

Table 30. Recovery rate in mast M1

Year-Month	V80	V60	V40	V20	V10	D76	D60	D20	VV80	VV40	T76	H76	T2	H2	P
18 Sep	58.7%	58.7%	58.7%	58.7%	58.7%	58.7%	58.7%	58.7%	58.7%	58.7%	58.7%	58.7%	58.7%	58.7%	58.7%
18 Oct	100.0%	100.0%	100.0%	100.0%	100.0%	100.0%	100.0%	100.0%	100.0%	100.0%	100.0%	100.0%	100.0%	100.0%	100.0%
18 Nov	100.0%	100.0%	100.0%	100.0%	100.0%	100.0%	100.0%	13.1%	100.0%	100.0%	100.0%	100.0%	100.0%	100.0%	100.0%
18 Dec	100.0%	100.0%	100.0%	100.0%	100.0%	100.0%	100.0%	0.0%	100.0%	100.0%	100.0%	100.0%	100.0%	100.0%	100.0%
19 Jan	65.6%	65.6%	65.6%	65.6%	65.6%	65.6%	65.6%	16.0%	65.6%	65.6%	65.6%	65.6%	65.6%	65.6%	65.6%
19 Feb	29.7%	29.7%	29.7%	29.7%	29.7%	29.7%	29.7%	29.7%	29.7%	29.7%	29.7%	29.7%	29.7%	29.7%	29.7%
19 Mar	100.0%	100.0%	100.0%	100.0%	100.0%	100.0%	100.0%	100.0%	100.0%	100.0%	100.0%	100.0%	100.0%	100.0%	100.0%
All data	79.8%	79.8%	79.8%	79.8%	79.8%	79.8%	79.8%	45.7%	79.8%	79.8%	79.8%	79.8%	79.8%	79.8%	79.8%

Table 31. Recovery rate in mast M5

Station	Start	End
SLS01	12/04/2018	12/12/2018
SLS02	12/04/2018	10/12/2018
SLS03	19/10/2017	12/12/2018
SLS04	28/07/2017	11/12/2018
SLS05	05/10/2017	12/12/2018
SLS06	04/10/2017	11/12/2018
SLS07	03/10/2017	10/12/2018
SLS08	20/10/2017	11/12/2018
SLS09	17/10/2017	10/12/2018

Table 32. Working periods for each station of the SLS network.

Col	Variable	Unit	Description
1	”timestamp”	–	Beginning of the 5-min block in format YYYY-MM-dd hh:mm:ss
2	”unixtime”	seconds	Beginning of the 5-min block, starts at 1970-01-01 00:00:00
3	”Bat_Avg”	Volts	Battery voltage. Average of 3 samples.
4	”T_BMP”		Temperature from barometer BMP085. Sample.
5	”P_BMP”		Pressure from barometer BMP085. Sample.
6	”Alt_BMP”		Barometric height from barometer BMP085. Sample.
7	”HFP_Avg”	W m^{-2}	Soil heat flux. Average of 3 samples.
8	”VWC”	%	Volumetric Water Content from CS650/5. Sample.
9	”TS(ºC)”	°C	Soil Temperature from CS650/5. Sample.
10	”T_HYT1_Avg”	°C	Air Temperature from HYT1. One-minute-average of 20 samples.
11	”T_HYT1_Std”	°C	Standard deviation of the Air Temperature from HYT1. One-minute-average of 20 samples.
12	”RH_HYT1_Avg”	%	Relative humidity from HYT1. One-minute-average of 20 samples.
13	”RH_HYT1_Std”	%	Standard deviation of Relative Humidity from HYT1. One-minute-average of 20 samples.
14	”T_HYT2_Avg”	°C	Air Temperature from HYT2. One-minute-average of 20 samples.
15	”T_HYT2_Std”	°C	Standard deviation of the Air Temperature from HYT2. One-minute-average of 20 samples.
16	”RH_HYT2_Avg”	%	Relative humidity from HYT2. One-minute-average of 20 samples.
17	”RH_HYT2_Std”	%	Standard deviation of Relative Humidity from HYT2. One-minute-average of 20 samples.
18	”T_HYT3_Avg”	°C	Air Temperature from HYT3. One-minute-average of 20 samples.
19	”T_HYT3_Std”	°C	Standard deviation of the Air Temperature from HYT3. One-minute-average of 20 samples.
20	”RH_HYT3_Avg”	%	Relative humidity from HYT2. One-minute-average of 20 samples.
21	”RH_HYT3_Std”	%	Standard deviation of Relative Humidity from HYT2. One-minute-average of 20 samples.
22	”u_Avg”	m s^{-1}	Wind vector u-component. 30-second-average of 30 samples.
23	”u_Std”	m s^{-1}	Standard deviation of u. 30-second-average of 30 samples.
24	”v_Avg”	m s^{-1}	Wind vector v-component. 30-second-average of 30 samples.
25	”v_Std”	m s^{-1}	Standard deviation of v. 30-second-average of 30 samples.
26	”wind_speed_Avg”	m s^{-1}	Wind speed. 30-second-average of 30 samples.
27	”wind_speed_Std”	m s^{-1}	Standard deviation of the wind speed. 30-second-average of 30 samples.
28	”dir_Avg”	°	Resultant mean wind direction in geographical coordinate system. 30-second-average of 30 samples.
29	”dir_Std”	°	Standard deviation of wind direction30-second-average of 30 samples.

Table 33. Output of the raw files from SLS stations (except for SLS04), including column, variable, unit and short description.

Table 34: Output of the raw file from SLS04, including column, variable, unit and short description. Averages and other statistics are calculated over one minute.

Col	Variable	Unit	Description
1	”TIMESTAMP”	–	Sampling time in format YYYY-MM-dd hh:mm:ss
2	”RECORD”	–	Record number from the starting date
3	”BattV_Min”	Volts	Battery Voltage minimum measurement within the block average.
4	”PTemp_C_Avg”	°C	Datalogger Panel Temperature. Average.
5	”PTemp_C_Std”	°C	Datalogger Panel Temperature. Standard deviation.
6	”AirTC1_Avg”	°C	CS215(1) Air Temperature at 205 cm. Average.
7	”AirTC1_Std”	°C	CS215(1) Air Temperature at 205 cm. Standard deviation.
8	”RH1_Avg”	%	CS215(1) Relative Humidity at 205 cm. Average.
9	”RH1_Std”	%	CS215(1) Relative Humidity at 205 cm. Standard deviation.
10	”AirTC2_Avg”	°C	CS215(2) Air Temperature at 30 cm. Average.
11	”AirTC2_Std”	°C	CS215(2) Air Temperature at 30 cm. Standard deviation.
12	”RH2_Avg”	%	CS215(2) Relative Humidity average at 30 cm. Average.
13	”RH2_Std”	%	CS215(2) Relative Humidity std at 30 cm. Standard deviation.
14	”WinsSpeed_WV_Avg”	m s^{-1}	Mean horizontal wind speed.
15	”WindDir_WV_Avg”	°	Unit vector mean wind direction.
16	”WindDir_WV_Std”	°	Standard deviation of wind direction calculated following Yamartino algorithm.
17	”WindSpeed_Avg”	m s^{-1}	Windspeed average.
18	”WindSpeed_Std”	m s^{-1}	Windspeed standard deviation.
19	”VWC_Avg”	m^3 m^{-3}	CS655 Volumetric water content. Average.
20	”VWC_Std”	m^3 m^{-3}	CS655 Volumetric water content. Standard deviation.
21	”EC_Avg”	dS m^{-1}	CS655 Bulk Electrical Conductivity. Average.
22	”EC_Std”	dS m^{-1}	CS655 Bulk Electrical Conductivity. Standard deviation.
23	”T_vwc_Avg”	°C	CS655 Soil temperature at -5 cm. Average.
24	”T_vwc_Std”	°C	CS655 Soil temperature at -5 cm. Standard deviation.

Col	Variable	Unit	Description
25	”P_Avg”	–	CS655 Soil Bulk Dielectric Permittivity. Average.
26	”PA_Avg”	nSec	CS655 Period. Average.
27	”VR_Avg”	–	CS655 Voltage ratio. Average.
28	”shf_mV_Avg”	mV	HFP01 mesured voltage at -8 cm. Average.
29	”shf_mV_Std”	mV	HFP01 mesured voltage at -8 cm. Standard deviation.
30	”shf_Avg”	W m^{-2}	Soil heat flux at -8 cm. Average.
31	”shf_Std”	W m^{-2}	Soil heat flux at -8 cm. Standard deviation.
32	”TS1_Avg”	°C	T107(1) soil temperature at -3 cm. Average.
33	”TS1_Std”	°C	T107(1) soil temperature at -3 cm. Standard deviation.
34	”TS2_Avg”	°C	Not Connected.
35	”TS2_Std”	°C	Not Connected.
End of Table 34			

Col	Variable	Unit	Description
1	”TIMESTAMP”	–	Sampling time in format YYYY-MM-dd hh:mm:ss
2	”RECORD”	–	Record number from the starting date
3	”Ux”	m s^{-1}	Horizontal wind in the x-axis (sonic coordinate system).
4	”Uy”	m s^{-1}	Horizontal wind in the y-axis (sonic coordinate system).
5	”Uz”	m s^{-1}	Vertical wind (sonic coordinate system).
6	”Ts”	°C	Sonic Temperature.
7	”co2”	mg m^{-3}	LI-7500 carbon dioxide mass density.
8	”h2o”	g m^{-3}	LI-7500 water vapour mass density.
9	”press”	kPa	LI-7500 system pressure.
10	”diag_csat”	–	CSAT3 diagnostic word.
11	”t_hmp”	°C	HMP45C Temperature.
12	”e_hmp”	kPa	HMP45C vapour pressure.

Table 35. Output of the raw files from the SEB station, including column, variable, unit and short description.

Table 36: Output of the flux file from the SEB station, including column, variable, unit and short description. Averages and other statistics are calculated over ten minutes.

Col	Variable	Unit	Description
1	”TIMESTAMP”	–	Sampling time in format YYYY-MM-dd hh:mm:ss
2	”RECORD”	–	Record number from the starting date
3	”Hs”	W m^{-2}	Sensible heat flux using sonic temperature
4	”Fc_wpl”	mg m^{-2} s^{-1}	Carbon dioxide flux, with Webb et al. term
5	”LE_wpl”	W m^{-2}	Latent heat flux, with Webb et al. term
6	”Hc”	W m^{-2}	Sensible heat flux calculated from Hs and LE_wpl
7	”tau”	kg m^{-1} s^{-2}	Momentum flux
8	”u_star”	m s^{-1}	Friction velocity
9	”Ts_mean”	°C	Average sonic temperature
10	”stdev_Ts”	°C	Standard deviation of sonic temperature
11	”cov_Ts_Ux”	°C m s^{-1}	Covariance of sonic temperature and horizontal wind (x-axis)
12	”cov_Ts_Uy”	°C m s^{-1}	Covariance of sonic temperature and horizontal wind (y-axis)
13	”cov_Ts_Uz”	°C m s^{-1}	Covariance of sonic temperature and vertical wind
14	”co2_mean”	mg m^{-3}	Average carbon dioxide density
15	”stdev_co2”	mg m^{-3}	Standard deviation carbon dioxide density
16	”cov_co2_Ux”	mg m^{-2} s^{-1}	Covariance of carbon dioxide density and horizontal wind (x-axis)
17	”cov_co2_Uy”	mg m^{-2} s^{-1}	Covariance of carbon dioxide density and horizontal wind (y-axis)
18	”cov_co2_Uz”	mg m^{-2} s^{-1}	Covariance of carbon dioxide density and vertical wind
19	”h2o_Avg”	g m^{-3}	Average water vapour density
20	”stdev_h2o”	g m^{-3}	Standard deviation of water vapour density
21	”cov_h2o_Ux”	g m^{-2} s^{-1}	Covariance of water vapour density and horizontal wind (x-axis)
22	”cov_h2o_Uy”	g m^{-2} s^{-1}	Covariance of water vapour density and horizontal wind (y-axis)
23	”cov_h2o_Uz”	g m^{-2} s^{-1}	Covariance of water vapour density and vertical wind
24	”Ux_Avg”	m s^{-1}	Average horizontal wind (x-axis)

Col	Variable	Unit	Description
25	”stdev_Ux”	m s^{-1}	Standard deviation of horizontal wind (x-axis)
26	”cov_Ux_Uy”	m^2 s^{-2}	Covariance of horizontal winds (x-axis and y-axis)
27	”cov_Ux_Uz”	m^2 s^{-2}	Covariance of horizontal wind (x-axis) and vertical wind
28	”Uy_Avg”	m s^{-1}	Average horizontal wind (y-axis)
29	”stdev_Uy”	m s^{-1}	Standard deviation of horizontal wind (y-axis)
30	”cov_Uy_Uz”	m^2 s^{-2}	Covariance of horizontal wind (y-axis) and vertical wind
31	”Uz_Avg”	m s^{-1}	Average vertical wind
32	”stdev_Uz”	m s^{-1}	Standard deviation of vertical wind
33	”press_mean”	kPa	Average barometric pressure
34	”t_hmp_mean”	°C	Average temperature from HMP45C
35	”h2o_hmp_mean”	g m^{-3}	Average water vapour density from HMP45C
36	”rho_a_mean”	kg m^{-3}	Average air density
37	–		
38	–		
39	”wnd_spd”	m s^{-1}	Horizontal wind speed (mean of the sonic wind speed)
40	”rslt_wnd_spd”	m s^{-1}	Resultant horizontal wind speed
41	”std_wnd_dir”	°	Standard deviation of wind direction
42	”Fc_irga”	mg m^{-2} s^{-1}	Carbon dioxide flux without the Webb et al. term
43	”LE_irga”	W m^{-2}	Latent heat flux without the Webb et al. term
44	”co2_wpl_LE”	mg m^{-2} s^{-1}	Carbon dioxide Webb et al. term due to latent heat flux
45	”co2_wpl_H”	mg m^{-2} s^{-1}	Carbon dioxide Webb et al. term due to (sonic) sensible heat flux
46	”h2o_wpl_LE”	W m^{-2}	Water vapour Webb et al. term due to latent heat flux
47	”h2o_wpl_H”	W m^{-2}	Water vapour Webb et al. term due to (sonic) sensible heat flux
48	”n_Tot”	samples	Number of samples in the statistics (fluxes, variances, means, ...)
49	”csat_warnings”	samples	Number of times any CSAT3 warning flag was set high
50	”irga_warnings”	samples	Number of times any LI-7500 warning flag was set high
51	”del_T_f_Tot”	samples	Number of delta temperature warnings from CSAT3

Col	Variable	Unit	Description
52	”sig_lck_f_Tot”	samples	Number of poor signal lock warnings from CSAT3
53	”amp_h_f_Tot”	samples	Number of amplitude high warnings from CSAT3
54	”amp_l_f_Tot”	samples	Number of amplitude low warnings from CSAT3
55	”chopper_f_Tot”	samples	Number of chopper warnings from LI-7500
56	”detector_f_Tot”	samples	Number of chopper detector from LI-7500
57	”pll_f_Tot”	samples	Number of chopper pll from LI-7500
58	”sync_f_Tot”	samples	Number of chopper synchronization warnings from LI-7500
59	”agc_Avg”	unitless	Average AGC from LI-7500
60	”panel_temp_Avg”	°C	Average datalogger panel temperature
61	”batt_volt_Avg”	Volts	Average battery voltage
62	”Rn_cnr1_Avg”	W m^{-2}	Average net radiation
63	”albedo_Avg”	unitless	Average albedo
64	”Rs_downwell_Avg”	W m^{-2}	Average downwelling short wave radiation
65	”Rs_upwell_Avg”	W m^{-2}	Average upwelling short wave radiation
66	”Rl_downwell_Avg”	W m^{-2}	Average downwelling long wave radiation, with temperature correction
67	”Rl_upwell_Avg”	W m^{-2}	Average upwelling long wave radiation, with temperature correction
68	”T_cnr1_Avg”	K	Average body temperature
69	”Rl_down_meas_Avg”	W m^{-2}	Average measured downwelling long wave radiation
70	”Rl_up_meas_Avg”	W m^{-2}	Average measured upwelling long wave radiation
71	”hfp01sc_1_Avg”	W m^{-2}	Average soil heat flux plate 1
72	”hfp01sc_2_Avg”	W m^{-2}	Average soil heat flux plate 2
73	”hfp01sc_3_Avg”	W m^{-2}	Average soil heat flux plate 3 - It does not work
74	”hfp01sc_4_Avg”	W m^{-2}	Average soil heat flux plate 4
75	”del_Tsoil(1)”	°C	Change in soil temperature 1
76	”del_Tsoil(2)”	°C	Change in soil temperature 2
77	”soil_water_T_Avg(1)”	m^3 m^{-3}	Mean soil volumetric water content 1, corrected for temperature
78	”soil_water_T_Avg(2)”	m^3 m^{-3}	Mean soil volumetric water content 2, corrected for temperature

Col	Variable	Unit	Description
79	”Tsoil_avg(1)”	°C	Average soil temperature 1
80	”Tsoil_avg(2)”	°C	Average soil temperature 2
81	”shf_cal(1)”	W m^{-2} mV^{-1}	In situ calibration for soil heat flux plate 1
82	”shf_cal(2)”	W m^{-2} mV^{-1}	In situ calibration for soil heat flux plate 2
83	”shf_cal(3)”	W m^{-2} mV^{-1}	In situ calibration for soil heat flux plate 3
84	”shf_cal(4)”	W m^{-2} mV^{-1}	In situ calibration for soil heat flux plate 4
85	”cs616_wcr_Avg(1)”	uSeconds	Average period of CS616(1)
86	”cs616_wcr_Avg(2)”	uSeconds	Average period of CS616(2)
End of Table 36			

B Sensors: Additional Information

For any additional information refer to the manufacturer specification sheet of each sensor:

B.1 WindScanners

Vaisala LEOSPHERE Scanning Lidar Windcube 200S

B.2 WLS70 Profiler

Vaisala LEOSPHERE LiDAR Remote Sensor Windcube70

B.3 Sonic Masts

- Gill Wind Master PRO, sonic anemometer in M2, M3 and M7.
  www.gillinstruments.com/products/anemometer/windmaster-pro.html
- METEK USA-1, sonic anemometer in M6.
  https://metek.de/product/usonic-3-scientific/
- Rotronic HM4 temperature and humidity sensors:
  https://www.rotronic.com/en/hm4-meteorology-probe.html

B.4 MP5 Mast

- METEK USA-1, sonic anemometers.
  https://metek.de/product/usonic-3-scientific/
- Vector A100LK, cup anemometers.
  https://www.windspeed.co.uk/ws/index.php?option=displaypage&Itemid=52&op=page&SubMenu=
- Thies Compact, wind vanes.
  https://www.thiesclima.com/en/Products/Wind-Compact/
- Ammonit P6312 temperature and humidity sensors.
  https://www.ammonit.com/en/products/sensors/temperature-humidity-sensors
- Vaisala PTB100A pressure sensor.
  https://www.vaisala.com/en/products/instruments-sensors-and-other-measurement-devices/instruments-industrial-measurements/ptb110

B.5 Conventional Masts

- Thies model 4.3350.00.000, cup anemometers.
  https://www.thiesclima.com/en/Products/Wind-First-Class/
- Thies Model 4.3121.33.000, wind vanes.
  https://www.thiesclima.com/en/Products/Wind-Classic/
- Young model27106-T, vertical anemometers.
  http://www.youngusa.com/products/7/60.html
- Galtec model KPK 1/6 temperature and humidity sensors.
  https://www.galltec-mela.de/productsheet/meteorological-design/pc-me-rc-me/c24_en.pdf
- Ammonit model AB 60 pressure sensor.
  https://www.ammonit.com/en/products/sensors/barometric-pressure-sensors

B.6 Surface Layer Stations (SLS)

- IST Hygrochip: Digital Humidity Sensor HYT-271.
  http://www.farnell.com/datasheets/1719946.pdf?_ga=2.96660767.1883403075.1556740712-1937404784.1537351306
- Gill Intruments: Windsonic Anemometer.
  http://gillinstruments.com/data/manuals/WindSonic-Web-Manual.pdf
- Hukseflux Thermal sensors: HFP01 (Heat Flux Plate).
  https://www.hukseflux.com/uploads/product-documents/HFP01_HFP03_manual_v1721.pdf
- Campbell Scientific: CS650/CS655 Water Content Reflectometers.
  https://s.campbellsci.com/documents/us/manuals/cs650.pdf
- Campbell Scientific: CS215 hygro-thermometer.
  https://s.campbellsci.com/documents/us/manuals/cs215.pdf
- Campbell Scientific: 107 Temperature probe.
  https://s.campbellsci.com/documents/us/manuals/107.pdf

B.7 Surface Energy Balance (SEB) Station

- Kipp&Zonen B. V.: CNR1 Net Radiometer.
  https://www.kippzonen.com/Download/85/Manual-CNR-1-Net-Radiometer-English
- LI-COR Inc.LI-7500 Open Path CO2/H2O Gas Analyzer.
  https://www.licor.com/documents/ij79q7adnx7ozr1r1yil
- Campbell Scientific: CSAT3 3-D Sonic anemometer.
  https://s.campbellsci.com/documents/us/manuals/csat3.pdf
- Vaisala: HMP45C hygro-thermometers.
  https://s.campbellsci.com/documents/af/manuals/hmp45c.pdf
- Hukseflux Thermal sensors: HFP01SC Heat Flux Plate (Self-calibrated).
  https://www.hukseflux.com/uploads/product-documents/HFP01SC_manual_v1624.pdf
- Campbell Scientific: TCAV averaging Soil Thermocouple Probe.
  https://s.campbellsci.com/documents/us/manuals/tcav.pdf
- Campbell Scientific: CS616 Water Content Reflectometer.
  https://s.campbellsci.com/documents/us/manuals/cs616.pdf

B.8 RASS-Sodar Profiler

Scintec WindRASS
https://www.scintec.com/english/web/Scintec/Details/A040040.aspx

C WindScanner & WLS70 Deployment

WindScanner #	Model-Serial	Nickname	Site deployed
WS1	WLS200S-13	Sirocco	Zulueta
WS2	WLS200S-07	Koshava	Zabalegui
WS3	WLS200S-03	Whittle	Elorz
WS4	WLS200S-10	Brise	Monreal
WS5	WLS200S-06	Sterenn	Otano

Table 37. WS deployment details

Figure 40. All WS systems side-by-side for CNR ranking and focus point adjustment.

C.1 WS1: Sirocco at Zulueta

Particularities of WS1 site:

- Due to land restrictions, WS1 had to be installed in a 2m platform in order to have a proper view towards the North Ridge, see figure 41;
- WS1 had a clear view to all measurement points of the North Ridge, as well as a good view to M7 (in the middle of the valley), Azimuth,Elevation,Range=164.89, 2.278, 2460.30, where the LOS sanity check was performed, see section 2.3.6. Figure 42 shows the panorama.

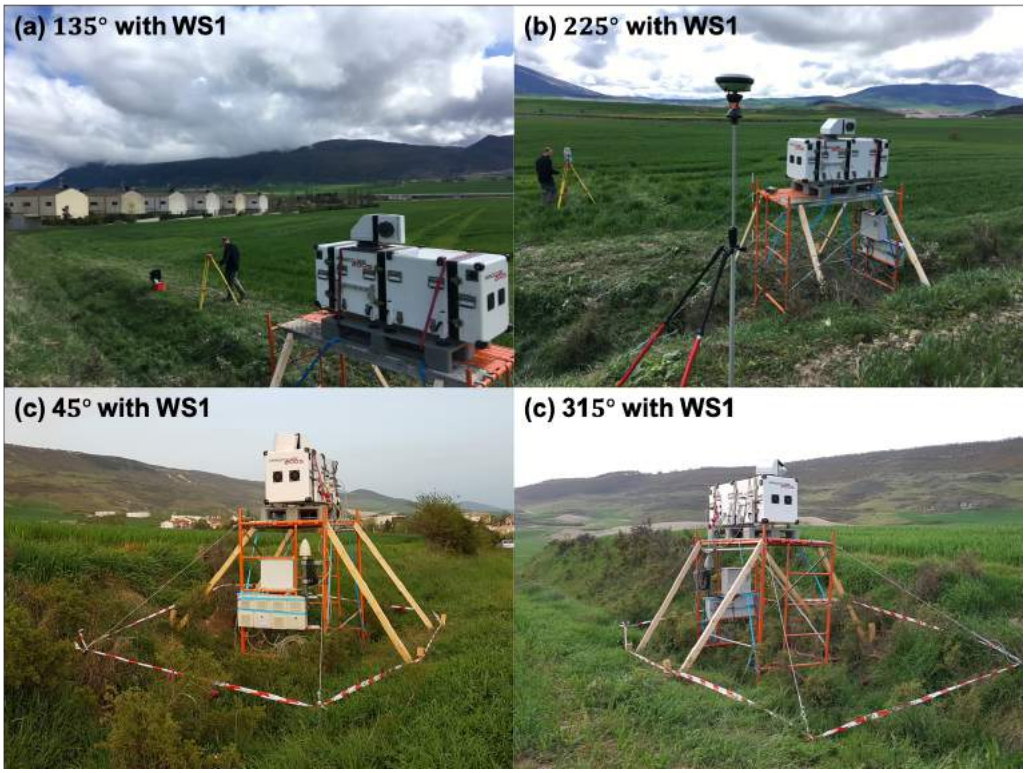

Figure 41. WS1 overview from 4 distinct positions

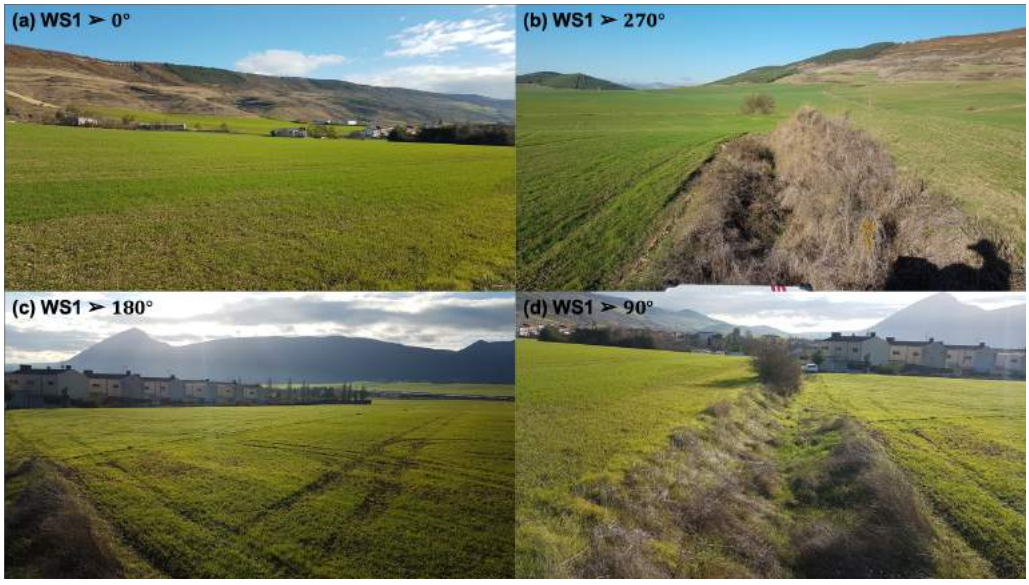

Figure 42. WS1 panorama towards all cardinal points

C.2 WS2: Koshava at Zabalegui

Particularities of WS2 site:

- WS2 was installed in the middle of the valley with easy access, along with M7, WindRASS, 1 SLS and the SEB, see figure 43 for an overview;
- WS2 is located in a clear and flat farm area, with clear view at all directions. Figure 44 shows the panorama of this system;
- WS2 has a close view to the M7 top with high elevation angle, Azimuth,Elevation,Range=$107.44, 44.108, 121.84$, but the system had a fatal failure during most the LOS Sanity Check campaign.

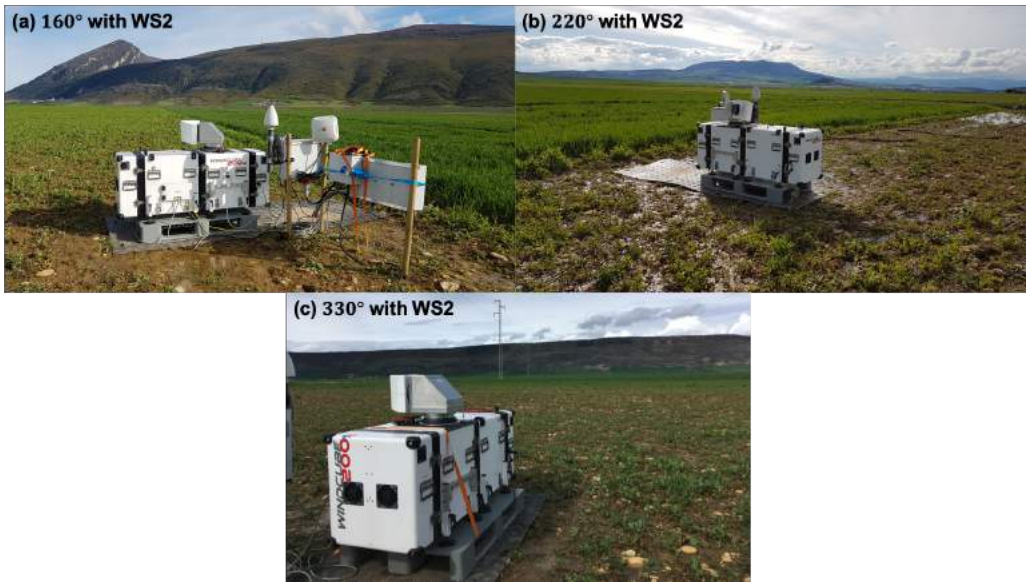

Figure 43. WS2 overview from 3 distinct positions: (a) 160°*, (b)* 220° *and (c)* 330°

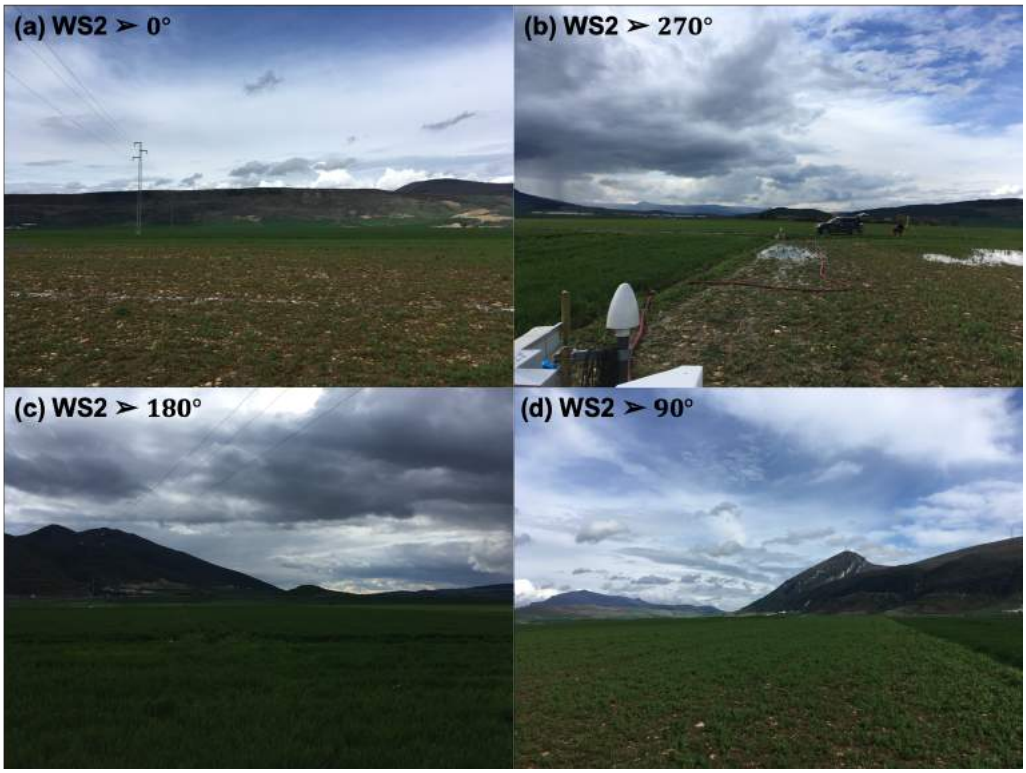

Figure 44. WS2 panorama with viewpoint from 4 cardinal points.

C.3 WS3: Whittle at Elorz

Particularities of WS3 site:

- In order to have a clear view to the North Ridge (Tajonar Hill) as well as good range for an RHI towards the South Ridge, WS3 was deployed on top of a 3m high platform, see an overview from different angles on figure 45;
- At the deployed location the system had a good 360° view and was able to reach the entire North Ridge and also perform the RHI towards the south, figure 46 shows the panorama from the system's point of view;
- During the north ridge, however, some obstacles were present, being possibly the platform itself (NW platform supporting pole, where a surveilance camera was installed), see figure 45b;
- WS3 has a clear view to the M7 top Azimuth,Elevation,Range=$226.66, 3.075, 1809.03$, making possible a sanity check with the other WS systems.

Figure 45. Overview of WS3 from 3 distinc angles: (a) 220°*, (b)* 45° *and (c)* 330°

Figure 46. WS3 panorama from 4 cardinal points

C.4 WS4: Brise at Monreal

Particularities of WS4 site:

- WS4 was deployed next to a transmission tower, due to power supply constraints, see figure 47;
- The position of WS4 provides a view of both the South Ridge as well as the transect, as the panorama shows on figure 48;

- Due to all restrictions, WS4 was in a position with potential obstacles for the scanning trajectory:
  - The South ridge scan from WS4 was compromised by the protection fence, see figures 47b and 49b.
  - The transect scan could be compromised by the vegetation height, specially during Summer, see figure 48b;
  - Transmission towers towards west of the system can block the transect scan at some points, see figure 48a and 48b.
- The final couple of points in WS4's south ridge scan hits the fence. Therefore, this can be used as a Hard Target sanity check to assess pointing accuracy;
- WS4 has a clear view to the M7 top Azimuth,Elevation,Range=$268.70, 1.127, 2895.82$, making possible a sanity check with the other WS systems.

Figure 47. WS4 deployment site next to a transmission tower.

Figure 48. WS4 panorama view from 3 relevant measurement angles.

Figure 49. Overview of WS4 site towards (a) 170°*, (b)* 180°*, (c)* 30° *and (d)* 330°.

C.5 WS5: Sterenn at Otano

Particularities of WS5 site:

- Deployed on the foothills of South ridge, facing the valley, see figure 50a;
- Restricted view towards the North, since it's bounded to perform an RHI aligned with the transect as well as an upwards LOS. Figure 50 show the deployment overview from 3 distinct angles;

- WS5 has a clear view to the M7 top Azimuth,Elevation,Range=331.24, 1.368, 1606.32, making possible a sanity check with the other WS systems.

Figure 50. Overview of WS5 site towards (a) 0° *(b)* 220° *and (c)* 150°.

C.6 WLS70 Deployment

Figure 51 shows a satellite view of WLS70 location and surroundings. The equipment is located on the Public University of Navarre (UPNA) campus of Agricultural studies, along with a meteorological weather station.

Particularities of WLS70 site:

- WLS70 is basically surrounded by crops to the south, small trees to the west and a warehouse to the east, see figure 52;
- The system is installed on a pallet and it's north alignment was checked and redone in distinct moments, see 2.6;

Figure 51. Satellite view of WLS70 location with 10 m *radius perimeter (yellow circle). Source: Google Earth*

Figure 52. Overview of WLS70 site towards (a) 315° *(b)* 350°*, (c)* 215° *and (d)* 45°*.*

D Met Masts Deployment

This sections aims to illustrate the surroundings of each mast site along with particularities of topography and landcover considering a fetch equals to the tower height. Other relevant details can be found on tables from Appendix A.

- XYZ Coordinates:
  - Sonic Masts: table 8;
  - Conventional masts: table 9;
- Boom height & direction, tower tilt: table 20.

D.1 M1: Cup Mast at Elorz (North)

Figure 53. M1 view with 80 m *radius perimeter around the mast location.*

Particularities of M1:

- M1 is surrounded by farmland with small and sparse trees 30 m to the south;
- To the east, M1 is close to the WS2 position and the Warehouse used for commissioning the experiment;
- Figure 53 shows the mast location with a 80 m radius perimeter. Hence, the topography is flat and landcover is uniform along this fetch;
- Figure 54 gives an overview of the mast as well as a sunflower farmland and trees to the south.

Figure 54. M1 overview from distinct viewpoints.

D.2 M2: Sonic Mast at Otano

Figure 55. M2 view with 80 m *radius perimeter around the mast location.*

Particularities of M2:

- M2 is surrounded by farmland with the Otano village road 80 m to the south as well as a channelized river;
- Figure 55 shows the mast location with a 80 m radius perimeter. Hence, the topography is flat and landcover is uniform along this fetch;
- Figure 56 gives an overview of the mast, which had the main computer and received data from all other sonic masts.
- M2 is about 500 m north of the South Ridge foothills, see figure 56c;

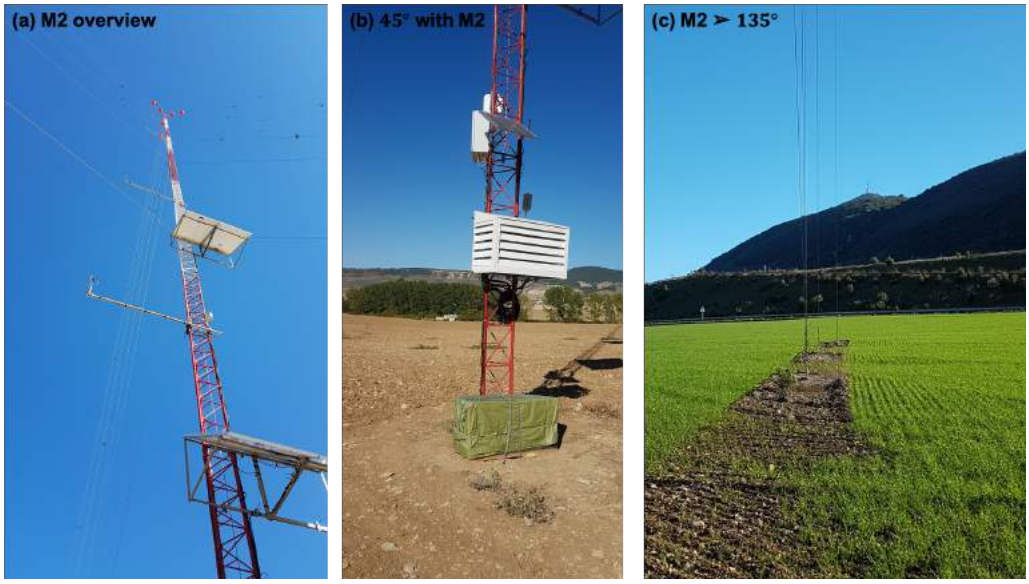

Figure 56. M2 overview from distinct viewpoints.

D.3 M3: Sonic Mast at Tajonar #1

Figure 57. M3 view with 80 m *radius perimeter around the mast location.*

Particularities of M3:

- M3 is located at the North Ridge foothills, surrounded by farmland 100 m south and low vegetation to the north, see figure 57;
- Figure 57 shows the mast location with a 80 m radius perimeter. A 14° slope is calculated along the prevailing wind direction. Also, there's a direction dependent landcover;
- Figure 58 gives an overview of the mast, which had a slightly different boom orientation from the other masts, see table 7.

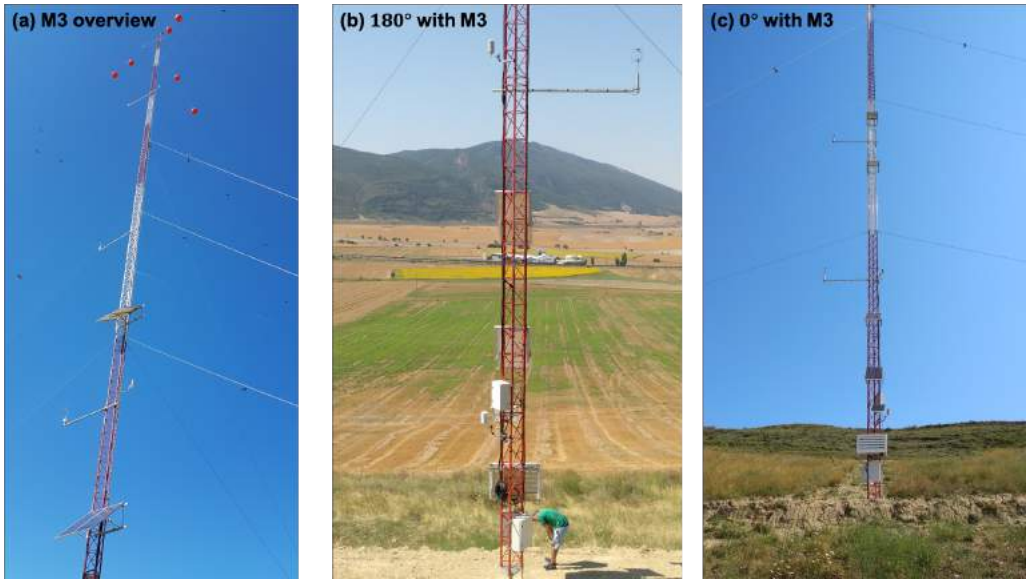

Figure 58. M3 overview from distinct viewpoints.

D.4 M5: Cup Mast at Elorz (South)

Figure 59. M5 view with 80 m *radius perimeter around the mast location.*

Particularities of M5:

- M5 is in the middle of the valley, surrounded by farmland from all directions;
- Figure 59 shows the mast location with a 80 m radius perimeter. Hence, the topography is flat and landcover is uniform along this fetch;
- Figure 60 gives an overview of the mast, which has a clear view from all directions and is also co located with the valley transect scan done by the WS systems.

Figure 60. M5 overview from distinct viewpoints.

D.5 M6: Sonic Mast at Tajonar #2

Figure 61. M6 view with 80 m *radius perimeter around the mast location.*

Particularities of M6:

- M6 is located at the North Ridge foothills, surrounded by low vegetation and with a patchy low height forest 80 m to the north;
- Figure 61 shows the mast location with a 80 m radius perimeter. A 14° slope is calculated along the prevailing wind direction;
- Figure 62 gives an overview of the mast, which, along with MP5, has METEK USA-1 sonics in contrast with Gill WM Pro sonics present in the other masts.

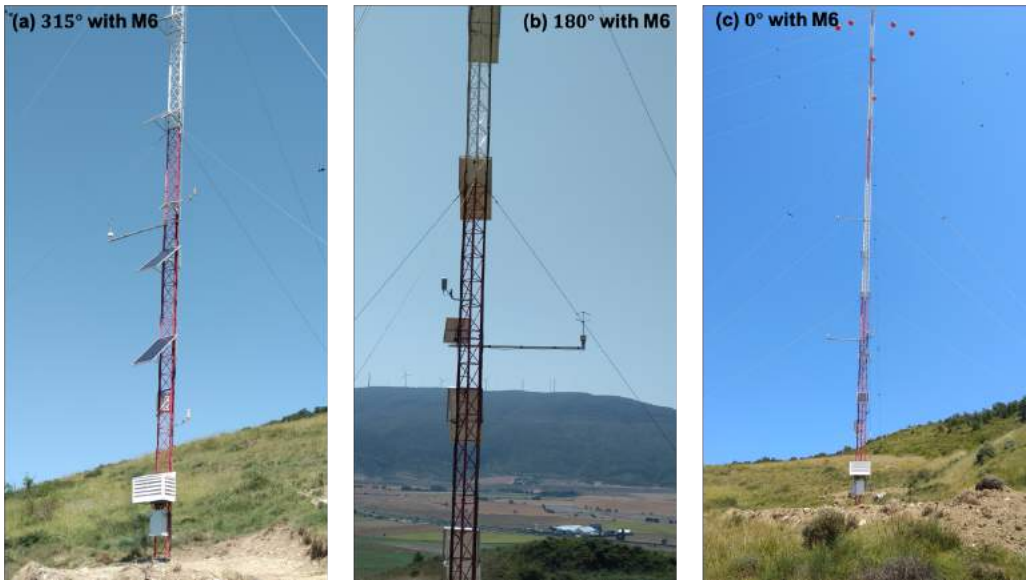

Figure 62. M6 overview from distinct viewpoints.

D.6 M7: Sonic Mast at Zabalegui

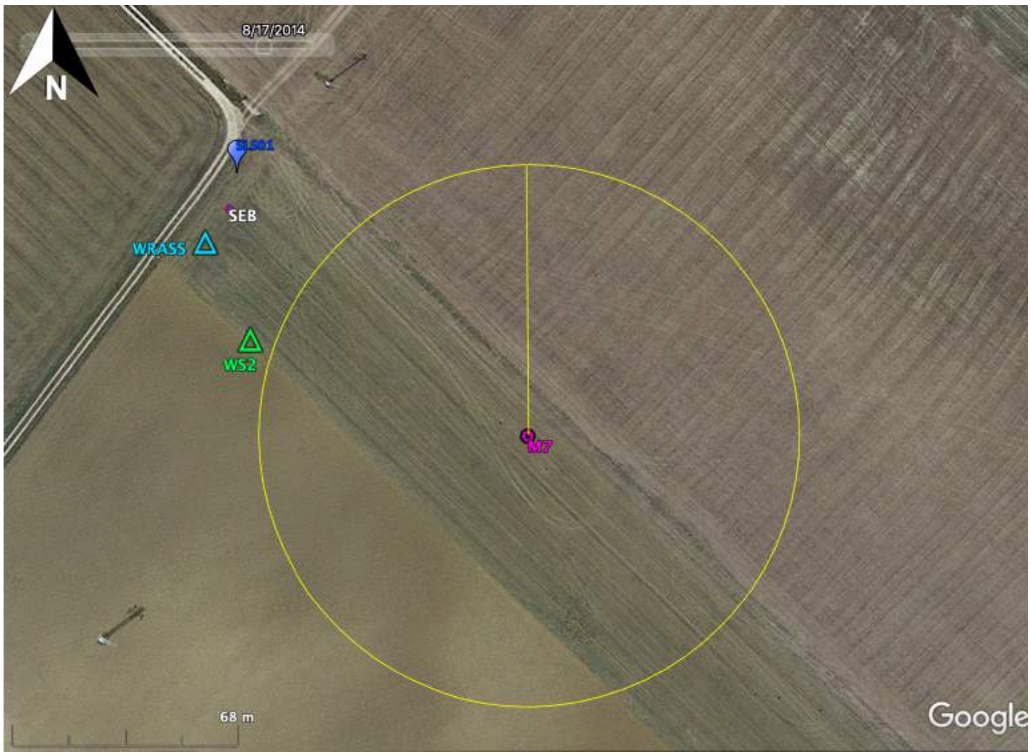

Figure 63. M7 view with 80 m *radius perimeter around the mast location.*

Particularities of M7:

- M7 is also in the middle of the valley, surrounded by farmland from all directions;
- Figure 63 shows the mast location with a 80 m radius perimeter. Hence, the topography is flat and landcover is uniform along this fetch;
- M7 position is considered a reference point, since other important sensors are present 100 m to the west, see figure 63, namely WS2, WRASS, SEB and SLS01;
- Figure 64 gives an overview of the mast, which has a clear view from all directions. Figure 64a also shows the tower twist, showing the reason for deviations in the boom directions for each height. The same can be observed for all masts in table 7.

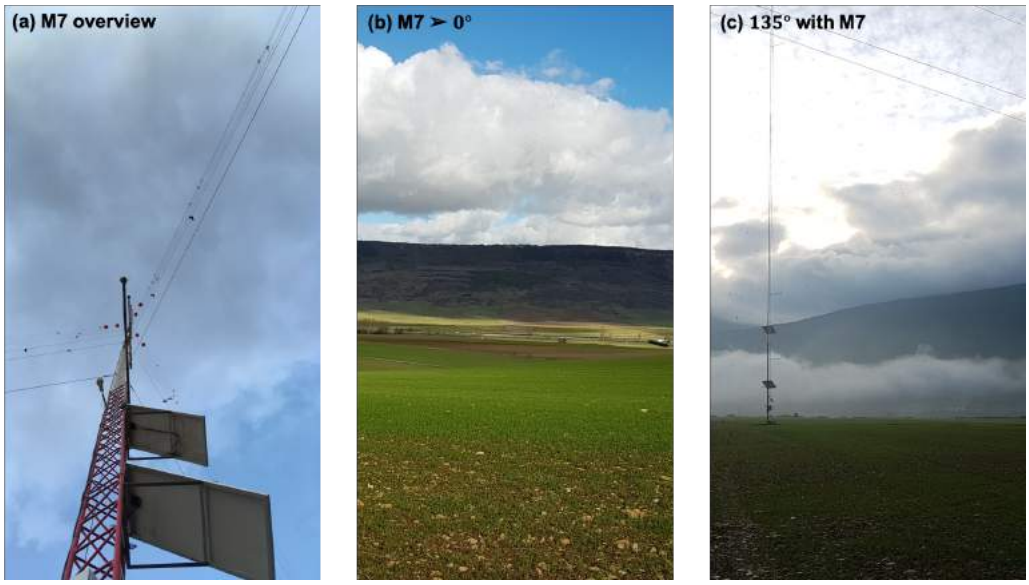

Figure 64. M7 overview from distinct viewpoints.

D.7 MP5: Reference Mast at CENER's Test Site

Figure 65. MP5 view with 120 m *radius perimeter around the mast location.*

Particularities of MP5:

- MP5 is located at the east end of CENER's Wind Turbine Test Site, on top of the South Ridge;
- MP5 location is surrounded by low vegetation and low bushes 100 m to the south;
- Figure 65 shows the mast location with a 120 m radius perimeter. A 5.7° slope is calculated along the prevailing wind direction;
- Figure 66 gives an overview of the mast, which has a busy array of booms at 40 m, but it's IEC compliant at the other heights (40 m and 118 m).

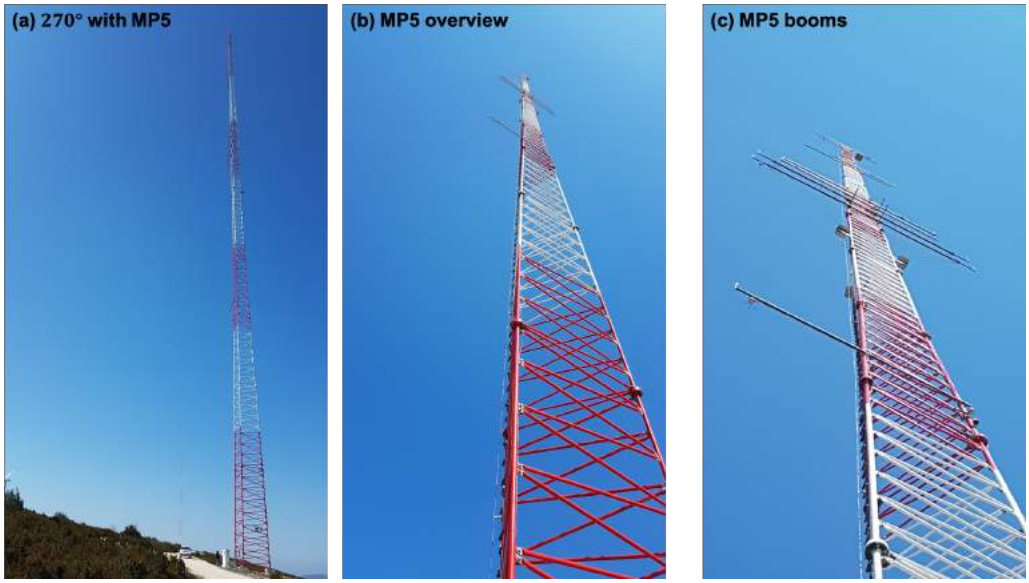

Figure 66. MP5 overview from distinct viewpoints.

E Atmospheric & Land Cover Conditions

E.1 Wind Regime

At this point, the analysis of wind characteristics during a longer measuring period at MP5 is presented.

The measuring period goes from 1st February 2011 till 31st January 2019. In this period, the mean wind speed at 118 m has been 8.55 m/s with a 87 % of data availability after data quality check.

Figure 67 shows the wind direction frequency at 118 meters height in MP5 mast. How it can be seen there are two predominant wind directions, near North (345º) and near South (165º).

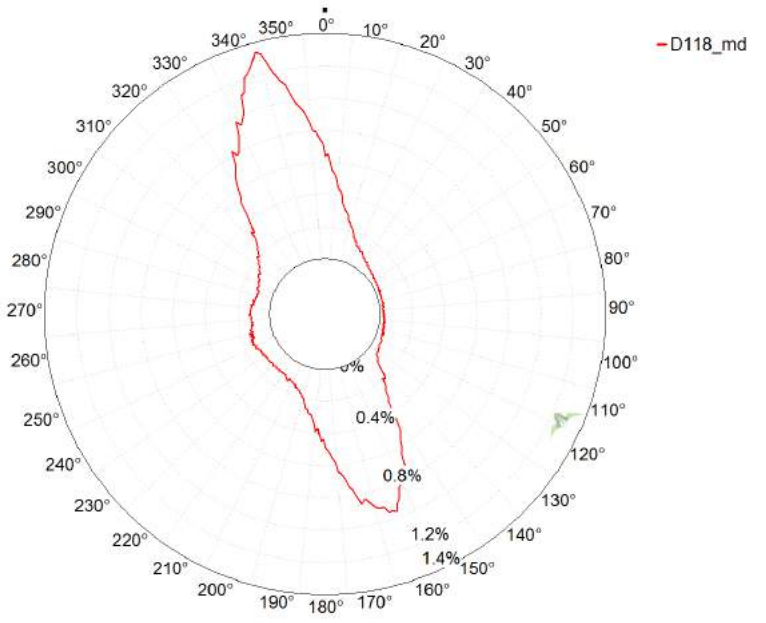

Figure 67. Wind Direction Frequency at 118 meters in MP5, from 01/02/2011 00:00 to 28/02/2019 24:00.

The frequency histogram for the measured period as well as the corresponding Weibull fit is presented in figure 68. Figure (a) shows the histogram for all the data; Figure (b) presents the histogram for data from the North direction (330º to 360º) where higher k_Weibull value but lower A_Weibul one; and Figure (C) shows the histogram for data from the South direction (180º to 150º) where there are higher wind speeds.

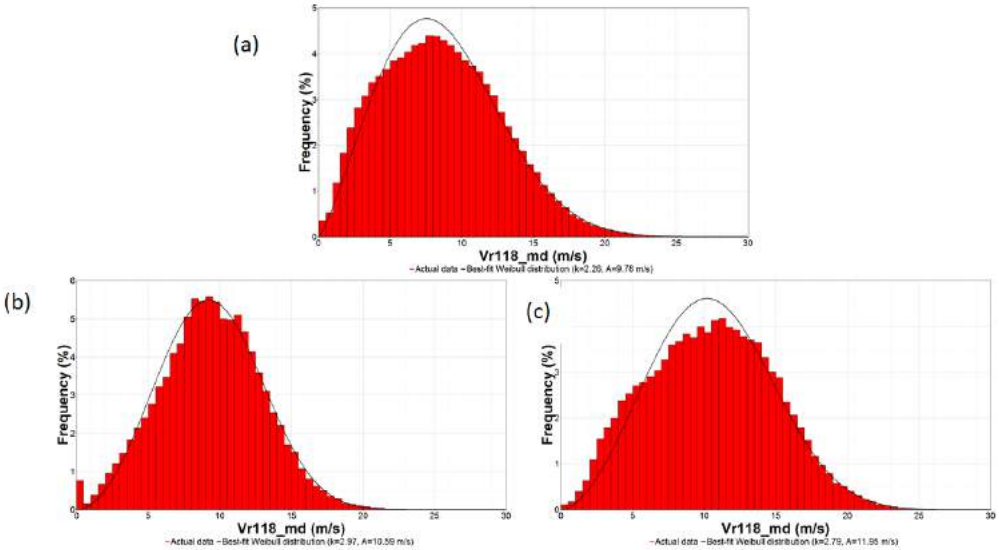

Figure 68. Histogram of wind speed frequency and Weibull fit curve for the MP5 at 118 m height, from 01/02/2011 00:00 to 28/02/2019 24:00. Figure (a) shows the histogram for all the data; Figure (b) presents the histogram for data from the North direction (330º to 360º) and Figure (C) shows the histogram for data from the South direction (180º to 150º).

Figure 69 shows the diurnal profile for the MP5 at 118 m height. As in previous figure, (a) shows the profile for all the data; Figure (b) presents the profile for data from the North direction (330º to 360º) and Figure (C) shows the profile for data from the South direction (180º to 150º). It can seen that there are a higher hourly variation for the south winds than for the northerly ones.

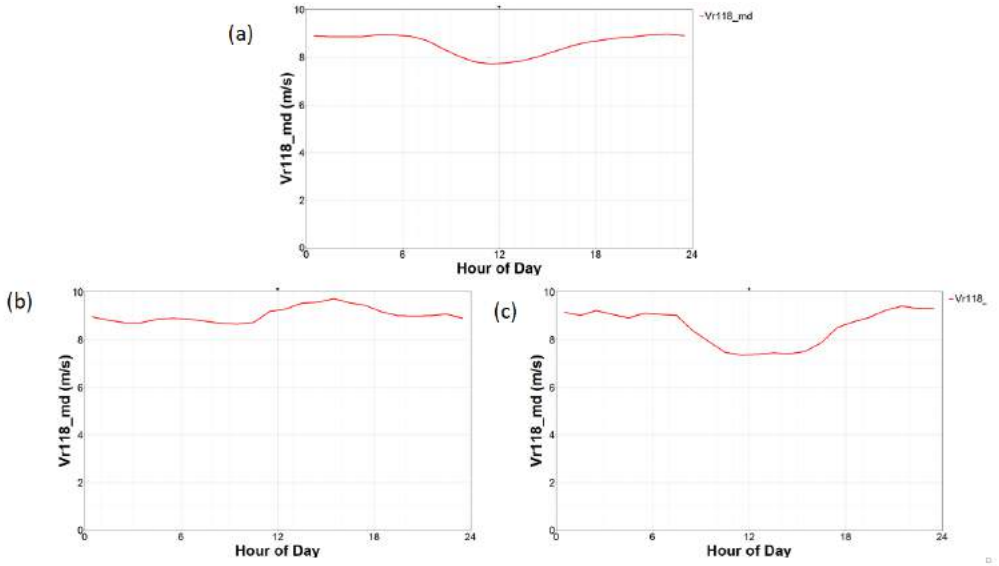

Figure 69. Diurnal profile for the MP5 at 118 m height, from 01/02/2011 00:00 to 28/02/2019 24:00. Figure (a) shows the profile for all the data; Figure (b) presents the profile for data from the North direction (330º to 360º) and Figure (C) shows the profile for data from the South direction (180º to 150º).

E.2 Clouds and Fog

As part of the site characterization, it is worth noticing frequent conditions of cloud cover in the site. Due to pressure systems and more than 400 m of height difference between the valley and the South Ridge, in many occasions the Alaiz Test Site is covered with clouds or tick fog.

Figure 70 shows an evening event where there is a tick cloud layer at about 1000 m a.g.l. which limits any kind of lidar measurements on the South Ridge. Figure 71 shows a morning event of low-level clouds as well as the presence of a fog at the WS position. This kind of condition is dissipated with the sunset and increase of the surface heat flux, however during this condition most of the valley transect can not be measured.

Figure 70. WS2 view towards 155° *with clouds covering the South Ridge (Alaiz Mountain). Picture taken on May 28th 2018 at 19h UTC*

Figure 71. WS2 view towards 155° *with low level clouds partial covering of the South Ridge (Alaiz Mountain). Picture taken on November 21st 2018 at 8h UTC*

E.3 Land Cover Change

Another aspect to consider, specially when assessing roughness length ($z0$) and surface heat fluxes is the temporal variation of the land use. Figures 72, E.3 and 74 try to show how drastic is the seasonal variation and, mainly, human activity (farming) on the land cover at ALEX17 domain.

Figures 72 and E.3 give an overview of the entire valley, from the viewpoint of WS5 looking north, towards the North Ridge. It is clear that the fall and spring seasons have distinct surface albedo, which will impact on heat flux measurements along the valley.

Figure 72. WS5 view towards North on October 25th 2018, during Fall season.

Figure 73. WS5 view towards North on April 7th 2018, during Spring season.

Figure 74 tries to exemplify the human farming and harvesting activity along the farm land, which dominates the valley. With plantations of sunflowers, rapeseed and barley the roughness length will change with the seasons.

Each farmland has one type of plantation, but in general the planting phase happens around February (or late Winter), where the crops grow until the harvest season in July (Summer). Therefore the large roughness length change happens in Spring to Summer, where the wind regime is actually lower.

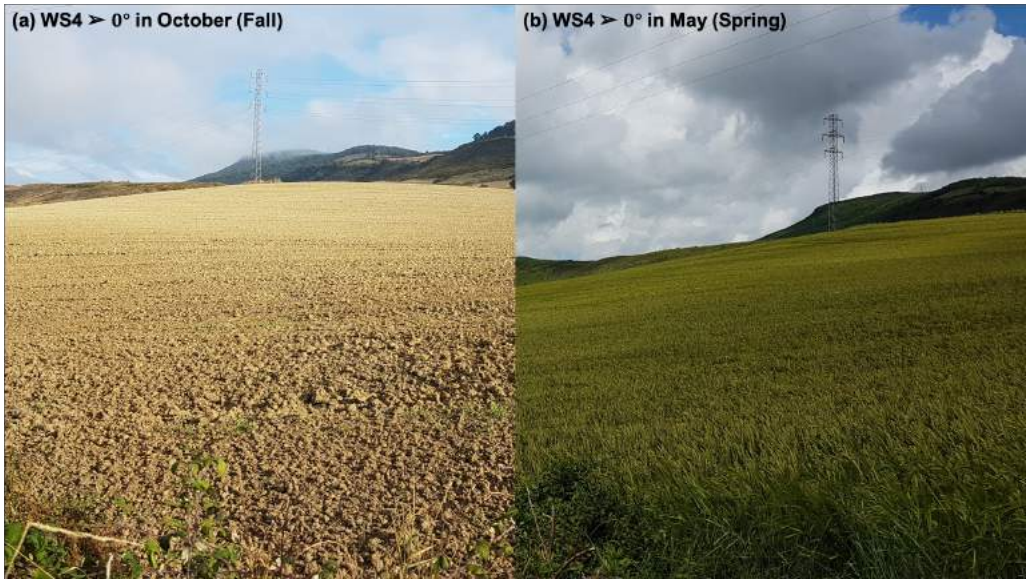

Figure 74. WS4 view towards North with comparison between Fall (a) and Spring (b) land cover.